Investigating the effects of loop modifications on the folding of outer membrane protein X

Simen Hermansen

The Department of Biosciences
The Faculty of Mathematics and Natural Sciences

UNIVERSITY OF OSLO

December 2020

Investigating the effects of loop modifications on the folding of outer membrane protein X

http://www.duo.uio.no/

Printed: Reprosentralen, University of Oslo

Acknowledgements

This thesis was carried out at the Department of Biosciences at the Univeristy of Oslo and funded by the National Institute of General Medical Sciences.

I would like to extend special thanks to my supervisors Professor Dirk Linke and Marcella Orwick Rydmark for letting me be a part of the Linke lab. You have both provided me with excellent support and advice throughout the project for which I am very grateful.

Special thanks go to all the members of the Linke group. Ina Meuskens helped me at all the stages of the project. Thank you for giving so much of your time to support me. Thanks to Athanasios Saragliadis. Your advice related to cloning was essential. Thanks to Daniel Hatlem, Hawseen Salah Khalil, Priya Kandanur and Kenneth Schneider for always answering my questions and making my stay in the lab highly enjoyable and productive.

Thanks to Professor Norbert Roos, Jens Wohlmann and Antje Hofgaard at the electron microscopy lab for your guidance and advice related to the transmission electron microscope.

Thanks to Professor Ute Krengel and Gabriele Cordara at the Deparment of Chemistry for providing the necessary facilities and advise on the crystallization experiments.

And finally, thanks to my family and friends for providing me with continued support throughout the thesis.

Table of Contents

Abstract

The surface of Gram-negative bacteria is perforated by β-barrel proteins called outer membrane proteins (OMPs). These β-barrels are integral to the outer membrane (OM) and are essential for the viability of the bacterial cell. OMPs often have large loops that protrude into the extracellular environment. These loops show promise for biotechnological applications and as therapeutic targets. The loops can be utilized to attach heterologous proteins at the surface of bacteria. Understanding how modifications to these loops affect the stability and folding of outer membrane proteins is essential for their efficient utilization for biotechnological purposes.

In this work, the small outer membrane protein OmpX was used a model system to examine the effects of loop insertions on folding and stability. The insertions were varied according to hydrophobicity and size. The effects of the loop inserts were determined by assaying folding into detergent micelles *in vitro* by SDS-PAGE. The folding capacity of the constructs were also examined *in vivo*, by isolating the OM of cells expressing the constructs.

The results indicate that folding of OMPs is effected by the hydrophobic character of the extracellular loops. Small insertions of five residues were found to improve the folding efficiency of OmpX, while large hydrophilic inserts reduced folding efficiency. All the constructs that were found to fold *in vitro*, could also do so in their native environment. One construct that could not fold *in vitro*, was transported to OM *in vivo*, but remained unfolded. The results have important biotechnological implications as they could improve the design and efficiency of recombinant OMPs used for surface display.

1. Literature Introduction

1.1 The Gram-negative Cell Envelope

The cell envelope is a composite structure that defines the boundary between the interior of the prokaryote cell and its external environment (Silhavy, Kahne, and Walker 2010). It includes the inner membrane (IM) and any other externally associated lipid bilayers, proteins or sugars. The physiological requirements of the envelope are numerous as prokaryotes rely on the structure for protection against environmental stressors, maintaining homeostasis and for directing of important cellular processes such as energy transduction, replication and motility. It is the intricate underlying structure of the envelope and the proteins lodged in its membrane layers that allows the envelope to attain these requirements. This project is focused on the structure and folding of the protein outer membrane protein X (OmpX) from the Gram-negative bacterium *Escherichia coli*.

The Gram stain

The envelope shows structural differences and adaptations between species dependent on their respective ecological niches. Basic envelope architecture has therefore been used for taxonomic classification of bacteria since the development of the "Gram-stain" (Gram 1884). The Gram-stain differentiates species into two major categories primarily based their retention of the dye crystal violet after incubation with iodine and washing with a decolorizer. Cells that can retain the dye appear dark purple and are described as being "Gram-positive". Cells that do not retain the dye appear clear and are "Gram-negative" (Moyes, Reynolds, and Breakwell 2009). Figure 1.1 shows the envelope of the Gram-negative bacterium *Escherichia coli*. Retention of the stain is primarily dependent on the thickness of the peptidoglycan cell wall, a common feature in the envelopes of prokaryotes. Peptidoglycan consists of glycan polymers cross-linked with short peptides. The glycan strands are made up of a repeating disaccharide (β-(1,4) linked GlcNAc and MurNAc) (Vollmer, Blanot, and Pedro 2008). Thicker layers of peptidoglycan results in the dye being retained. Consequentially, cells that stain Gram-positive have a thick layer of peptidoglycan. The Gram-positive envelope consist of 30-70% peptidoglycan, while the Gram-negative envelope consist of less than 10% peptidoglycan (Schleifer and Kandler 1972). The most important function of the peptidoglycan cell wall is to maintain physiological turgor pressure, cell shape and to steer cell division (Typas et al. 2011).

1.1.1 The outer membrane

Since Gram-negative cells have thinner layers of peptidoglycan, they require additional structures to maintain turgor pressure. For the vast majority of Gram-negative cells this compensation comes in the form of a second membrane attached to the ex-

terior of the peptidoglycan layer, called the outer membrane (OM) (Rojas et al. 2018). The membrane that surrounds the interior of the cell (cytoplasm) is called the inner membrane (IM). Prokaryotes with envelopes that contain two membranes are called diderms and are considered phylogenetically distinct from bacteria with a single membrane (Sutcliffe 2010). "Diderm" and "Gram-negative" is generally used synonymously since the presence of the OM reduce entry of crystal violet and is correlated with a thin layer of peptidoglycan.

In *E. coli* the OM is an asymmetrical lipid bilayer, where the inner leaflet is composed of phospholipids and the outer leaflet is composed of lipopolysaccharides (LPS). This makes the OM structurally distinct from the IM, which is a symmetrical bilayer with phospholipids in the inner and outer leaflet. LPS is a large molecule that consist of three parts. Lipid A is the lipophilic part that makes up the outer leaflet of the outer membrane. The head group of lipid A consists of a glucosamine disaccharide typically substituted with two phosphate groups attached to six acyl chains (Silhavy, Kahne, and Walker 2010). Lipid A can be crosslinked through electrostatic interactions by divalent cations (Mg^{2+}/Ca^{2+}) into a highly rigid membrane that creates a barrier to hydrophilic compounds (Clifton et al. 2015). Lipid A is further modified with two carbohydrate moieties; the core oligosaccharide and the o-antigen. The oligosaccharides protrude into the extracellular environment and creates an effective barrier to hydrophobic compounds (Sperandeo, Martorana, and Polissi 2017). The structure of the carbohydrate moieties of LPS is highly regulated and varies between species. It can therefore be used as a "fingerprint" for identification and classification of species (Caroff and Novikov 2020).

The IM and OM also differs fundamentally in the topology of the proteins that occupy their respective lipophilic sections. While the vast majority of integral outer membrane proteins share a β-barrel fold, cytoplasmic membrane proteins consist of integral α–helices. The OM is densely packed with β-barrel proteins. An estimated 50% of the surface area of the OM consists of β-barrel proteins (Horne, Brockwell, and Radford 2020). The outer membrane β-barrel proteins are therefore important for the structural integrity of the OM and are referred to as outer membrane proteins (OMPs). Lipoproteins can be attached to the inner leaflet of the OM by a lipid anchor. It is murein lipoprotein (LPP) that covalently attaches the OM the peptidoglycan layer (Silhavy, Kahne, and Walker 2010).

The space between the OM and the IM is called the periplasm. The total distance from the IM to the OM in *E. coli* is $\tilde{1}65$Å, making it a relatively thin compartment (Plummer and Fleming 2016). As the periplasm is a compartment separated from the cytoplasm its characteristics can be regulated independently (Silhavy, Kahne, and Walker 2010). The periplasm contains a variety of enzymes and chaperones. The enzymes would be toxic to the cell if it was not separated from the cytoplasm (S. I. Miller and Salama 2018). The chaperones are important for quality control of protein folding during stressful situations and are essential for folding of OMPs (Duguay and Silhavy 2004). The periplasm is devoid of ATP, so all chaperones and enzymes must function without any direct energy source (Wülfing and Plückthun 1994).

E. coli is a bacterium adapted to the mammalian gut and is the archetypal example of a Gram-negative diderm with LPS. *E. coli* is commonly uses as a model species for the study of prokaryotes and for heterologous expression of protein (Rosano and Ceccarelli 2014). The K-12 laboratory strain of E. coli does not produce the O-antigen as a part of

its LPS (Lerouge and Vanderleyden 2002). Figure 1.1 depicts all the common features of the Gram-negative outer membrane in *E. coli*. In *E. coli* the outer membrane is 7nm thick (Park et al. 2015). Murein lipoprotein and Outer membrane protein A bind to peptidoglycan and ensures that the outer membrane is securely attached to the cell (Silhavy, Kahne, and Walker 2010).

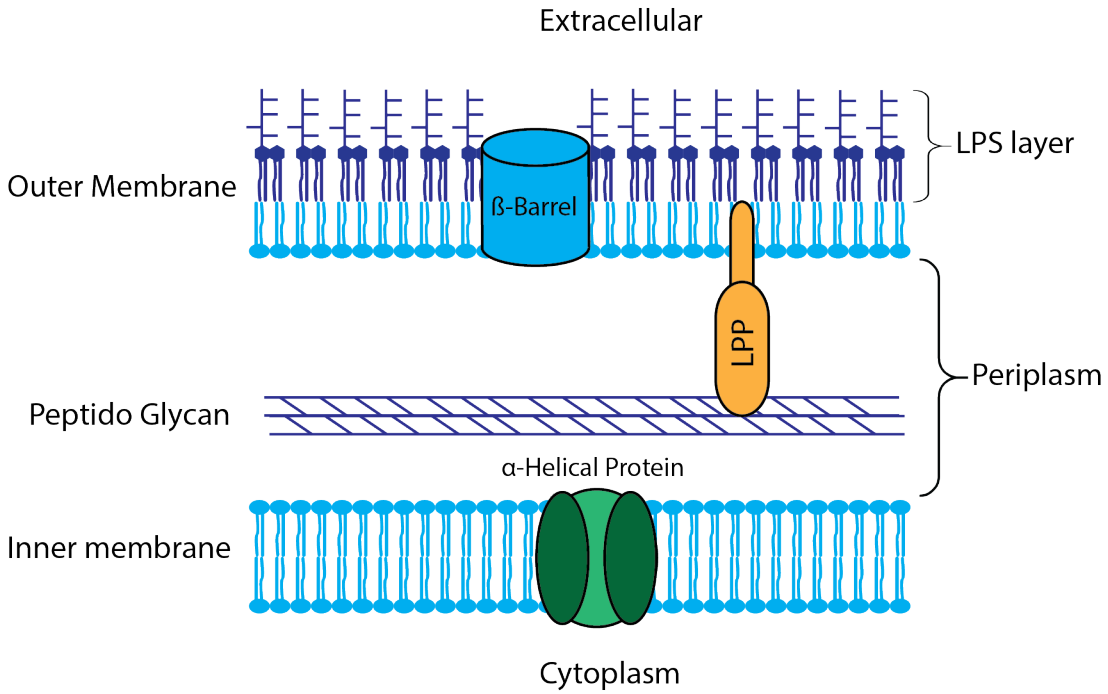

Figure 1.1: The Gram-negative cell envelope. The OM is an asymmetrical bilayer that contain integral β-barrel protein. The periplasmic space separates the OM from the IM and contains the peptidoglycan cell wall. The cell wall is attached to the OM by the lipoprotein LPP. The IM surrounds the cytoplasm and contains integral α-helical protein.

Evolution of the outer membrane and antibiotic resistance

The OM is an evolutionary ancient structure. The exact origin of the Gram-negative envelope architecture is not known (Megrian et al. 2020). One theory explains that the first diderm probably evolved from a sporulating monoderm ancestor(Vollmer 2012) under the selective pressure of antibiotics (Gupta 2011). The OM provides the cell with an extra protective layer and the necessary tools to combat antibiotics. Several of the known mechanisms of antibiotic resistance involve modifications to the envelope. Modifications to the general porins can prevent diffusion of antibiotics into the periplasm (I. Ghai and S. Ghai 2018). Periplasmic enzymes can chemically modify the antibiotic to prevent it from doing harm, and integral transporters can remove them from the cell (Blair et al. 2015). The utility of the Gram-negative envelope in combating antibiotics has caused Gram-negatives to make up the majority of the high priority multi drug-resistant bacteria listed by the CDC (Ventola 2015).

1.2 Outer Membrane Protein - Structure, function and folding

1.2.1 Structure of Outer Membrane β-barrel Protein

Geometrical features

OMPs have a ß-barrel structure. A ß-barrel is a ß-sheet that has been twisted and coiled into a cylinder, where the first (N-terminal) strand of the sheet is hydrogen bonded to the last (C-terminal strand). In OMPs the β-sheet is antiparallel. The overall geometric features of ß-barrels can be described by two parameters; the strand number (n) and shear number (S) (Murzin, Lesk, and Chothia 1994). These parameters can be used to compare the structure of different ß-barrels regardless of their primary structure. The strand number simply designates the amount of strands in the barrel. Each strand in the barrel is hydrogen bonded to both of its neighbors, where the strands are separated by a constant distance b (3Å). The hydrogen bonding occurs between the amide hydrogen and carbonyl oxygen on the backbone of the strands. Most ß-barrels have an even number of strands. Water-soluble ß-barrels tend to have fewer strands than the transmembrane ß-barrels. No characterized transmembrane ß-barrel has been found with less than eight strands. The OM domain of the Type 2 secretion system (GspD) is an example of a large multimeric β-barrel, with 60 transmembrane strands (Yan et al. 2017).

The shear number indicates the degree to which the strands are tilted (α), relative to lateral axis of the membrane. To calculate S, the barrel should be drawn two-dimensionally (Figure 1.2). This is done by cutting the barrel at the position of the last residue in the first strand and "flattening/rolling" the barrel out. The shear number is calculated by drawing a line from the position of the cut residue, parallel to the hydrogen bonds, around the barrel until the same strand has been reached. The shear is then given by the number of residues required to reach the starting residue again (on the same strand). Residues are separated by a constant distance a (3.8Å). If S is positive it means the ß-barrel is "right-handed", which is the case for all characterized OMPs (Murzin, Lesk, and Chothia 1994).

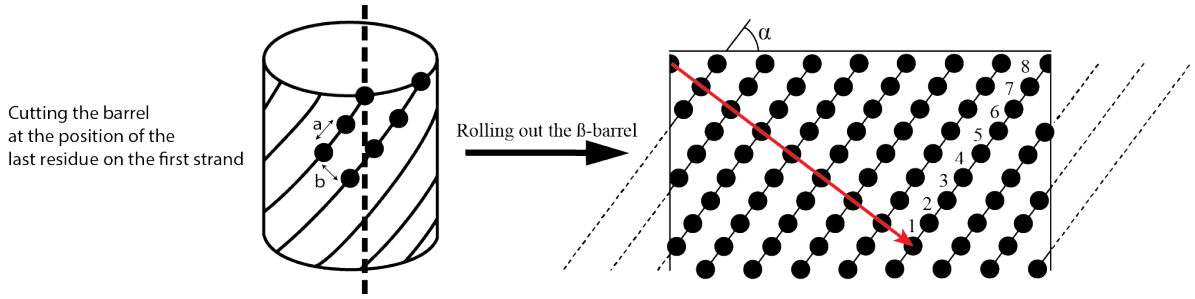

Figure 1.2: The process of calculating the shear number (S). The depicted protein has eight strands and a shear of 8. The relationship between the tilt of the strands (α) and S is given by $tan(\alpha) = (S * n)/(n * b)$. Black dots represents the carbon Cα of the residues in the protein. Each residue is separated by a constant distance a (along the strand) and each strand is separated by constant distance b (length of the hydrogen bonding). The figure is adapted from Schulz 2003.

S and n is related in such a way, that with each additional strand, the offset between the N-terminal and C-terminal strand increase. The total shear therefore increases with each additional strand. The 8-stranded ß-barrel OmpA has a shear of 10, while the 16-stranded OmpF has a shear of 20. The theoretical optimal shear for a strand number is S=n+4 (Murzin, Lesk, and Chothia 1994). Residue packing in the lumen of the barrel or interactions between external residues and the membrane cause deviations from this relationship.

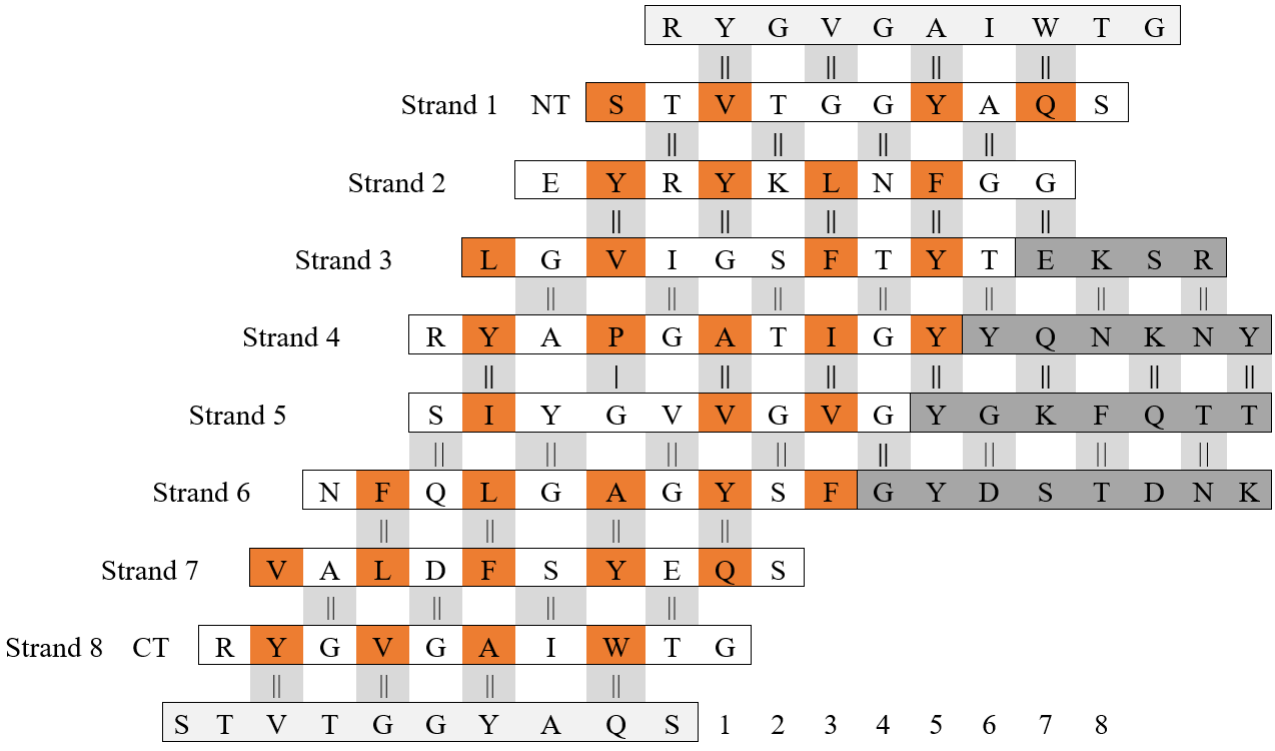

Figure 1.3: Hydrogen bonding between the transmembrane ß-strands of OmpX. Hydrogen bonding is marked by "||". Residues that are pointed into the lipid bilayer are marked in orange. Strands 3, 4, 5 and 6 form an extended ß-sheet in the extra-cellular environment that is marked in grey. The figure highlights the offset between strands. The total offset (or the shear number) between strand 1 and 8 is eight residues.

Figure 1.3 shows the hydrogen-bonding network between the ß-strands of OmpX and the offset between neighboring strands. For the off-set strands to fit inside a lipid bilayer they must be tilted accordingly. The extensive hydrogen bonding network of the ß-barrel renders OMPs highly resilient towards unfolding (Schiffrin, Brockwell, and Radford 2017). High stability might be a prerequisite for proteins that are placed in OM, as the OM is subjected to harsh environmental conditions (R. Koebnik, Locher, and Van Gelder 2000). The stability of the ß-barrel is responsible for the characteristic heat-modifiability of OMPs, which can be used to examine their folding by SDS-PAGE (section 1.2.3).

Common residue patterns in OMPs

The ß-strands of OMPs have residues alternating between facing the barrel core and the lipid bilayer core in a "dyad-repeat" pattern (William C Wimley 2003). The residues facing the bilayer core are more hydrophobic while the interior tends to be filled with more hydrophilic residues (Figure 1.4A). In smaller ß-barrels like OmpX the internal residues are packed closely together where they form strong electrostatic interactions (P. Rath, Sharpe, and Hiller 2020). The pattern of an electrostatic core and hydrophobic exterior means that OMPs can be described as reverse micelles (Figure 1.4B). Figure 1.4C shows the residue packing in the interior of OmpX. Aromatic residues in membrane protein are distributed towards the membrane interface where they form an "aromatic girdle" (figure 1.4C). The aromatic residues form interactions with the lipid head groups and are important for structural stability (Hong et al. 2007). The pattern is noticeable in both α-helical membrane proteins and ß-barrel membrane proteins.

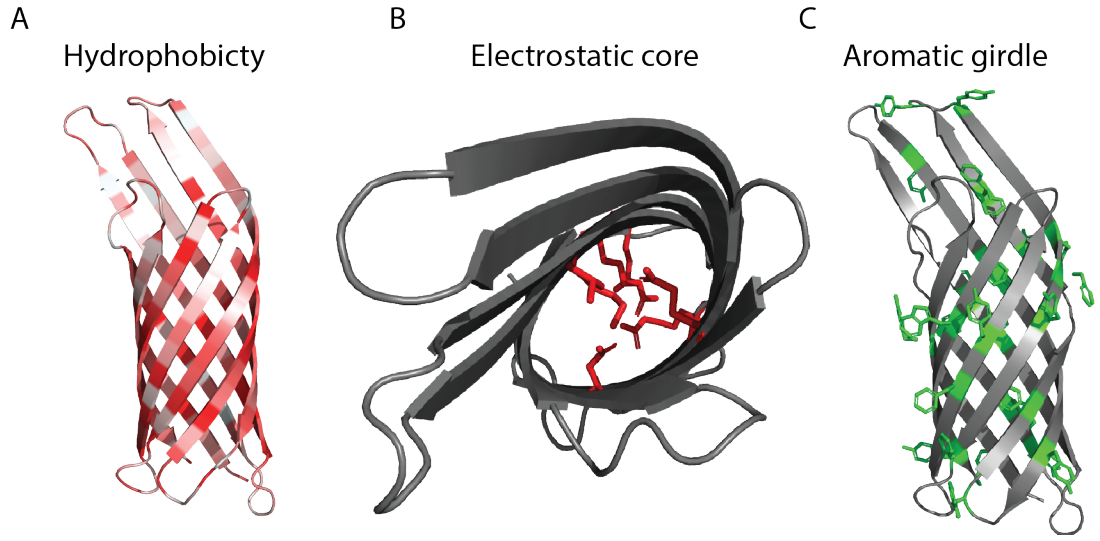

Figure 1.4: Common residue patterns in OMPs exemplified with OmpX. A) Residues are colored from white to red according to their hydrophobicity. Red residues are more hydrophobic and tend to be pointed towards the lipid bilayer. B) The electrostatic core (red residues) of OmpX (P. Rath, Sharpe, and Hiller 2020). C) Aromatic residues (marked in green) are distributed towards the bilayer interfaces. The figures was drawn with PyMol and the PDB is 1QJ8 (Vogt and Schulz 1999).

External arginine and lysine residues are sometimes located towards the terminal ends of the trans-membrane strands. These residues are charged, with a relatively long

aliphatic chain. The chains are believed to be pointed towards the membrane interface where the charged group is exposed to the membrane water interface (Deol et al. 2004). In some cases, positively charged residues on the surface of the barrel can form LPS binding sites (Ferguson et al. 2000).

1.2.2 Structure, function and applications of loops in outer membrane protein

It is the OMPs that provide the OM with features beyond that of a rigid barrier, turning it into a highly advanced interface. OMPs have several different functions in the OM. Their most obvious function is the formation of pores for nonspecific diffusion and facilitated transport of nutrients. They can also function as enzymes, adhesins or as membrane anchors for extra-cellular domains (R. Koebnik, Locher, and Van Gelder 2000). The biological function of most OMPs is closely tied to the extra cellular loops that connect the transmembrane ß-strands of the barrel.

The loops in OMPs connect adjacent beta strands in opposing directions. The ß-strands alternate between being connected at the periplasmic and extracellular side of the OM. Starting from the N-terminus the extracellular loops are labeled as loop 1, loop 2, etc. The periplasmic loops are often described as turns. The periplasmic turns and extracellular loops tend to be structurally distinct. On average, the periplasmic turns are composed of four to five residues, and they mostly seem to function as strand connectors (Franklin and Slusky 2018). This is in stark contrast with the extra-cellular loops which can be much longer, with extensive secondary structure (R. Koebnik, Locher, and Van Gelder 2000). The difference in structure between the periplasmic and extracellular loops makes the OMPs, perhaps predictably, as asymmetric as the membrane bilayer in which they reside. It is often possible to determine the orientation of OMPs in the OM by examining the length of loops on opposite sides of the barrel. As the loops are suspended in the hydrophilic environment, they are necessarily more hydrophilic compared to the transmembrane regions. Molecular dynamic simulations suggests that the extracellular loops of OMPs are more disordered and mobile compared to the trans-membrane regions (Cox et al. 2008).

The extracellular loops and the periplasmic turns of OMPs have been subject to a wide variety of mutational studies to examine their biological function. Loops have been found to be involved in pathogenesis (Maruvada and K. S. Kim 2011), they are essential for the function of the BAM complex (Browning et al. 2013), and the proteolytic activity of OmpT. The effect on the structure and stability have also been studied. In the trimeric porin OmpF, the loops are important for the structural stability of the protein. Loop 3 is folded into the core of the ß-barrel where it restricts the diameter of the channel, and loop 2 stabilize trimerization (Phale et al. 1998). Aside from specific examples the loops do not appear to be as essential for structural stability. When all the extracellular loops of OmpA where shortened, the mutated protein could still fold into the native β-barrel *in vivo* (Ralf Koebnik 1999). Similarly, insertion of 21 residues (a multiple cloning site) into the loop 2 and 3 of OmpA did not interfere with membrane assembly *in vivo* (Freudl 1989). In general, most structural studies indicate that the extracellular loops are permissible to modifications without compromising the stability of the ß-barrel. This feature makes the loops of OMPs an attractive target for genetic

modifications, with several possible biotechnological applications (Parwin, Kalan, and Srivastava 2019). Loops have been used for surface display of epitopes (Lång 2000; Rice et al. 2006), for bio adsorption of metals (Xu and S. Y. Lee 1999) and display of trypsin cleavage sites (R. Koebnik and Braun 1993; Ried et al. 1994), all without causing any significant perturbations to the ß-barrel structure.

1.2.3 Electrophoretic mobility of membrane proteins

Sodiumdodecylsulfate-polyacrylamide gel electrophoresis (SDS-PAGE) is a method for separation of proteins on the basis on their molecular weight. First, the protein is denatured by SDS. SDS binds to the protein and form an anionic SDS/protein complex where the intrinsic charge of the protein is masked. Only the primary structure of the protein is preserved when SDS is bound. When the SDS/protein complex is loaded onto a poly-acrylamide gel and separated by electrophoresis the observed mobility should only depend on the molecular weight of the protein (Manns 2011).

The method is quite reliable for determining molecular weight of most proteins, however, the observed electrophoretic mobility of membrane proteins tends to deviate from what is expected of their molecular weight. Folded OMPs exhibit "heat-modifiability" where the observed electrophoretic mobility change after the SDS/OMP complex is heated (figure 1.5). Before heating the SDS/OMP complex is rich in ß-strands, while after heating, the protein becomes unfolded (Nakamura and Mizushima 1976). It is apparent that the ß-barrel structure of OMPs is resistant to denaturation by SDS, and that the folded SDS/OMP complex has a different electrophoretic mobility compared to the unfolded/ heated complex. The unfolded SDS/OMP has an electrophoretic mobility expected of its molecular weight. Anomalies in electrophoretic mobility are also observable in α-helical membrane protein (A. Rath, Cunningham, and Deber 2013).

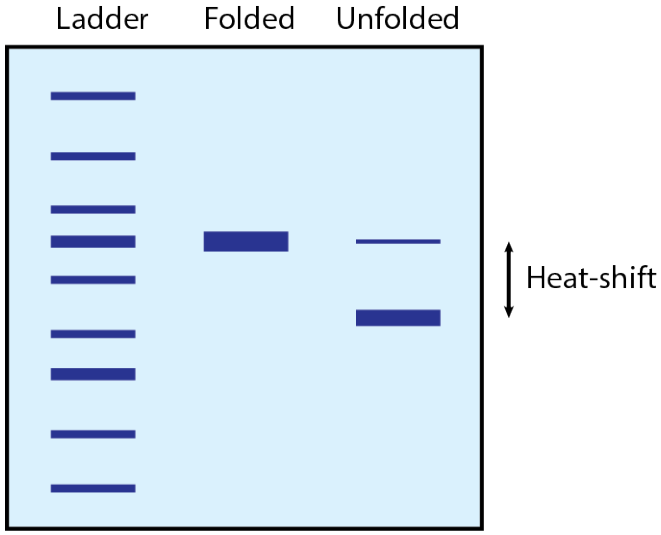

Figure 1.5: Heat-modifiability of Outer Membrane Protein observed with SDS-PAGE. OMPs resist denaturation by SDS at room temperature. Upon heating, the protein unfolds and run runs with an electrophoretic mobility that is different to the folded protein. The unfolded protein has an apparent molecular weight that is more accurate to the true weight of the protein.

Heat-modifiability is a useful tool for studying folding of OMPs, as the folded state of the protein can be determined simply by SDS-PAGE (Jörg H. Kleinschmidt 2006).

The shift in mobility between the folded and unfolded protein is mainly caused by differences in bound SDS and depend on the concentration of acrylamide in the gel (Heller 1978; A. Rath, Glibowicka, et al. 2009). In the end, whether the folded OMP has a higher or lower mobility than its unfolded counterpart depends a great deal on the composition of the gel, and the size of the ß-barrel.

1.2.4 *In vivo* biogenesis of outer membrane proteins

Folding and integration of OMPs into the OM is a complex process that requires the unfolded protein to interact with all the layers of the envelope without aggregating or misfolding. The first step in the pathway of trafficking envelope proteins to their designated location in the cell, is to separate them from the cytoplasmic proteins. Once they are recognized, they are targeted for translocation or integration at the IM. Envelope proteins are recognized by a cleavable N-terminal signal-peptide (Tsirigotaki et al. 2017). The signal peptide varies in composition but is generally 16-20 amino acids long, with a hydrophobic α-helical domain. The helical domain is flanked by a cleavage motif at its C-terminus while the N-terminus of the signal peptide tends to be positively charged. Translocation through or integration into the cytoplasmic membrane is eventually completed by one of three possible membrane protein complexes; the SecYEG translocon, the YidC insertase or the Tat system (Ross E. Dalbey and Kuhn 2012).

The general secretion pathway

In the case of OMPs, the translocation trough the inner membrane is dependent on the general secretion (Sec) pathway and the SecYEG translocon. Around 96% of proteins targeted for the envelope utilize this pathway (Tsirigotaki et al. 2017). The SecYEG translocon is a transmembrane protein complex in the IM membrane. It is an essential component of the pathway as it is involved in secretion of unfolded proteins to the periplasm, or insertion of helical membrane proteins to the cytoplasmic membrane (Denks et al. 2014). SecY is the largest subunit of the complex and it forms the channel that allows proteins to cross the cytoplasmic membrane. The channel can also open laterally for insertion of helical transmembrane domains into the membrane (Denks et al. 2014). SecE and SecG are integral proteins that stabilize the conformation of SecY in the membrane during translocation (Denks et al. 2014).

Unfolded proteins with the appropriate signal peptide (pre-protein) can be targeted towards SecYEG by a post-translational pathway or by a co-translational pathway (Tsirigotaki et al. 2017). Which pathway the pre-protein takes depend on what factor that bind the signal peptide. The co-translational pathway is preferred for integral IM proteins, while secreted protein prefer the post-translational pathway (Hegde and Bernstein 2006). The co-translational pathway involves binding of Signal Recognition Particle (SRP) to ribosome nascent protein. SRP then bind its receptor at the cytoplasmic membrane (FtsY). SRP and FtsY then disassociates by GTP hydrolosys and the ribosome nascent protein is inserted into the protein conducting channel of SecYEG (Tsirigotaki et al. 2017). In eukaryotes, SRP arrest translation of the protein. In *E. coli*, SRP does not arrest translation, and the nascent protein must reach SecYEG before translation is completed (Powers and Walter 1997).

The post-translational pathway relies mainly on the chaperone SecA. SecA can bind the ribosome nascent protein or the fully translated pre-protein free in the cytosol. SecA also binds SecY and use ATP hydrolysis and the proton motive force to push the protein through the channel (Chatzi et al. 2014). The pathway is aided by other chaperones such as Trigger Factor (TF) and SecB. TF can also bind the ribosome nascent protein while SecB can only bind the fully translated pre-protein. The chaperones maintain the unfolded state of the pre-protein and ensures it remains compatible with the SecYEG translocase (Chatzi et al. 2014).

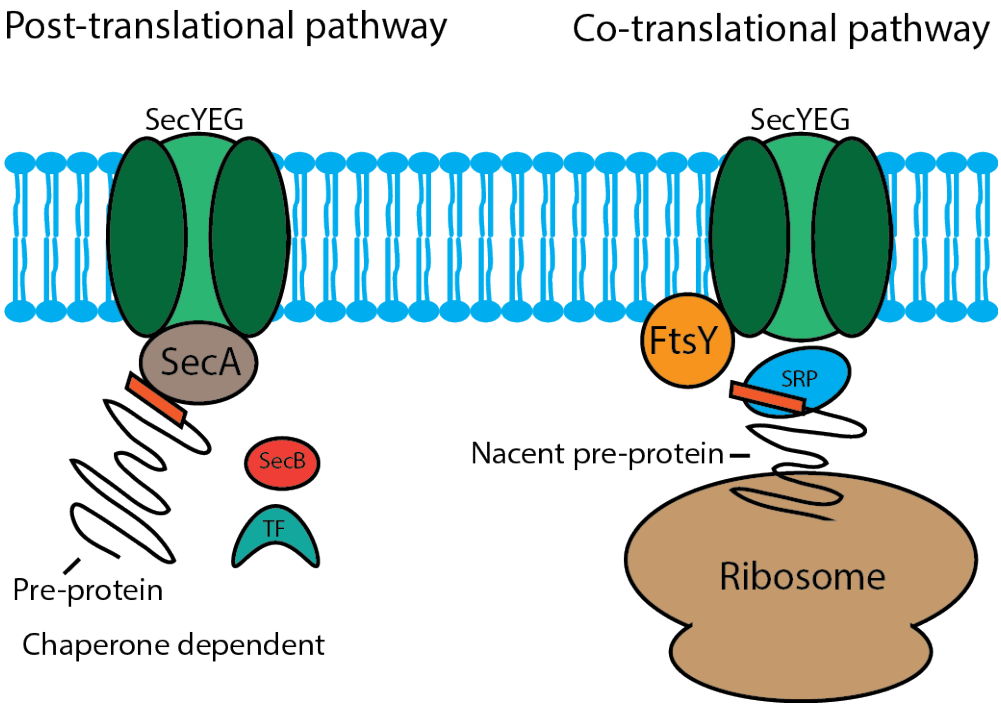

Figure 1.6: Secretion of pre-protein to the periplasm of Gram-negative bacteria. OMPs are transported through the IM by the action of the general secretion machinery (SecYEG). Protein with the signal peptide attached (pre-protein) follow one of two possible pathways. The post-translational pathway is chaperone dependent, and relies mainly on SecA to push unfolded protein through SecYEG by ATP hydrolysis. The co-translational pathway involves binding of SRP to nacent pre-protein. SRP bind its membrane receptor (FtsY). SecYEG cause FtsY and SRP to disassociate and the nascent protein is inserted into the channel of SecY.

The periplasm and the periplasmic chaperones

After translocation through the cytoplasmic membrane is complete, the pre-protein is still tethered to the membrane by the helical domain of the signal peptide. Proteolytic cleavage by the type 1 signal peptidase is necessary before the unfolded OMP can be released to the periplasmic space (Paetzel, Ross E Dalbey, and Strynadka 2000).

The periplasm is an aqueous environment in which unfolded OMPs would normally aggregate. Aggregation in the periplasm is prevented by the action of multiple chaperones that can bind unfolded OMPs, and preserve them in state that is competent for folding into the OM. OMPs can take several pathways through the periplasm (Hagan, Silhavy, and Kahne 2011). Which chaperone that is required depends on the state of the unfolded protein (Hussain, Peterson, and Bernstein 2020). Most OMPs appear to

be transported by the chaperone SurA (Ross E. Dalbey and Kuhn 2012). SurA is not essential as there are several other chaperones available in the periplasm that can complement SurA (Plummer and Fleming 2016). DegP and Skp are examples of chaperones connected to the σ^E-stress response and can complement SurA (Mogensen and Otzen 2005). The stress response is triggered upon accumulation of unfolded protein in the periplasm and usually activated at elevated temperatures (Duguay and Silhavy 2004). Up to 24 monomers of DegP can assemble into a cage-like structure that surrounds misfolded protein, after which it also functions as a protease (Krojer et al. 2008).

The BAM complex

In Gram-negative bacteria OMPs are folded and inserted into the OM by the action of the β-barrel assembly machinery (BAM). Homologs of BamA is present in the OM of mitochondria and chloroplasts (Noinaj, Kuszak, Gumbart, et al. 2013). The BAM complex consists of a 16-stranded OMP (BamA) and four associated lipoproteins (BamB, BamC, BamD and BamE) (Knowles et al. 2009). The BAM complex is essential for basic functioning of diderm prokaryotes as the OM cannot function as intended without OMPs. The mechanisms of how the complex inserts and folds OMPs into the OM remains to be completely understood. The mechanism is of special interest as it is essential for cell viability, and since the BAM complex is exposed at the OM, it is a promising target for development of novel antibiotics (Wu et al. 2020).

BamA has five periplasmic polypeptide transport-associated (POTRA) domains and is the most important monomer in the BAM complex (Wu et al. 2020). It is BamA that allows for passive entry of OMPs to the OM and facilitates protein folding. The folding mechanism of the BAM complex is probably linked to conformational changes in the N- and C-terminal strands of BamA (Wu et al. 2020). The terminal strands are short with reduced hydrogen bonding and do not fit within the dimensions of the OM. The strands cause local perturbations in the OM and thereby create a point of entry for unfolded OMPs (Doerner and Sousa 2017). According to a "budding/template model", the terminal strands can open laterally for entry of OMPs to the OM and act as a template for unfolded OMPs to form hydrogen bonds (J. Lee, Tomasek, et al. 2019; Tomasek et al. 2020). The exact function of the POTRA domains is not known, but they are believed to interact with unfolded protein in the periplasm and aid in protein folding (Knowles et al. 2009). The lipoproteins utilize the POTRA domains to assemble with BamA (Bakelar, Buchanan, and Noinaj 2016). The exact function of the associated lipoproteins is not fully understood. BamD is the only lipoprotein that is essential for the viability of the BAM-complex, while knocking out the other lipoproteins reduce the efficiency of OMP assembly (Wu et al. 2020). Figure 1.7 summarizes the general steps involved in the processing of OMPs after they are transported through the IM.

1.2.5 *In vitro* folding of outer membrane protein

The ability to fold OMPs *In vitro* has enabled the study of folding dynamics and protein structure of OMPs. The experimental process generally starts by expressing protein without the signal peptide. Without the signal peptide, the protein aggregates in the cytosol and accumulate in inclusion bodies. Expression into inclusion bodies is often preferred to overexpression to the membrane, as purifying inclusion bodies is rela-

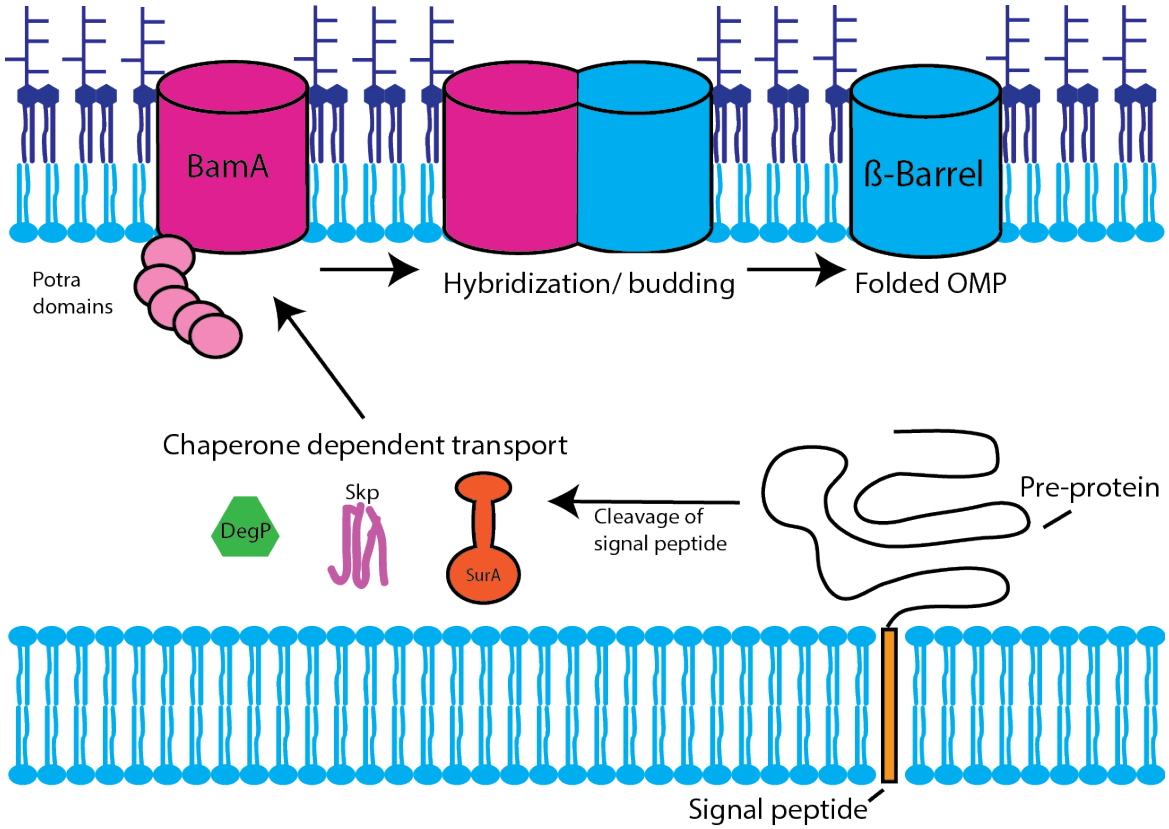

Figure 1.7: Folding of OMPs in the OM of Gram-negative bacteria and transport through the periplasm.

tively simple and delivers higher yields. Overexpressing protein to the membrane can have toxic effects by stalling the membrane insertion machinery (Popot 2014). Cell-free expression systems can also be utilized (Hussain, Peterson, and Bernstein 2020).

Protein can be recovered from its aggregated state in the inclusion bodies with a denaturant. Chaotropic agents like urea and guanidine hydrochloride are commonly used to dissolve OMPs into a soluble, unfolded state. Rapid dilution of the unfolded OMP with an appropriate folding media must then be performed for the protein to enter its folded state. In the case of OMPs, the folded state refers to any conformation where the ß-barrel has formed. OMPs with 16 β-strands or less can generally be folded *in vitro* (Popot 2014). Larger and more complex OMPs such as the 26-stranded LptD require the BAM-complex to fold (J. Lee, Tomasek, et al. 2019). The folding media must provide a suitable hydrophobic environment for the protein. Lipid bilayers, detergent/lipid micelles, detergent micelles or amphipols are commonly utilized (Popot 2014). Dilution of the denaturant makes it energetically unfavorable for the protein to stay unfolded in solution which promotes spontaneous formation of the folded ß-barrel within the provided hydrophobic environment. OMPs can only fold in detergent micelles if the detergent concentration is above the critical micellar concentration (CMC). Mild zwitterionic detergents or uncharged detergents can be utilized for folding OMPs. OMPs generally cannot fold in detergent micelles with a strong surface charge (J. H. Kleinschmidt, Wiener, and Tamm 1999). Folding into lipid bilayers is not possible if phospholipids native to the IM are used. It is possible that OMPs are adapted to prevent insertion into the IM where they could exhibit serious toxic effects

(Patel et al. 2009). OMPs fold more efficiently in bilayers composed of lipids with shorter acyl chains (Burgess et al. 2008).

In vitro folding kinetics

The folding kinetics of OMPs at high concentrations of detergent, lipid or amphipol to protein can be described by a single exponential function (Equation 1.1) when analyzed by SDS-PAGE (Jörg H. Kleinschmidt 2006).

$$X_F(t) = 1 - e^{-kt} \tag{1.1}$$

X_F is the fraction of folded protein at time t, and k is the rate constant. At time = 0, the fraction of folded protein is zero. This model works on the assumption that all the protein folds given enough time, and that all protein folds according to the same kinetic pathway. These assumptions do not generally hold true under several conditions. Folding protocols that involve rapid dilution of OMPs will cause some protein to aggregate when the concentration of the denaturant becomes too low. Outside of optimal folding temperatures this effect becomes more pronounced (Maurya, Chaturvedi, and Mahalakshmi 2013). To account for the portion of protein that cannot fold, an additional parameter (A_f) can be added to Equitation 1.1 that represents the yield of folded protein (Equation 1.2). A_f must then be between 1 and 0.

$$X_F(t) = A_f \times (1 - e^{-kt}) \tag{1.2}$$

It has been described that OMPs can follow different kinetic pathways in parallel, at different folding rates (Jörg H. Kleinschmidt 2015). In these cases, a second exponential can be added to the model to account for the alternative, slower folding kinetic (Equation 1.3).

$$X_F(t) = 1 - [A_f e^{-k_1 t} + (1 - A_f) e^{-k_2 t}] \tag{1.3}$$

In this case, A_f represents the contribution of the fastest folding pathway to the final yield of folded protein. k_1 and k_2 are the rates for the faster and slower folding kinetics respectively (Patel et al. 2009). The functions can be fitted to real data by non-linear least squares regression.

In vitro folding intermediates

Analyzing heat-shifts in OMPs by SDS-PAGE makes it possible to differentiate the completely folded protein from unfolded protein. Folding intermediates cannot be observed directly with this method. To analyze folding intermediates alternative methods must be employed that rely on, for example, circular dichroism or fluorescence quenching. Using these methods, it has been proposed that *In vitro* folding into lipid bilayers, after rapid dilution of protein in urea, follows a folding pathway with at least three distinctive steps (Surrey and Jähnig 1995). The first step involves the transition of the unfolded protein in urea (U_W) to an intermediate state in water (I_W). From I_W the protein may transition into an aggregated state (A) or into a membrane-associated state (I_M). In the aggregated state the protein loses its capability to fold. From I_M the protein will eventually transition into the native folded state (F_M). A model for the transition

of I_M to F_M has been described based on fluorescence quenching (J. H. Kleinschmidt, Wiener, and Tamm 1999). It was found that the polypeptide chain initially remains flat on the surface of the bilayer. The β-strands then start to associate into the β-barrel simultaneously as the protein penetrates the lipid bilayer (Figure 1.8a). In this model the extracellular loops penetrate the bilayer first (Jörg H. Kleinschmidt et al. 2011). It is not known if this model is applicable to folding in detergent micelles (Figure 1.8B).

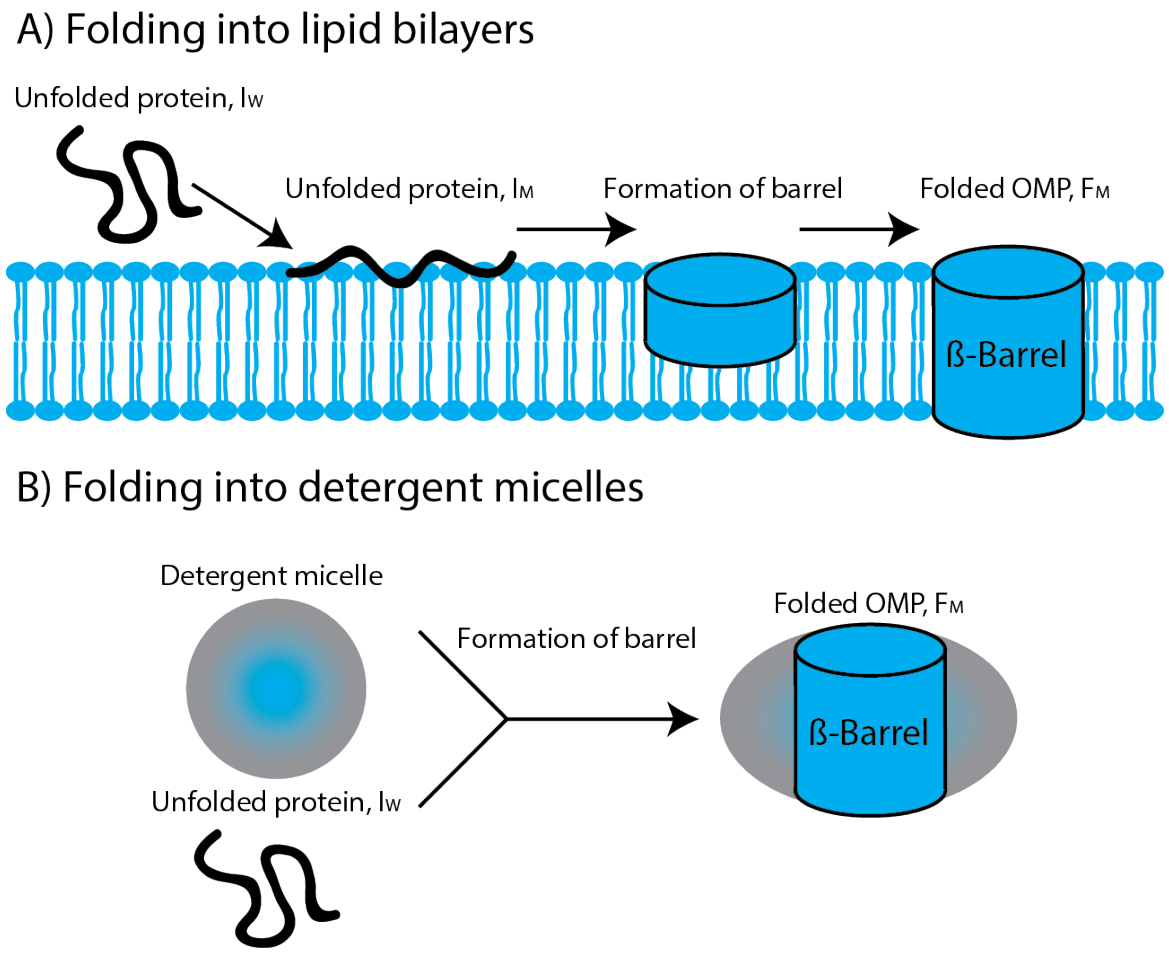

Figure 1.8: Model for *in vitro* folding of OMPs. A) Proposed mechanism for folding into lipid bilayers (J. H. Kleinschmidt, Wiener, and Tamm 1999). The unfolded OMP initially stick to the surface of the bilayer. The ß-strands then starts to assemble into a ß-barrel as they pass through the lipid bilayer. B) It is not known if folding into detergent micelles works by the same mechanism.

1.2.6 Outer membrane protein X

OmpX belongs to a group of small integral membrane proteins in Gram-negative bacteria. The protein was first characterized in *Enterobacter cloacae* (Stoorvogel, Bussel, and Klundert 1991) and the later in *E. coli* (Mecsas et al. 1995). The extracellular loops show a high degree of sequence variation between homologs, while the barrel domain is more conserved (Yamashita et al. 2011). With the signal peptide cleaved off, OmpX in *E. coli* has a molecular weight of 16.5 kDa, and with just eight transmembrane β-strands, the protein is one of the smallest characterized OMPs. Several functions has

been attributed to OmpX, such as surface adhesion (Otto and Hermansson 2004) and serum resistance (Lin, Huang, and Zhang 2002)(Lin, Huang and Zhang, 2002), but no mechanism have been described that can explain how the protein could carry out these possible functions.

The crystallographic structure of OmpX in E.coli revealed that the extra cellular loops 2 and 3 forms a four-stranded β-sheet that extends from the β-barrel (Vogt and Schulz 1999). The sheet is believed to be related to its biological function. It is not known if the β-sheet forms regularly *In vivo* where the loops would be in contact with the LPS layer. Regardless of its biological function, OmpX has been used extensively to study folding and structure of OMPs. As a model system, OmpX is ideal because of its relatively simple structure and low toxicity when expressed at high levels *E. coli*.

2. Aim and strategy

The mechanism of how OMPs fold both *in vitro* and *in vivo* remains to be completely understood. OMPs consists of an integral amphipathic ß-barrel, where each ß-strand is connected by a hydrophilic loop that extends into the aqueous environment. In bacterial cells, OMPs are folded into the OM by the BAM-complex (Wu et al. 2020). Smaller OMPs can also fold independently of the BAM-complex *in vitro*, given the presence of a suitable hydrophobic environment, such as detergent micelles or liposomes (Popot 2014).

The aim of this project was to better understand how the composition and length of the loops affects the folding of OMPs into detergent micelles *in vitro*, and into the OM *in vivo*. We believed that increasing the size and reducing the hydrophobicty of the loops would be detrimental for folding. This hypothesis was derived from observations of how OMPs fold into lipid bilayer *in vitro*. When OMPs fold into lipid bilayers the loops appear to pass through the hydrophobic interior of the bilayer (J. H. Kleinschmidt, Blaauwen, et al. 1999). We hypothesized that the mechanism of how the ß-strands and loops partitions themselves according to a ß-barrel *in vitro*, would be dependent on interactions between the hydrophilic loops and the hydrophobic interior of the detergent micelle. Understanding how the loops of OMPs affect folding is valuable because of their potential biotechnological applications for presenting heterologous protein to the bacterial surface (Lång 2000).

The small eight stranded OMP, OmpX, folding into SB12 detergent micelles was used a model system to study folding. To test our hypothesis we aimed to introduce a set of different inserts into loop 2 and 3 of OmpX, varied according to size and hydrophobicty. The effects by the loop inserts on folding would then be determined by measuring the folding kinetic of the OmpX constructs.

We were also curious to examine the effects on folding *in vivo*, as no published mechanism of how the BAM-complex folds OMPs involves the hydrophilic loops. If the loops affected folding *in vivo*, it could have implication for our understanding of the BAM-complex functions. To determine the if the inserts affected folding *in vivo*, the outer membrane was purified from *E. coli* expressing the constructs. Folding capacity *in vivo* could then be determined by the presence and integration of the constructs in the purified outer membrane fractions.

3. Materials and Methods

3.0.1 Bacterial strains - Preparation and growth conditions

The bacterial strain utilized for this project are listed in Table 3.1.

Table 3.1: Overview of bacterial strains and purpose of usage

Strain	Purpose	Resistance	Reference
TOP10	Cloning		Invitrogen
BL21-Gold (DE3)	Phage transduction	Tet	Studier and Moffatt 1986
BW25113Δ*ompX*	Phage transduction	Kan	Baba et al. 2006
Bl21-GOLD (DE3)Δ*ompX*	Protein expression	Tet/Kan	Invitrogen

Lysogeny broth (LB) (Bertani 1951) was used as media for growth in liquid culture. Cell count in liquid culture was measured by tracking optical density at 600nm (OD_{600}) with an Eppendorf BioPhotometer. Cultures with optical densities outside of the linear range (>0.8) were diluted appropriately for accurate measurement. LB agar was used for growth on plates and selection of pure colonies. See Appendix 2 for chemical components of LB and LB agar. Antibiotics were used as selective markers for growth of pure colonies. Table 3.2 gives the stock and working concentrations of antibiotics utilized in this project.

Table 3.2: Antibiotics used for growth of pure cultures

Antibiotic	Stock concentration	Working concentration	Company
Ampicillin	100 mg/ml	100 μg/ml	AppliChem
Kanamycin	100 mg/ml	50 μg/ml	AppliChem
Tetracycline	5 mg/ml	10 μg/mL	AppliChem

Bacterial strains were prepared for long tern storage by inoculating overnight culture (1 mL, 37 °C) in LB (50mL, 37 °C) with the appropriate antibiotic Table 3.1. The bacterial culture was grown at 37 °C with 200 rpm shaking, until the culture reached an OD_{600} of 0.5. 1200µL of the bacterial culture was then mixed with glycerol (600 µL, 60% (v/v), VWR) in a 1.8 mL cryotube (Nunc™) and preserved at -80 °C.

Transformation-competent cells were prepared with transformation and storage solution (TSS) (Chung, Niemela, and R. H. Miller 1989). Components of TSS are listed in Appendix 2. Overnight culture of the bacterial strain (1 mL, LB, 37 °C) was inoculated in LB with the appropriate antibiotic and grown until an OD_{600} of 0.5. The culture was then cooled down on ice and spun down with an Allegra X-30R Centrifuge (4000 rcf, 4

°C, 10 min). The cell pellet was suspended in 5 mL TSS (4 °C). 200 µL aliquots of TSS competent cells were extracted and stored at -80 °C.

3.0.2 Cloning and PCR

Plasmids

Plasmids utilized for this project are listed in Table 3.3. Sequence variants of pET3bOmpX and pETOmpX8f-3b generated for this project are listed in Table 3.6. Plasmids were preserved for long-term storage in ddH_2O at -20 °C.

Table 3.3: Plasmids used for expression of OmpX constructs

Name	Description	Reference
pET3bOmpX	Induced expression of OmpX without the signal peptide.	Pautsch et al. 1999
pETOmpX8f-3b	Expression of OmpX with the signal peptide	Arnold et al. 2007
pETOmpX88-3b	Induced expression of duplicated OmpX without the signal peptide	Arnold et al. 2007
pET-22b(+)	Empty vector control	Novagen

Primer design

All primers used for making sequence variants of pET3bOmpX and pETOmpX8f-3b are listed in Appendix 3 with optimal annealing temperatures and PCR buffer compositions. Primers were designed to amplify the plasmid along with additional 5'-end, non-annealing, overhangs that contained the insert sequences. Overhangs were included on the reverse and forward primers for the larger (>15 nucleotides) inserts. Primers were ordered from ThermoFisher and diluted in ddH2O to a concentration of 100 µM. Phosphorylated working stocks were prepared by incubating primers with T4 Polynucleotide Kinase (T4 PNK solution is in Appendix 2).

Polymerase chain reaction

The polymerase chain reaction was utilized for linearization and mutation of pET3bOmpX and pETOmpX8f-3b. Primers were phosphorylated before PCR. Table 3.4 shows the standard temperature cycling program. Table 3.5 shows the buffer composition for the standard PCR reaction. Phusion® HF DNA polymerase was used for the majority of the PCR reactions. Q5® High-Fidelity DNA polymerase was used for certain primer combinations when phusion did not work. The GC enhancer was only included with certain reactions. Annealing temperatures and specific buffer compositions are listed in Appendix 3 for the appropriate primer combinations. The PCR was carried out in

PCR strip tubes (Axygen®) in a BioRad c1000 Touch™ Thermal Cycler. The enzymes and buffer were from New England Biolabs.

Table 3.4: Thermocycling program.

Step		Time
Initiation	94	3 minutes
Denaturation	94	30 seconds
Annealing	Variable	15 seconds
Extension	72	3 minutes
Final extension	72	5 minutes
Cycles	30	

Table 3.5: Standard PCR master mix

Components	Volume
Buffer	10 μL
dNTPs	1 μL
Forward primer	2.5 (6 μM)
Reverse primer	2.5 (100 μM)
Template DNA	2 ($\sim$50 ng/μL)
(GC enhancer)	(10 μL)
ddH_2O	31.5 μL (21.5 μL)
Polymerase	0.5 μL
Total	50 μL

Reaction products (5 µL) were diluted in 6xDNA loading buffer and analyzed by agarose gel electrophoresis at 100 mV for 30 min. Separated DNA bands were visualized and imaged with a BioRad Gel DocTM XR+. Composition of buffers are given in Appendix 2.

Blunt-end ligation and transformation

The PCR produced mutated linearized plasmids according to the specific primer pair. The PCR product was made into functional plasmids with blunt-end ligation. PCR product was first incubated with 1 µL Dpn1 for one hour at 37 °C to remove methylated template DNA. Dpn1 was inactivated by heating the reaction at 80 °C for twenty minutes. Dpn1 digested PCR product (0.5 µL) was then incubated with 0.5 µL T4 DNA ligase in 9 µL of 1xT4 DNA buffer overnight (16 °C), to carry out the blunt-end ligation. Table 3.6 lists all generated sequence variants of pET3bOmpX and pETOmpX8f-3b. All of the used enzymes were bought from New England Biolabs.

Table 3.6: Generated sequence variants

Name	Mutation	Primer Pair
SPLATx1 L2	pS54G55insSPLAT	1 and 3
SPLATx2 L2	pS54G55insSPLATSPLAT	8 and 11
SPLATx4 L2	pS54G55insSPLATSPLATSPLATSPLAT	14 and 15
SPLATx1 L3	pP96T97insSPLAT	4 and 6
SPLATx2 L3	pP96T97insSPLATSPLAT	4 and 9
SPLATx4 L3	pY95P96insSPLATSPLATSPLATSPLAT	16 and 17
SPLATx4 L2+L3	pS54G55insSPLATSPLATSPLATSPLAT, pY95P96insSPLATSPLATSPLATSPLAT	14 and 15, 16 and 17
AGPGAx1 L2	pS54G55insAGPGA	2 and 3
AGPGAx2 L2	pS53G54insAGPGAAGPGA	10 and 7
AGPGAx4 L2	pS53G54insAGPGAAGPGAAGPGAAGPGA	18 and 19
AGPGAx1 L3	pP96T97insAGPGA	5 and 6
AGPGAx2 L3	pT97Y98insAGPGAAGPGA	12 and 13
AGPGAx4 L3	pT97Y98insAGPGAAGPGAAGPGAAGPGA	20 and 21
AGPGAx4 L2+L3	pS53G54insAGPGAAGPGAAGPGAAGPGA pT97Y98insAGPGAAGPGAAGPGAAGPGA	18 and 19 20 and 21
$\Delta 94 \rightarrow 98$	p94E_Y98del	22 and 23
ΔY87 $\rightarrow$ T93, ΔK99 $\rightarrow$ G106	pY87_T93del, pK99_G106del	24 and 25

Ligated plasmids were transformed into TSS competent TOP10 cells. Blunt-end ligation reaction product (5 µL) was added to 50 µL of competent cells (4 °C) and left to rest for 30 minutes on ice before a heat shock at 42 °C for 45 seconds in a water bath. Heat shocked cells were left to recover for two minutes on ice. Transformed cells were then plated out on LB agar plates with ampicillin and left at 37 °C over night for colony growth. Single colonies were picked and transferred to 5 mL of LB with ampicillin and left to grow overnight (37 °C, 200 rpm).

Plasmids were purified from the bacterial culture using the QIAprep® Spin MiniPrep kit according to manufacturer's protocol, and eluted with 50 µL of ddH_2O. The quality of the purified plasmids was estimated with a NanoDrop (Saween Werner) spectrophotometer. The plasmids were sequenced for verification with LightRun™ (Eurofins Genomics) Sanger sequencing (Sanger and Coulson 1975). Primer 26 and 27 were used for sequencing (Appendix 3). DNA modifications in the sequencing data were detected by doing a pairwise sequence alignment with pET3bOmpX. The sequence alignment was

done with EMBOSS Needle (Madeira et al. 2019).

3.0.3 SDS-PAGE

Sodium dodecyl sulfate (SDS) poly acrylamide gel electrophoresis (PAGE) was used for analysis of whole cell lysates, *in vitro* folding assays and OM preps. The composition of relevant buffers are listed in Appendix 2. Novex™ WedgeWell™ 4-20% Tris-Glycine pre-cast gels were used for all the experiments. A VWR 250 V power source and a xCell SureLock™ Electrophoresis Cell was used for the electrophoresis. Gels were run for 55 minutes at 225V. The electrophoresis cell was kept on ice for the duration of the electrophoresis.

For visualization of protein bands, the gels were incubated with coomassie Brilliant Blue R250 (SIGMA) overnight. The gels were then destained for an appropriate amount of time ($\sim$3 hours) to remove background stain. The gels were incubated in distilled water ($\sim$20 minutes) to enlarge them before they were imaged. Relevant buffer compositions are given in Appendix 2. Stained gels were imaged with a Molecular Imager Gel Doc™ XR+ on a white light conversion screen (BioRad). The brightness and contrast of the imaged gels were adjusted with the Image Lab™ software to visualize the separated bands. The gamma was set to 1.4 and the lower range of the frequency distribution histogram was omitted to remove background noise.

3.0.4 Phage Transduction

A kanamycin resistance cassette was transferred from "BW25113Δ*ompX* " in the Keio collection (Baba et al. 2006) to BL21-Gold (DE3) by P1 phage transduction (Lennox 1955). BW25113Δ*ompX* has the gene *ompX* swapped out for a kanamycin resistance cassette. Transduction of the kanamycin resistance then cause deletion of the gene *ompX*. Centrifugation steps was carried out with a VWR MICRO STAR 17R centrifuge.

The donor phage lysate was prepared by inoculating BW25113Δ*ompX* in LB (10 mM CaC_2, Merck). The culture was left to grow (37 °C, 200 rpm) until an OD_{600} of 0.5 was reached. Five aliquots (100 µL) were taken from the culture and added to an equal volume of five dilutions (100 to 10-4) of P1 phage lysate respectively. The samples were incubated at 37 °C for twenty minutes without shaking. Samples were then diluted into 0.8% liquid top agar (1 mM CaC_2, 45 °C) and poured out onto LB agar plates. The plates were left to incubate over night (37 °C). The top agar was scraped off a selected semi-confluent plate and mixed vigorously with 2 mL LB and 50 µL chloroform (Sigma-Aldrich) before being spun down (5000 rcf, 4 °C, 10 min). The resulting supernatant (BW25113Δ*ompX* phage lysate) was taken out and 50 µL chloroform was added. The Δ*ompX* BW25113 phage lysate was stored at 4 °C.

An overnight culture of the acceptor strain (BL21-Gold (DE3)) was inoculated in LB (10mm $CaCl_2$) and grown (37 °C, 200rpm) until an OD600 of 1 was reached. Four aliquots (1 mL) were taken out and incubated with four dilutions of the BW25113Δ*ompX* phage lysate: 10-4, 10-6, 10-8 and 10-10 respectively. The samples were then left to incubate for twenty minutes before the infection was stopped by the addition of 100 µL sodium citrate (100 mM, Merck). The samples were then vortexed and spun down (5000 rcf, 10 min). The pellet was washed by suspending the pellet in LB (100mM

sodium citrate) and centrifuged (5000 rcf, 10 min). The pellet was once more resuspended in fresh LB (10mM sodium citrate) and incubated for 1 hour (37 °C, 200 rpm). After the incubation the cells were centrifuged (5000 rcf, 10 min) and resuspended in 100µL LB before they were plated out on LB agar plates (50µg/µL kanamycin, 10 mM sodium citrate) and incubated overnight (37 °C).

For verification of successful transfer of the kanamycin resistance casette into BL21-GOLD (DE3), healthy colonies were tested for growth in selective liquid media. Cultures that could grow in tetracycline and kanamycin were deemed successful. Additionally, the deletion of *ompx* was tested for by western blotting of whole cell lysates of transfected colonies.

3.0.5 Western Blotting

Western blotting was used to verify the deletion of ompX in *E. coli* BL21-Gold (DE3)Δ*ompX*. The composition of the relevant buffers for the electrophoretic blotting are listed in Appendix 2. Whole cell lysates of bacterial cultures were first separated by SDS-PAGE electrophoresis as described above (section 3.0.3). Filter paper and a 0.45 µm PVDF membrane were cut to the same size as the gel (~ 100 cm^2), and the membrane was soaked in ethanol for 5 minutes to activate it. All the layers of the electrophoretic blotting sandwich were pre-incubated in the transfer buffer for 5 minutes. The PVDF membrane was placed beneath the poly-acrylamide gel during the semi-dry transfer. Three layers of filter paper were placed below the gel, and three were also placed above the membrane. Air bubbles were carefully removed from the blotting sandwich by light rolling with a glass syringe. Transfer from the poly-acrylamide gel to the PVDF membrane was done with a TE70X semi-dry transfer unit and a VWR 250 V power source at 360 mA for 45 minutes with a maximum voltage of 30 V. The membrane was then used for immunological detection of OmpX. The poly-acrylamide gel was stained with Coomassie R after the transfer for comparison (Appendix 4).

The PVDF membrane blotted with protein from whole cell lysates (section nn) was blocked for 60 minutes at room temperature in 10mL TBS-T (2% BSA). An anti-OmpX antibody was used as the primary antibody (Arnold et al. 2007). Goat anti-rabbit IgG-HRP was used as the secondary antibody (Santa Cruz Biotechnology). Anti-OmpX antibodies were added (1/2500) and left to incubate for 60 minutes at room temperature. The blot was washed three times with 10 mL TBS-T and then incubated with the HRP-conjugate anti-rabbit secondary antibody (1/2500) in 10 mL TBS-T (2% BSA) for 60 minutes at room temperature. Finally, the blot was washed three times with 10 mL TBS-T and once with 10 mL TBS. The membrane was then incubated in 10 mL of working detection reagent (ECL western blotting substrate) for 2 minutes according to the manufacturers protocol. The blot was imaged with an Image Station 4000R Pro (Kodak) and analyzed with the Carestream molecular imaging software. Relevant buffer compositions are listed in Appendix 2.

3.1 Protein expression and purification

3.1.1 Protein overexpression

BL21-GOLD (DE3)Δ*ompX* was used for protein production. The strain was made TSS competent and transformed with the appropriate plasmid. Purified plasmid was added to 50µL of competent cells (4 °C) and incubated for 30 minutes on ice before heat shock at 42 °C in a water bath for 45 seconds. Heat shocked cells were left to recover for two minutes on ice. Transformed cells were then plated out on LB agar plates with ampicillin and left at 37 °C over night for colony growth. Overnight cultures were prepared with freshly transformed colonies. All constructs (with and without the signal peptide) were expressed from the pET3b plasmid.

Constructs without the signal peptide were expressed as inclusion bodies. 500 mL LB was inoculated with 5 mL of overnight culture and grown at room temperature to an optical density between 0.8 – 1.0. Protein production was induced with IPTG (1 mM, VWR chemical), and incubated overnight (37 °C, 200 rpm). The culture was then spun down and the inclusion bodies were harvested and washed (section 3.1.3).

The pET3b plasmid exhibited a high degree of leaky expression and IPTG induction seemed to hamper integration into the OM. Constructs with the signal peptide were therefore expressed by autoinduction in LB. Transformed colonies were inoculated in 50 mL LB and incubated overnight at room temperature. Cells were then harvested for outer membrane purification after a minimal OD_{600} of 0.8 had been reached (section 3.1.2).

3.1.2 Outer membrane preperations

Cultures corresponding to a 40 mL bacterial culture with an OD_{600} of 1.0 was centrifuged (4000 rcf, 10 minutes) and resuspended in 1.5 mL HEPES buffer (pH 7.4, 10 mM $MgCl_2$, 4 °C) with DNase (0.1 mg/mL, Sigma-Aldrich) and lysozyme (0.1 mg/mL, AppliChem). The cells were incubated for 15 minutes on ice and then transferred to a 2 mL Micro tube (SARSTEDT AG & Co) with 250 µL Zirconia/Silica Beads (0.1mm dia, BioSpec Products). Cells were then lysed with a FastPrep™ FP120 cell disruptor. The cells were shaken three times for 40 seconds at 6.5 m/s. Cells were cooled for two minutes on ice between runs. Intact bacteria and cell debris were pelleted by a brief centrifugation step (12,000 rcf, 1 minute). The resulting supernatant was centrifuged (16,000 rcf, 30 minutes) to pellet whole membranes. The IM fraction of the membrane pellet was dissolved by resuspending the membranes in 200 µL HEPES (pH 7.4) and then adding 200 µL of 2% N-lauryl Sarcosine (Sigma-Aldrich). The membrane pellet was incubated for 30 minutes on a VWR Tube Rotator in the detergent-rich buffer at room temperature. The non-dissolved OM was pelleted by centrifugation (16,000 rcf, 30 minutes). The OM pellet was washed twice with 500 µL HEPES buffer (pH 7.4) without resuspending the pellet, and then re-centrifuged as above. After washing, the pellet was resuspended in 60 µL HEPES buffer (pH 7.4). 30 µL of the suspension was incubated in 500µL of 6M urea (100mM glycine, 80 mM HEPES, pH 7.4) for 30 minutes on a VWR Tube Rotator to remove protein only peripherally attached, rather than integrated into the OM. Urea washed membrane fractions were then centrifuged (16,000

rcf, 30 minutes) and resuspended in 30 µL HEPES (pH 7.4. The OM preparations were diluted with 10 µL 4x SDS buffer and then analyzed by SDS-PAGE electrophoresis (section 3.0.3). Centrifugation steps were carried out with a Microstar 17R (VWR) at 4 °C.

3.1.3 Inclusion body purification and protein solubilization

Cells from overnight bacterial cultures expressing inclusion bodies (500 ml) were spun down with an Avanti J-265 XP centrifuge (4000 rcf, 30 minutes). The cell pellet was resuspended in 1x PBS with DNAse (0.1 mg/ml) and lysozyme (0.1 mg/ml) and incubated on ice for 15 minutes. The cells were then lysed by three passages through a French® Pressure Cell Press at 10000 psi. Inclusion bodies were separated from the lysate by centrifugation (4000 rcf, 10 minutes) with an Allegra X-30R centrifuge. The inclusion bodies were washed once with 20 mL detergent rich 1x PBS buffer (1% Triton X-100, VWR) and three times with 20 mL 1x PBS buffer. Washed inclusion bodies were resuspended in 1x PBS and stored at -80 °C.

For solubilization of protein, the inclusion bodies were incubated in urea buffer (8M, pH8, 40mM Tris) at room temperature until they turned transparent. Insoluble debris was removed by centrifugation (12,000 rcf, 10 minutes) and the unfolded protein in the supernatant could then be purified for crystallization by anion exchange chromatography or used directly for the folding assays (section 3.2) . The protein concentration was estimated by measuring absorbance at 280 nm with a BioPhotometer (Eppendorf). The extinction coefficient was determined with the ProtParam software (Gasteiger et al. 2005) to be 34840 $M^{-1}cm^{-1}$.

3.1.4 Anion exchange chromatography

OmpX88 solubilized from inclusion bodies with urea buffer was purified for 2D crystallization using anion exchange chromatography. The NGC™ Chromatography System and a HiTrap™ Q HP column (GE Healthcare) were used for this. The compositions of relevant buffers are listed in Appendix 2. All buffers were degassed before being used for chromatography.

The column was equilibrated in 5 column volumes (CV) of urea buffer. The urea concentration in the urea-solubilized OmpX88 solution was adjusted to 6M and filtered through a 0.22 µM filter (Sarstedt) before being loaded onto the column using a Superloop (GE healthcare). The column was washed with urea buffer (3 CV). The protein was eluted using a salt gradient over 10 CV (0-1M NaCl). Urea-solubilized OmpX88 routinely eluted when the salt concentration reached approximately 100 mM NaCl. Elution of protein was monitored by measuring absorption at 280 nm. Eluted fractions were analyzed with SDS-PAGE and protein was concentrated by centrifugal concentrator with a 10,000 Da molecular weight cut-off (Vivaspin 20, Sartorius).

3.2 *In vitro* folding of OmpX

3.2.1 Folding assay

The protein was folded *in vitro* by diluting the urea-solubilized protein in refolding buffer (1% SB12). For the *in vitro* folding assays, the protein concentration was first adjusted to 1.9 mg/ml. The protein was then diluted 1:20 into refolding buffer and incubated at 15 °C on a PCMT Thermo-Shaker (1000 rpm). Samples were taken at specific time points and quenched in an equal volume of ice cold 4x SDS buffer. The heat modifiability of samples was analyzed using SDS-PAGE. Relevant buffers are listed in Appendix 2.

3.2.2 Gel densitometry

Images of the folding assay were converted to 8-bit grey scale with the Image Lab™ software. Gel densitometry was done with ImageJ (Schindelin et al. 2012) by measuring the integrated density of the separated bands using the "analyze gel" command. Background noise was removed with the "subtract background" command with a rolling ball radius of 50 pixels. The fraction of folded protein at each time point was calculated according to equation 3.1.

$$\text{Fraction of folded protein} = \frac{\text{Folded protein}}{\text{Folded protein + Unfolded protein}} \tag{3.1}$$

Fraction of folded protein at time = 0 was assumed to be 0. Nonlinear least squares regression was used to fit the equations listed in the introduction to the collected data with R. Equation 1.2 produced the best fit to the data

3.3 2D crystallization of OmpX88

3.3.1 Detergent exchange

OmpX88 was purified by anion exchange (section 3.1.4) and refolded *in vitro* into SB12 detergent micelles (section 3.0.3). The protein was then reconstituted into 1.85% n-Octyl ß-D-glucopyranoside (OG, Glycon) for 2D crystallization. The detergent exchange was done using the NGC™ Chromatography System and a HiTrap™ Q HP column (GE Healthcare). The column was equilibrated in the refolding buffer (3 CV). OmpX88 folded in SB12 was loaded on the column with a Superloop (GE healtcare). The detergent was exchanged with a gradient (3 CV) to 100% OG (1.85%). The column was then washed (3 CV) with OG (1.85%). Protein reconstituted into OG was eluted with a salt gradient as described before (gradient over 10 CV, 0-1M NaCl, section 3.1.4).

3.3.2 Detergent dialysis

Crystallization was tested with two types of lipid; *E. coli* polar lipid extract and 1,2-dimyristoyl-sn-glycero-3-phophocholine (DMPC). Lipids were first dissolved in chloroform (Sigma-Aldrich) and methanol (Sigma-Aldrich) (1:1) in a round bottom flask. A Buchi R-210 rotovapor was used to remove liquid and to deposit a dry lipid film. The lipid film was then dissolved in 1.85% OG to a lipid concentration of 5 mg/mL. The following lipid/detergent micelles were incubated with the protein/detergent micelles for 60 minutes at room temperature at various lipid/detergent ratios prior to dialysis. The dialysis was carried out according to published screening recommendations (C. Kim et al. 2010; Nannenga et al. 2013). Detergent dialysis was carried out for different crystallization conditions using a home-built dialysis block adapted from C. Kim et al. 2010 (Appendix 4). A dialysis membrane with a molecular weight cut-off of 25,000 Da (ZelluTrans) was used for detergent removal. Buffers were exchanged daily for two weeks to ensure complete detergent removal.

3.3.3 Negative stain and electron microscopy

After dialysis, the samples were negatively stained with 1% (w/v) uranyl acetate (Electron Microscopy Sciences). Carbon coated grids (300 mesh, Cu, Electron Microscopy Sciences) were glow discharged in air (200 mmHg) for 45 seconds at 350 V. 2 µL of sample were applied to the carbon coated side of the grid and incubated for 20 seconds. Excess sample was then removed by holding the edge of the grid to a filter paper. The grid was then washed once by incubating the face of the grid in 50 µL ddH_2O. Excess liquid was removed with filter paper and the face of the grid was then placed on a 20 µL drop of uranyl acetate (1%) and immediately dried with filter paper and washed with ddH_2O as before. The grid was incubated for an additional 20s on a 20µL drop of uranyl acetate (1%), dried and washed with ddH_2O, and dried in air until the sample was ready for the microscope. The stained samples were examined with a JEOL 1400plus TEM: 120 kV transmission

4. Results and discussion

4.1 Design of loop inserts

In this work the contribution of the extracellular loops on folding of OMPs were explored by introducing peptides of various lengths into loop 2 and loop 3 of OmpX from *Escherichia coli*. Two types peptides were tested in this study. The amino acid sequence of the two inserts where SPLAT and AGPGA. The inserts were used individually, or repeated twice and four times in loop 2 and loop 3. The inserts repeated twice are called SPLATx2 and AGPGAx2. The inserts repeated four times are called SPLATx4 and AGPGAx4. Additional constructs were made with SPLATx4 and AGPGAx4 introduced to both loop 2 and 3 at the same time. The location of the inserts are given by either "L2" or "L3", which designates loop 2 and loop 3 respectively. Table 4.1 lists the tested inserts and provides some relevant physiochemical properties.

Table 4.1: Physiochemichal properties of the loops inserts. Hydrophobicity was calculated according to the Wimley-White hydrophobicity scale. The calculations illustrate the differences in hydrophobicity between the inserts, and they do not take into account C- and N-terminal groups. The SPLAT insert partitions into hydrophobic environments more favorably than the AGPGA insert.

Insert	Molecular weight	pI	Hydrophobicity (Wimley-White)
SPLAT	469.54	5.24	+0.1 Kcal * mol^{-1}
SPLATx2	939.08	5.24	+0.2 Kcal * mol^{-1}
SPLATx4	1878.16	5.24	+0.4 Kcal * mol^{-1}
AGPGA	353.38	5.57	+3.44 Kcal * mol^{-1}
AGPGAx2	706.76	5.57	+6.88 Kcal * mol^{-1}
AGPGAx4	1413.52	5.57	+13.76 Kcal * mol^{-1}

Both the SPLAT inserts and the AGPGA inserts contains proline. Proline applies rigid constraints on the backbone due to its ring structure that prevents rotation around the Cα-N bond. Proline is frequently found in protein turns as its regular conformation is beneficial for loop formation (Klose et al. 1988). The isoelectric points of the inserts were relatively similar. The SPLAT insert had a ~30% higher molecular weight compared to the AGPGA insert. The main difference between the inserts are related to the change in hydrophobicity as the peptides are repeated. The hydrophobicity was calculated according to the Wimley-White hydrophobicity scale (William C. Wimley and White 1996). The hydrophobicity values are the associated change in free energy as the peptide transitions from an aqueous environment to a hydrophobic environment. Large positive changes in the associated free energy make these transitions more unfavorable.

The SPLAT insert contains a balance of hydrophobic and hydrophilic residues. Leucine residues in particular partitions into hydrophobic phases favorably according to the scale. Consequentially, when the SPLAT insert is repeated, there is a relatively small change hydrophobicity. The AGPGA insert, in contrast, does not partition favorably into hydrophobic environments. Partitioning of glycine is especially energetically unfavorable. Therefore, when the AGPGA insert is repeated the overall hydrophobicity of the insert decreases.

4.2 Creation of an *ompX* knockout strain by P1 phage transduction

In this work a variety of OmpX constructs were expressed *in vivo* in BL21-Gold (DE3). BL21-Gold (DE3) is a bacterial strain of *E. coli* developed for protein expression (Studier and Moffatt 1986). However, native OmpX can be expressed at relatively high concentrations which would could mask expression of the OmpX construct(Molloy et al. 2000). A knockout of *ompx* in BL21-Gold (DE3) was created to avoid the background of native OmpX. This knockout strain was created by P1 phage transduction. Removing background of other OMPs is not a problem since OmpX has much lower molecular weight compared to the most common OMPs in *E. coli*. Deleting an excessive amount of OMPs cause structural disturbances to the OM rendering the cell vulnerable to lysis. Overexpression of OmpX also cause decreased expression of other OMPs (Stoorvogel, Bussel, and Klundert 1991).

BW25113Δ*ompx* from the Keio collection (Baba et al. 2006) was used as the donor strain for the transduction. A pET vector that contained *ompX* (pETOmpX8f-3b) was used to induce expression of OmpX in the knockout strain. The knockout was confirmed by western blotting of whole-cell lysates collected from transformed and untransformed cells before induction, 3 hours after induction and after an over-night incubation. The primary antibody (anti-OmpX) is derived from rabbit serum and can only bind unfolded OmpX (Arnold et al. 2007). A HRP linked anti-rabbit antibody was used as the secondary antibody. Figure 4.1 shows the result of the western blotting.

OmpX in urea and SB-12 detergent micelles was used as controls of the unfolded and folded protein respectively. No protein was detected in the *in vitro* folded sample, confirming that the antibody cannot bind folded protein. A single band is visible in BL21-Gold (DE3), corresponding to the molecular weight of OmpX. In the untransformed knockout strain no band is detectable at any time point which confirms the knockout. The transformed knockout strain has a two bands appearing at all timepoints at molecular weight similar to OmpX. The second band that appears is likely non-processed pre-protein with the signal peptide (+2.2 kDa). The presence of OmpX in the uninduced sample indicates a high degree of leaky expression from the pET3b vector. Transformed samples also has an extra band at approx. 35 kDa, and uninduced samples shows an extra band below 70kDa. It is not known what these bands correspond to. It is possible that the 35kDa bands is caused by dimerization/ aggregation of OmpX (Winther 2015). Due to time constraints, the knockout could not be confirmed by DNA sequencing.

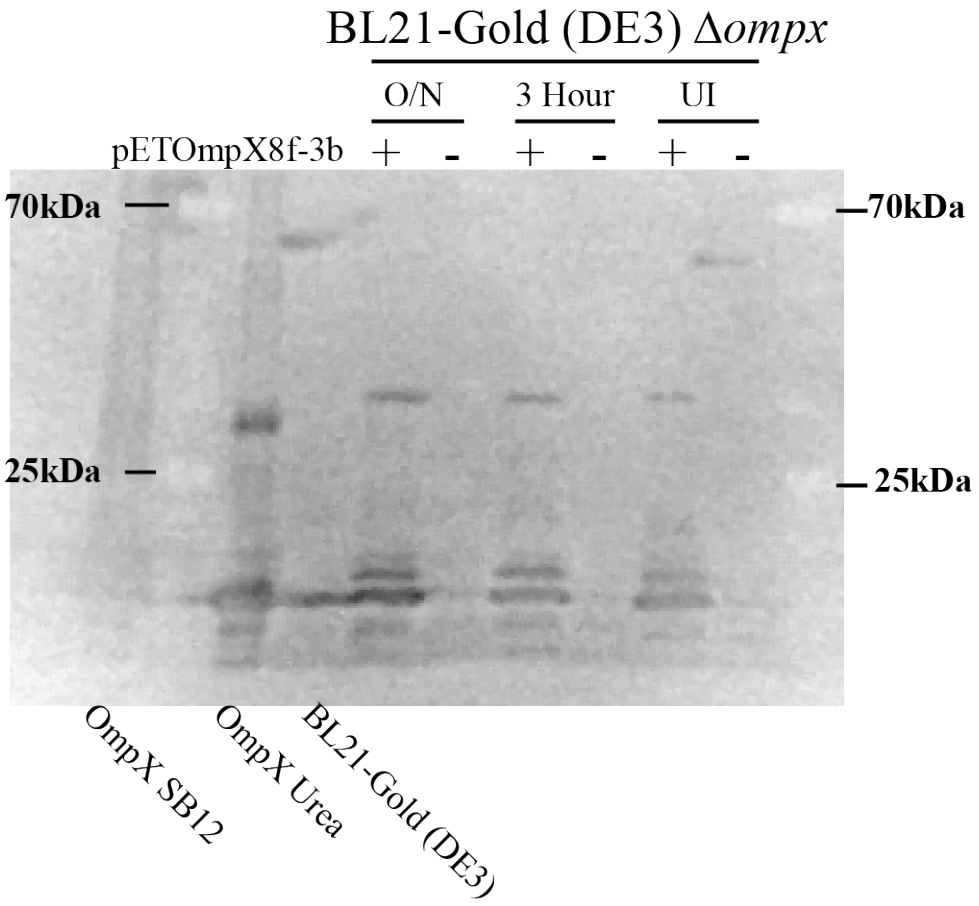

Figure 4.1: Western blotting of OmpX from whole cell lysates, denatured inclusion bodies and SB12 detergent micelles. anti-OmpX was used for immunological detection of OmpX. The antibody can only bind unfolded OmpX. BL21-Gold (DE3)Δ*ompX* was transformed with pETOmpX8f-3b and induced with 1mM IPTG. Whole cell lysates were sampled 3 hours after induction and after an over-night (O/N) incubation. BL21-Gold (DE3), OmpX in urea, OmpX folded in SB12 and an uninduced (UI) sample was used as controls. OmpX was not detected in the untransformed knock-out strain which confirms the knockout of *ompx*.

4.3 *In vitro* folding assays

Insertions to the extracellular loops of OmpX modulate folding kinetics

We wanted to understand how the extra-cellular loops of OMPs affect folding. Inserts with different physiochemical characteristics (table 4.2) were systematically introduced to the loops of OmpX. OmpX carrying the different inserts were then folded into SB-12 detergent micelles at 15°C to determine if the inserts caused variations in the folding kinetics. The effects of loop hydrophobicity and size were explored in this study.

The kinetics of the OmpX constructs were determined by SDS-PAGE and gel densitometry. Folding of OMPs can be determined by SDS-page because of their characteristic heat-shift (section 1.5). Upon folding the apparent molecular weight of OMPs change (Noinaj, Kuszak, and Buchanan 2015). Electrophoretic separation of OMPs then results in two distinctive bands, were one band is the folded protein and the other band is the unfolded protein. The amount of folded protein in a sample can then be determined by gel densitometry (P. Rath, Sharpe, Kohl, et al. 2019). The densitometry data of the folding kinetics were fit to equation 1.2 by nonlinear least square regression in R. This model has two parameters. A_f is the parameter for the final folding yield, and k is the parameter for the folding rate. Figure 4.2 shows two replicates of the WT (wild type) OmpX folding kinetic. The two replicates are made from the same batch of inclusion bodies. A single observation was made at each time point in the folding kinetic of the constructs.

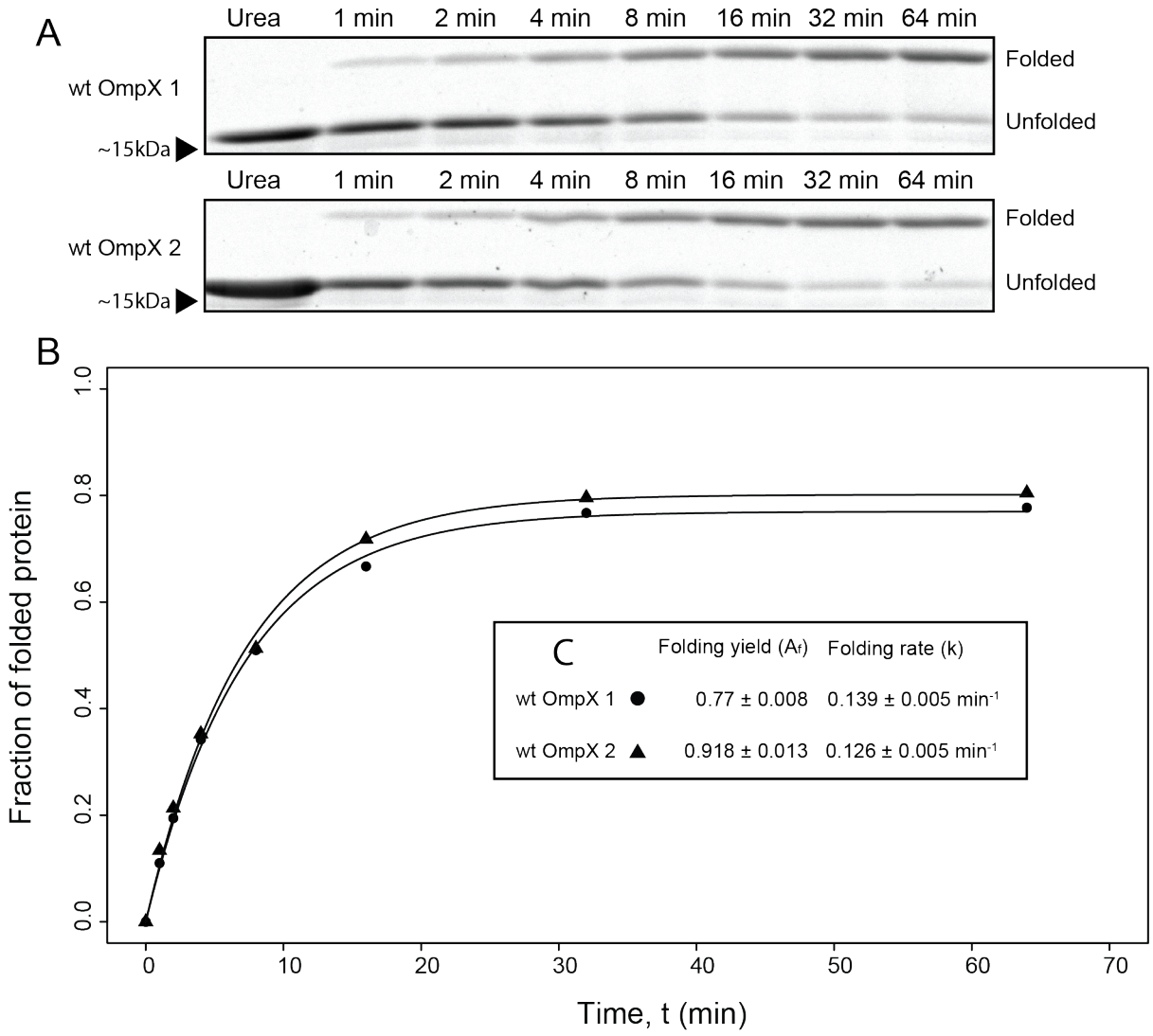

Figure 4.2: (A) SDS-PAGE showing the time course of OmpX folding into SB12 detergent micelles. Folding was performed at 15°C. Two replicates of WT OmpX was collected (B) Fraction of folded protein as a function time determined by densitometry. Equation 1.2 was fitted to the data (solid lines). (C) Parameters estimations of the models fitted to the densitometry data.

WT OmpX 1 had a yield of 77% and a rate of 0.14 min^{-1} and was selected for comparison to the remaining constructs. The estimated folding rate for OmpX folding into SB12 detergent micelles at 15°C is about four times as slow as the reported rate for folding into PC10:0 lipid bilayers (0.59 min-1) at 25°C (P. Rath, Sharpe, Kohl, et al. 2019). Observing the folding kinetic at slow rates is beneficial as it becomes easier to detect possible variations between constructs. As only 77% folded after 64 minutes, it shows that a portion of the protein cannot fold. Equation 1.1 does not take into account protein that cannot fold and was therefore inappropriate for modeling the folding kinetic. The likely explanation for the portion of protein that remains unfolded is aggregation. If 20% of the protein becomes aggregated after dilution in the folding buffer then the amount of protein that would be observed as folded at each time point will be reduced by 20%. It is also possible that some protein becomes trapped in an intermediate conformation in the folding pathway, as has been observed when OmpA was folded into lipid bilayers (Jörg H. Kleinschmidt 2015). Equation 1.3 was also fitted to the data, but was discarded in favor of equation 1.2, as the extra parameters in this equation did not provide a statistically significant improvement in the residuals. The equations are described in section 1.2.5 in the introduction.

There was an approx. 4% difference in the estimated parameters for the yield and rate between WT OmpX 1 and WT OmpX 2 (figure 4.2). The largest source of error in the estimation is likely tied to the collection of the densitometry data. As the integrated density of the folded band becomes smaller, it becomes more difficult to separate the signal from the noise. This is visible in figure 4.2, where the differences in the data becomes more larger, later in the kinetic. Ideally, three replicates should be done for each observed time point to average out the variation. A complete set of replicates could not be completed due to time constraints. As the protein was solubilized from inclusion bodies directly, and not purified by anion exchange, some unrelated protein appears in the gels. These unrelated proteins would could cause variations in the estimated protein concentration between the samples. Uncropped gels of the *in vitro* folding assays are listed in Appendix 4.

Figure 4.3 and 4.4 shows the folding kinetic of the AGPGA inserts in loop 2 and loop 3 respectively. All of these constructs folded *in vitro*. Most of the constructs showed improved folding yield and folding rate compared to WT OmpX. AGPGA insertions into loop 2 provided a moderate improvement in both folding yields and rates compared to WT OmpX. While a single AGPGA insert in loop 3 increased the yield, further repeats negatively affected the folding yield, where AGPGA x1 L3 had 91% folding yield while AGPGA x4 L3 only had a 44% folding yield. Interestingly, while the yield was reduced, the folding rate of AGPGAx4 L3 remain unchanged compared to the WT OmpX. AGPGA x1 L3 had the highest folding rate of all the insertions at 0.28 min^{-1}, which is double to the rate of WT OmpX. AGPGA x2 shows some abnormalities. AGPGA x2, folds at a relatively higher rate when inserted in loop 2 (0.22 min^{-1}) and slowly in loop 3 (0.1 min^{-1}). While both loops are sensitive to insertions, it seems that increasing the length of loop 2 actually improves the overall folding efficiencies within loop 2. In contrast, while a single AGPGA insertion in loop 3 improves the situation, duplication of this insert is deleterious to both estimated folding yields and rates.

The same set of insertions were completed with the SPLAT insert. Figures 4.5 and 4.6 shows the folding kinetics of SPLAT inserts in loop 2 and loop 3 respectively. The SPLAT inserts all showed improved folding yields compared to the WT OmpX when

inserted into either loop 2 or loop 3. This indicates that loop hydrophobicity plays some role in the folding. Even an 80 residue insertion (SPLATx16 L2) was able to fold, even though the rate was considerably slower as the maximum yield was not reached even after 64 minutes. While the folding rates were similar to WT OmpX in the singular SPLAT insert constructs, the rate decrease with repeat inserts.

Figure 4.7 shows the folding kinetics of the double insertions (loop 2 and loop 3 simultaneously). AGPGA x4 L2+L3 did show heat-modifiability and a folding kinetic could therefore not be captured. SPLAT x4 L2+L3 could fold and even had a higher yield compared to the wt, but folded at a much slower rate (0.035 min^{-1}). It is possible that AGPGAx4 L2+L3 still folds, but that the inserts has rendered the construct less resistant to SDS. A semi-native SDS-PAGE or circular dichroism can be done to test if the construct can fold (Noinaj, Kuszak, and Buchanan 2015).

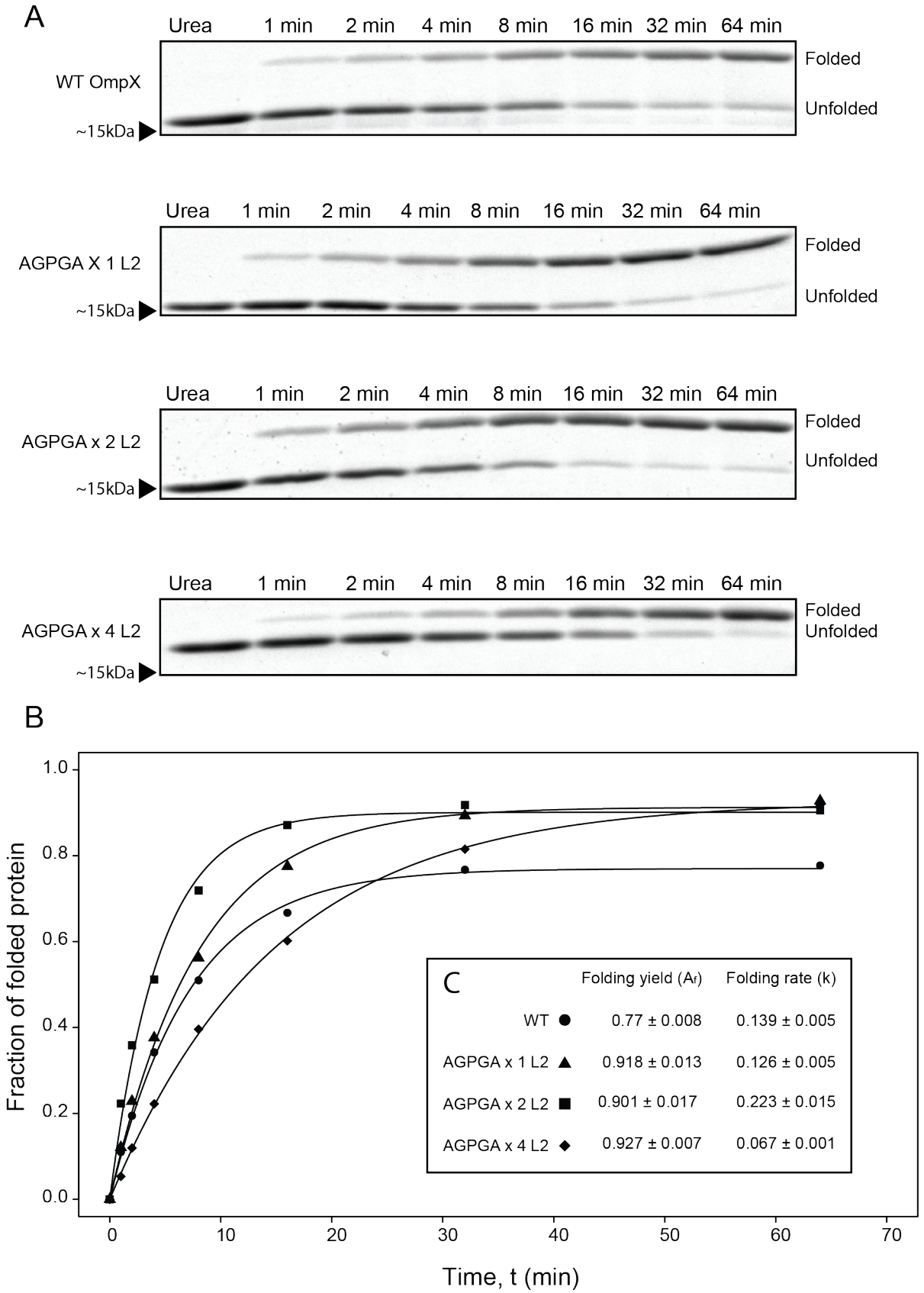

Figure 4.3: (A) SDS-PAGE showing the time course of OmpX constructs with AGPGA inserts in loop 2. (B) Fraction of folded protein as a function time determined by densitometry. Equation 1.2 was fitted to the data (solid lines). (C) Parameters estimations of the models fitted to the densitometry data.

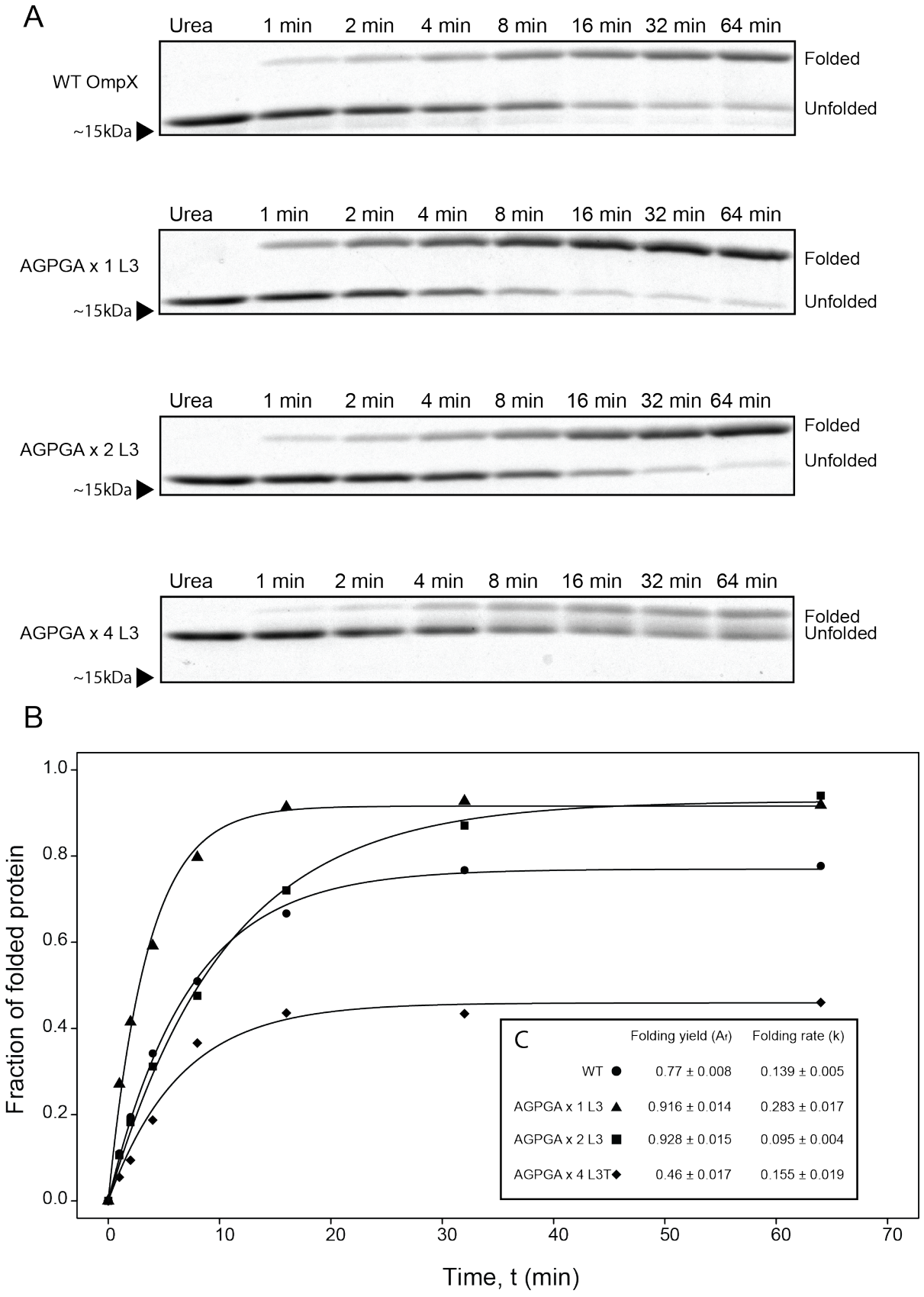

Figure 4.4: (A) SDS-PAGE showing the time course of OmpX constructs with AGPGA inserts in loop 3. (B) Fraction of folded protein as a function time determined by densitometry. Equation 1.2 was fitted to the data (solid lines). (C) Parameters estimations of the models fitted to the densitometry data.

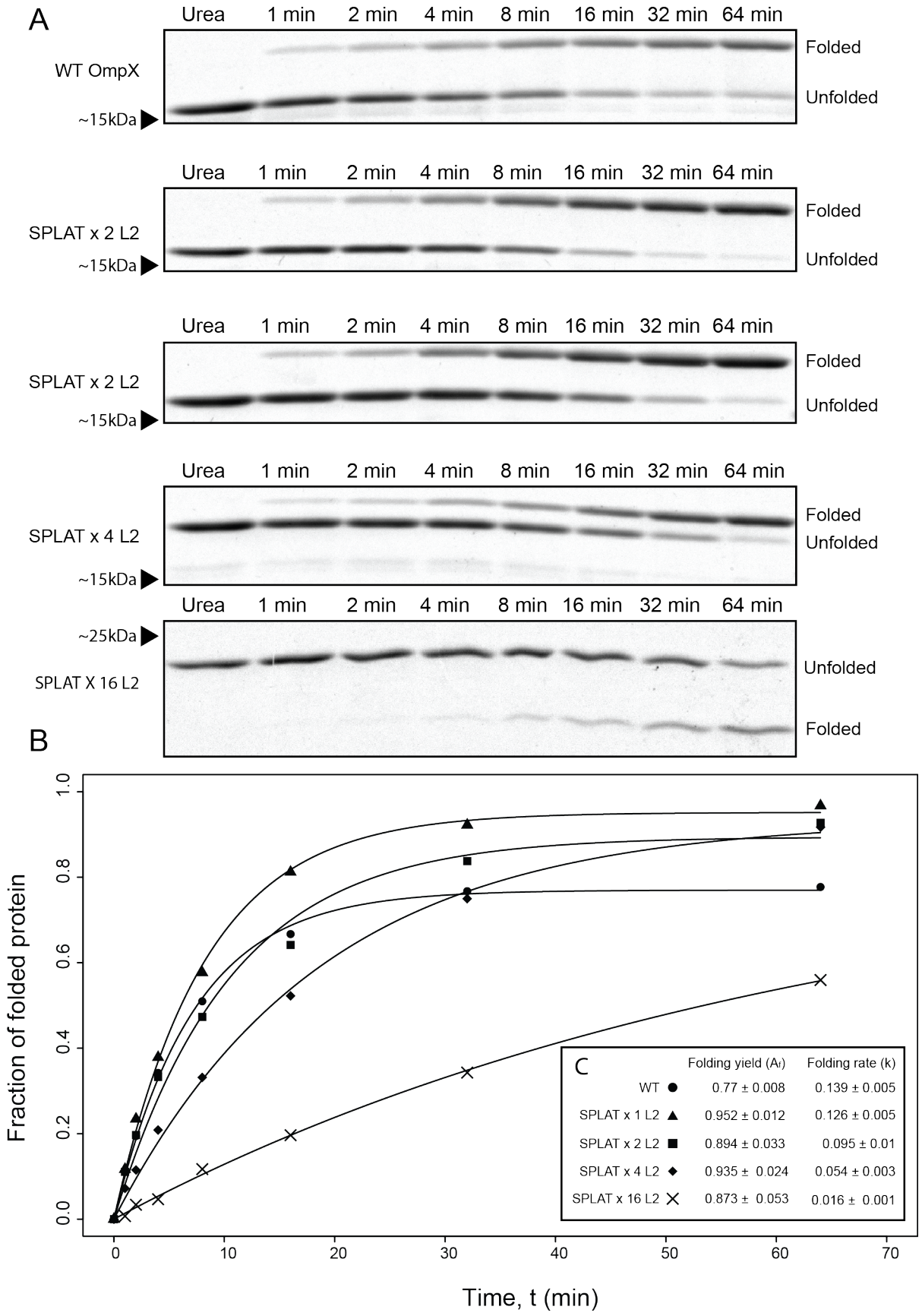

Figure 4.5: (A) SDS-PAGE showing the time course of OmpX constructs with SPLAT inserts in loop 2. (B) Fraction of folded protein as a function time determined by densitometry. Equation 1.2 was fitted to the data (solid lines). (C) Parameters estimations of the models fitted to the densitometry data.

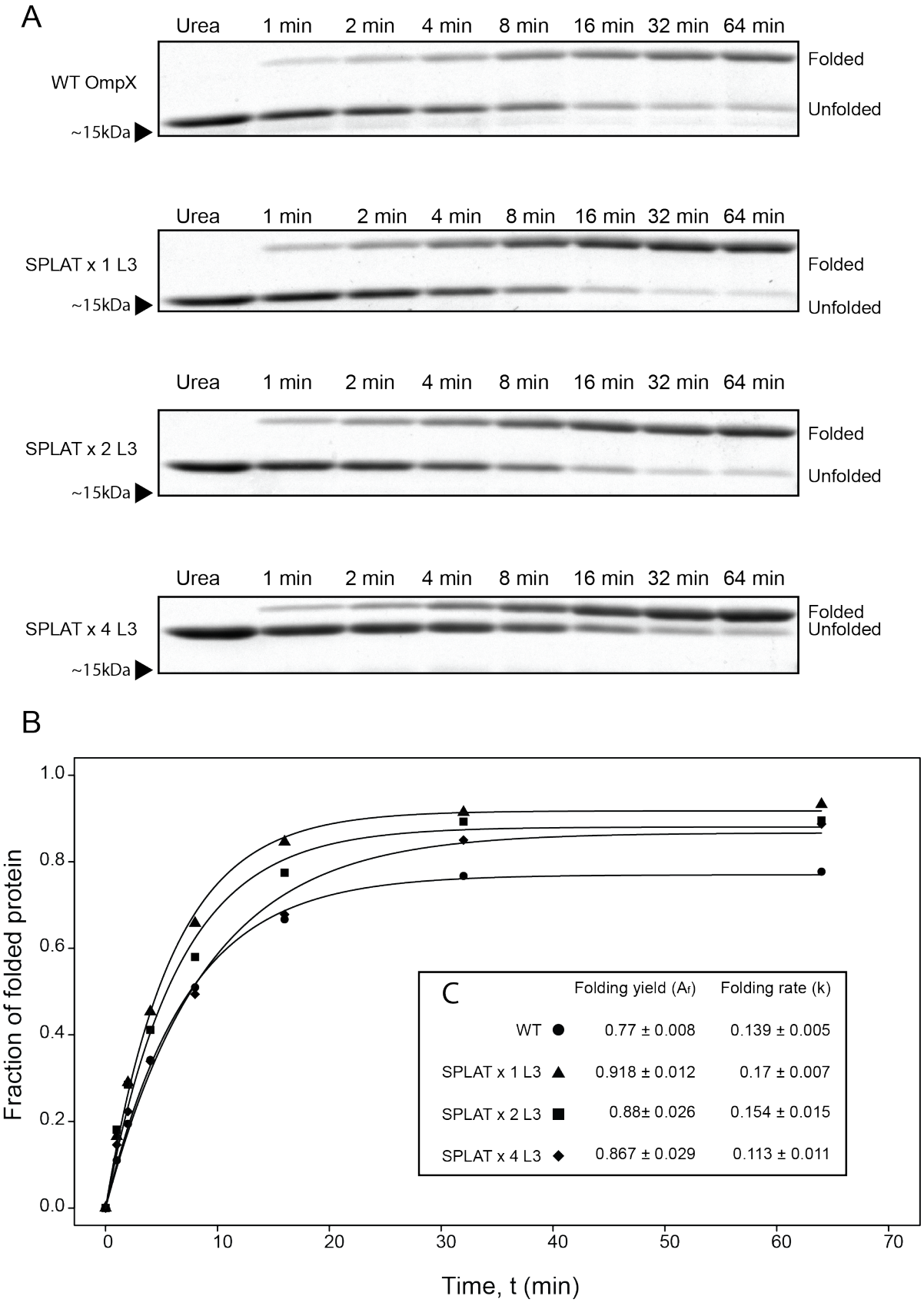

Figure 4.6: (A) SDS-PAGE showing the time course of OmpX constructs with SPLAT inserts in loop 3. (B) Fraction of folded protein as a function time determined by densitometry. Equation 1.2 was fitted to the data (solid lines). (C) Parameters estimations of the models fitted to the densitometry data.

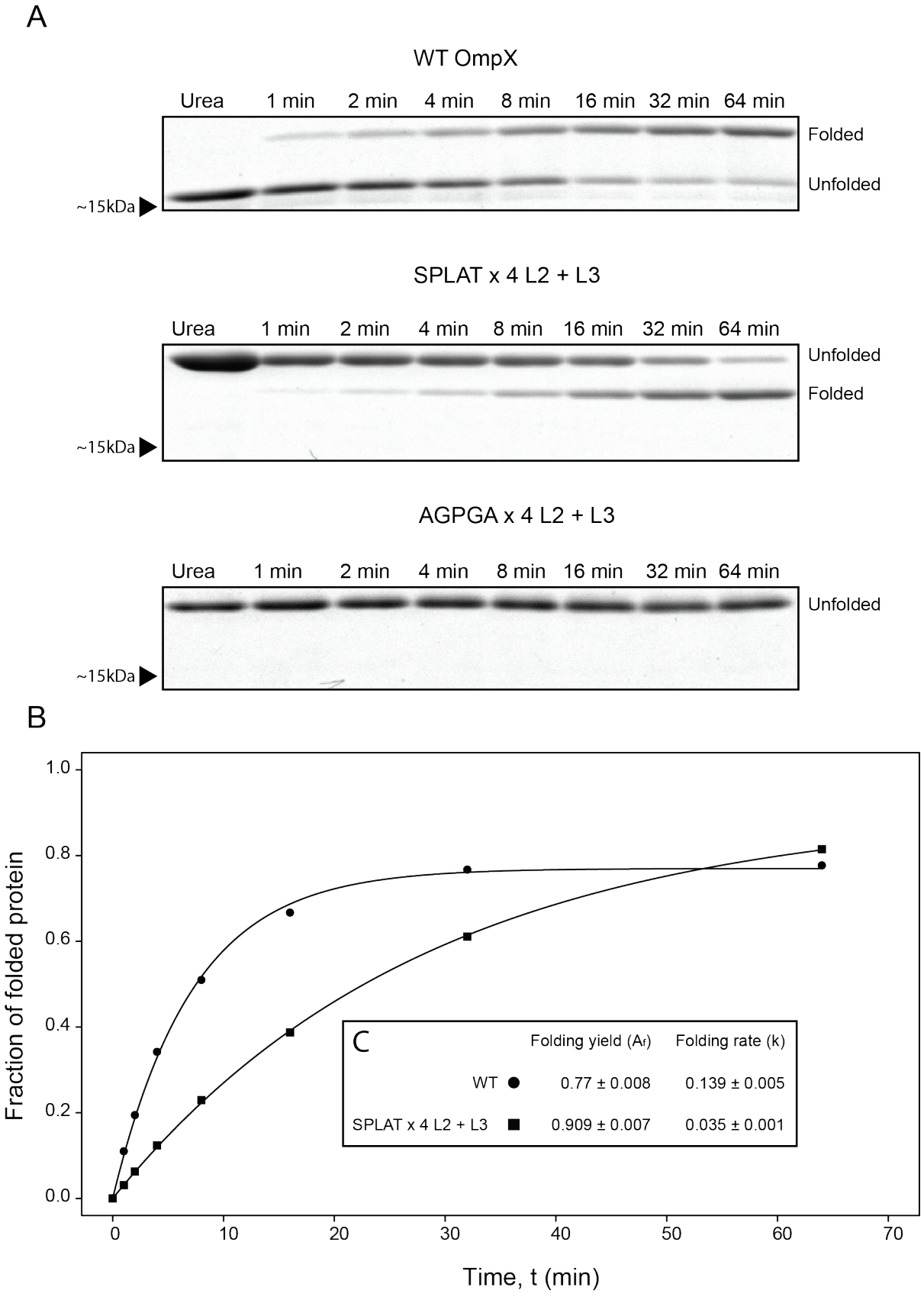

Figure 4.7: (A) SDS-PAGE showing the time course of the OmpX constructs with SPLATx4 and AGPGAx4 in loop 2 and 3. AGPGAx4 L2+L3 could not fold. (B) Fraction of folded protein as a function time determined by densitometry. Equation 1.2 was fitted to the data (solid lines). (C) Parameters estimations of the models fitted to the densitometry data.

Table 4.2 lists all of the parameter estimations for the different constructs. All of the constructs followed a single exponential rate law as previously reported for OmpX (P. Rath, Sharpe, Kohl, et al. 2019). Overall, a pattern emerges for the SPLAT inserts: a single insert improves folding yields, and repeating the inserts further then decrease the rate at which the protein folds, without affecting the yield. This pattern is less consistent with the AGPGA inserts. While AGPGA inserts improve folding yields in loop 2, it reduces the folding yields when inserted into loop 3. This suggest that the ability for L3 to make favorable hydrophobic contacts with a membrane is critical for OmpX insertion and folding. OmpX appear to be less dependent upon favorable hydrophobic interactions between loop 2 and the membrane. It is possible that differences in the folding kinetics are caused by unpredictable secondary structure formations in the different loop insertions.

Table 4.2: Parameter estimations on the folding kinetic of OmpX constructs. Parameters were estimated by non-linear least squares regression in R.

Model	Folding yield (A_f)	Folding rate (k)
WT OmpX 1	0.769832 ± 0.008496	0.139209 ± 0.004812
WT OmpX 2	0.801612 ± 0.012745	0.140459 ± 0.007008
AGPGAx1 L2	0.912688 ± 0.012671	0.125919 ± 0.005354
AGPGAx2 L2	0.90089 ± 0.01701	0.22356 ± 0.01461
AGPGAx4 L2	0.926675 ± 0.006863	0.067226 ± 0.001297
AGPGAx1 L3	0.91608 ± 0.01482	0.28307 ± 0.01665
AGPGAx2 L3	0.927758 ± 0.015014	0.095222 ± 0.004415
AGPGAx4 L3	0.45936 ± 0.01703	0.15544 ± 0.01849
SPLATx1 L2	0.951524 ± 0.012058	0.122569 ± 0.004728
SPLATx2 L2	0.89435 ± 0.03314	0.09518 ± 0.01010
SPLATx4 L2	0.934543 ± 0.024248	0.053626 ± 0.003372
SPLATx16 L2	0.873064 ± 0.053086	0.015918 ± 0.001447
SPLATx1 L3	0.91759 ± 0.01214	0.16952 ± 0.00733
SPLATx2 L3	0.88033 ± 0.02646	0.15391 ± 0.01481
SPLATx4 L3	0.86680 ± 0.02908	0.11290 ± 0.01131
SPLATx4 L2L3	0.9085631 ± 0.0074909	0.0352053 ± 0.0005995
$\Delta 94 \rightarrow 98$	0.939075 ± 0.008803	0.299691 ± 0.010336

If a reduction in folding yield is caused by aggregation before the protein can associate with the membrane, it means that the inserts prevents aggregation in solution prior to inserting into and folding within the detergent micelle. OMPs initially associate with the membrane (I_M) before they transition into their native conformation (F_M) when folding *in vitro*(Surrey and Jähnig, 1995). Since the larger insertions cause decreased folding rates without reducing the folding yield, it is likely that they are affecting the

transition from IM to FM. If the insertions affected the folding while the protein remained in solution they would surely cause increased aggregation. Uncropped/ unmodified gels of the folding assays are listed in Appendix 4.

The proposed mechanism for folding of OMPs into lipid bilayers *in vitro*involves simultaneous formation of all transmembrane β-strands within the lipid bilayer (J. H. Kleinschmidt, Blaauwen, et al. 1999). According to this model, the extracellular loops pass through the bilayer before the transmembrane β-strands. In this work, *in vitro* folding into zwitterionic detergent micelles was studied. It is possible that folding into detergent micelles follows a similar mechanism to the one proposed for folding into lipid bilayers. If this is the case, then it is arguable that modifications to the loops that alter their physical properties should change their ability to pass through the detergent micelles, and change the folding capacity of the protein. Modifications could also prevent secondary structure formation in the loops that could affect folding in a similar manner. Secondary structure in the inserts is, however, unlikely because of the structural constraints imposed by the included proline residues.

Interestingly, the apparent molecular weight of the folded constructs were similar to the apparent molecular weight of WT OmpX regardless of the size of the insert. Differences in molecular weight due to the loop inserts were only visible when the protein was unfolded. Figure 4.8 shows the heat shifts of the SPLAT inserts in loop 2, highlighting this observation.

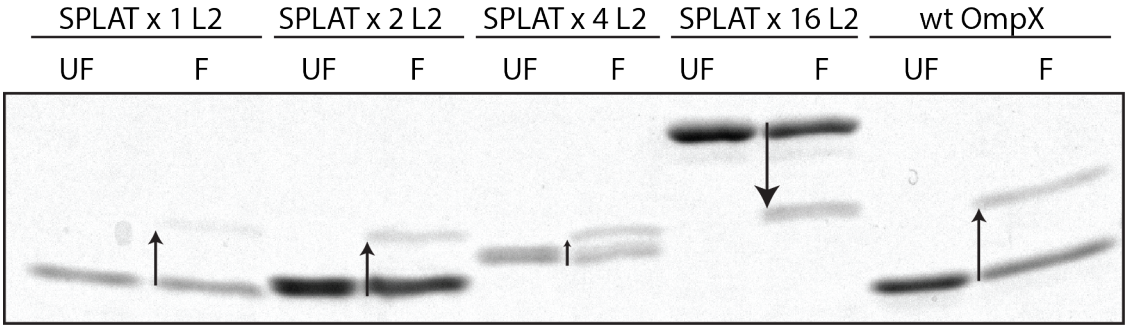

Figure 4.8: Folding shift of the constructs with inserts in loop 2. The molecular weight of the unfolded band increase with larger inserts. The position of the folded band do not change to the same degree and appear similar between the constructs. The arrow marks the direction of the shift. Protein was folded into SB12 detergent micelles at 15 °C. The unfolded controls are from protein in urea.

Outer membrane ß-barrels folded in SB12 likely forms some kind of SDS/SB12/ß-barrel complex when incubated in SDS. This complex would have defined radius and surface charge. The electrophoretic mobility is largely determined by the friction between the SDS/protein complex and the gel, and the charge of the complex (Chrambach and Rodbard 1971). Since the mobility of the folded band does not change after loop insertions it means that the insertions does not significantly affect the radius of the SDS/SB12/ß-barrel complex, which would increase/ decrease friction. It also means that the amount of bound SDS remains unchanged. This is possible since the loops protrude into the environment when the ß-barrel is folded. The size of the particle is primarily determined by the size of the ß-barrel, not the loops. This means that loop insertions should only cause minimal changes in friction. The loops are also quite hydrophilic, and it is unlikely that the loops can bind SDS when the protein is folded.

Since the amount of bound SDS remains the same, there should be no large difference in the charge of the SDS/SB12/ß-barrel complex. Since the loop insertions does not change the electrophoretic mobility of the folded protein, it indicates that the loop insertions does not affect the trans membrane domain.

Overall the results clearly state that the composition of the extra cellular loops affect folding efficiency of OMPs. Depending on their composition, loop modifications could either improve folding efficiency as was observed with the singular inserts, significantly decrease the folding rate as was observed with the large SPLAT inserts or cause aggregation/ prevent folding as was observed with the large AGPGA insert in loop 3. These results have implications for the biotechnological applications of OMPs. Care should be taken when the loops are modified to prevent reduction in folding yields or aggregation. Large modifications/insertions to the loops might reduce folding rate, but it should not prevent formation of the ß-barrel as long as the overall hydrophobicity remains unchanged.

Deleting different sections of loop 3 in OmpX affects folding kinetics

After observing that loop insertions can affect folding kinetics we became interested to see if deletions could have similar effects. The kinetics of folding of two deletion constructs were determined by SDS-PAGE in the same way as with the insertion constructs. The deletion constructs have residues removed from loop 3 of OmpX.

Strands 5 and 6 form an extended β-sheet in the X-ray structure of OmpX (Vogt and Schulz 1999). In contrast, the β-sheet this region appear more flexible in NMR structures (Fernández, Hilty, et al. 2004). Strand 5 and 6 are connected by loop 3. Molecular dynamics simulations also suggest that the loop regions are more flexible in the NMR structures compared to X-ray structures of OmpX (Cox et al. 2008). Examining the Cα secondary structure predictions for this region of an NMR structure reveals that the ß-strand propensity is similar to the X-ray structure, but somewhat reduced (Fernández, Adeishvili, and Wüthrich 2001). It should be noted that the RMSD of the loop regions are especially high in both solved X-ray and NMR structures.

Two deletion constructs in loop 3 were made to test the proposed flexibility of loop 3. One construct was made where the residues connecting the extended β-strands in the X-ray structure was deleted (ΔE94 $\rightarrow$ Y98). A second construct was also made by deleting the extended β-strands (ΔY87 $\rightarrow$ T93, ΔK99 $\rightarrow$ G106) that appear in the X-ray structure, and leaving the proposed loop region. The rationale behind the deletions were that if loops 2 and 3 form a rigid ß-sheet, as is suggested by the X-ray structure, the ß-barrel should lose its capacity to fold if the five residues that connect the strands in loop 3 were deleted. If the extended strands are rigid, they should not be able to bend into a loop. The other deletion construct was used to test if residues at the tip of loop 3 can function as a loop by themselves.

Figure 4.9 shows the folding kinetic of the deletion constructs. The deleted residues in the two constructs are marked in red. ΔE94 $\rightarrow$ Y98 folded at the highest rate (0.3 min^{-1}) and had the highest yield (94%) of all the tested constructs. Since a loop must be present to connect strands 5 and 6, this provides strong evidence for the fact that the tips of ß-strand 5 and 6 to not form a strong hydrogen-bonded network in this construct, and are able to adopt a more flexible loop-like structure in order to connect strands 5 and 6 to one another. It should be noted that the five deleted residues in this construct (EYPTY), at the tip of loop 3, do not partition into hydrophobic phases favorably according to the Wimley-White scale. This provides strong support for the hypothesis that the loop hydrophobic index plays a critical role ß-barrel protein folding *in vitro*.

The double deletion (ΔY87 $\rightarrow$ Y93, ΔK99 $\rightarrow$ G106) left the residues EYPTY to connect the transmembrane ß-strands. These deletions prevented the construct from folding *in vitro*. These results indicate that EYPTY cannot function as a loop as is indicated in the X-ray structure. The loss of folding capacity *in vitro*might be a result of deleting too much of the extended ß-strands. Two tyrosine residues that are placed in proximity to the bilayer interface were deleted. Aromatic residues that interact with the interface are important for structural stability. More deletion constructs should be made to identify how much of the loop that is required for the protein to fold.

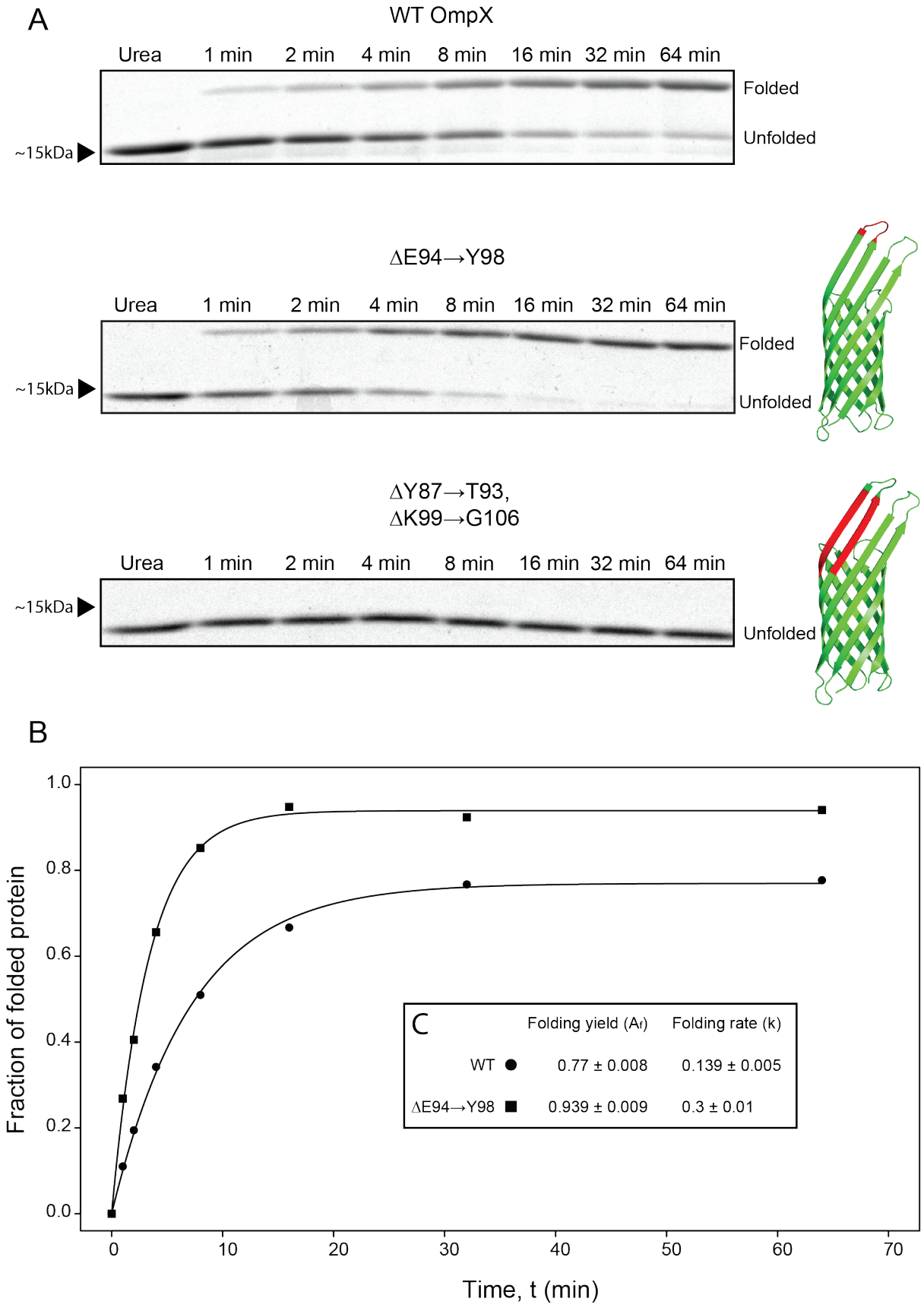

Figure 4.9: A) SDS-PAGE showing the time course of the OmpX deletion constructs folding into SB12 detergent micelles. ΔY87 $\rightarrow$ Y93, ΔK99 $\rightarrow$ G106 could not fold. The location of the deletions in OmpX are marked in red. The structure of OmpX was drawn in PyMol (PDB code:1QJ8). (B) Fraction of folded protein as a function time determined by densitometry. Equation 1.2 was fitted to the data (solid lines). (C) Parameters estimations of the models fitted to the densitometry data.

4.4 Outer membrane isolations

The mechanism of folding OMPs *in vivo* is markedly more complicated than the process of folding OMPs *in vitro*. In the cell it is the BAM-complex that allows OMPs to fold into the OM (Wu et al. 2020). Most practical applications of OMPs involves expressing them to the bacterial surface (Lång 2000). It was therfore important to examine if the loop inserts prevented the constructs from folding into the OM or if they stalled the mechanism by which the BAM-complex integrates OMPs to the OM.

To test if the OmpX constructs (table 4.1) could fold *in vivo* they were expressed with the signal peptide by auto induction in BL21-Gold (DE3)Δ*ompX*. The insoluble fractions of induced cultures was collected and the outer membrane was then isolated by selective detergent solubilization. If the expressed OmpX constructs exhibited heat modifiability and resisted a wash with urea it was indicative that the construct could fold *in vivo*. If the protein was not integrated into the OM, and was instead peripherally attached, the urea wash would remove the protein from the sample.

Figure 4.10 shows the expression of WT OmpX and SPLAT x1 L2 compared to an empty vector control (pET-22b(+)). The empty vector shows large bands around 25kDa and 35kDa. The molecular weights of these bands likely corresponds to OmpF (37kD), OmpC (38kDA) and OmpA (35kDa), three of the most highly expressed endogenous OMPs in *E. coli* (Meuskens et al. 2017). Overexpression of OmpX results in a reduction of these proteins as previously reported in *Enterobacter cloacae* (Stoorvogel, Bussel, and Klundert 1991), and the appearance of a band with a molecular weight corresponding to OmpX. Upon heating, a clear shift is observed in the apparent molecular weight OmpX. This heat shift is caused by denaturation of the β-barrel. A similar pattern with WT OmpX was observed in SPLAT x1 L2, which indicates that the loop insert did not prevent formation of the native ß-barrel. The large bands at approximately the same intensity as WT OmpX indicate that the folding efficiency is similar to WT OmpX. An unidentifiable band at 25 kDa appeared in all OM preparations. This protein did not exhibit any heat modifiability and was not affected by OmpX expression.

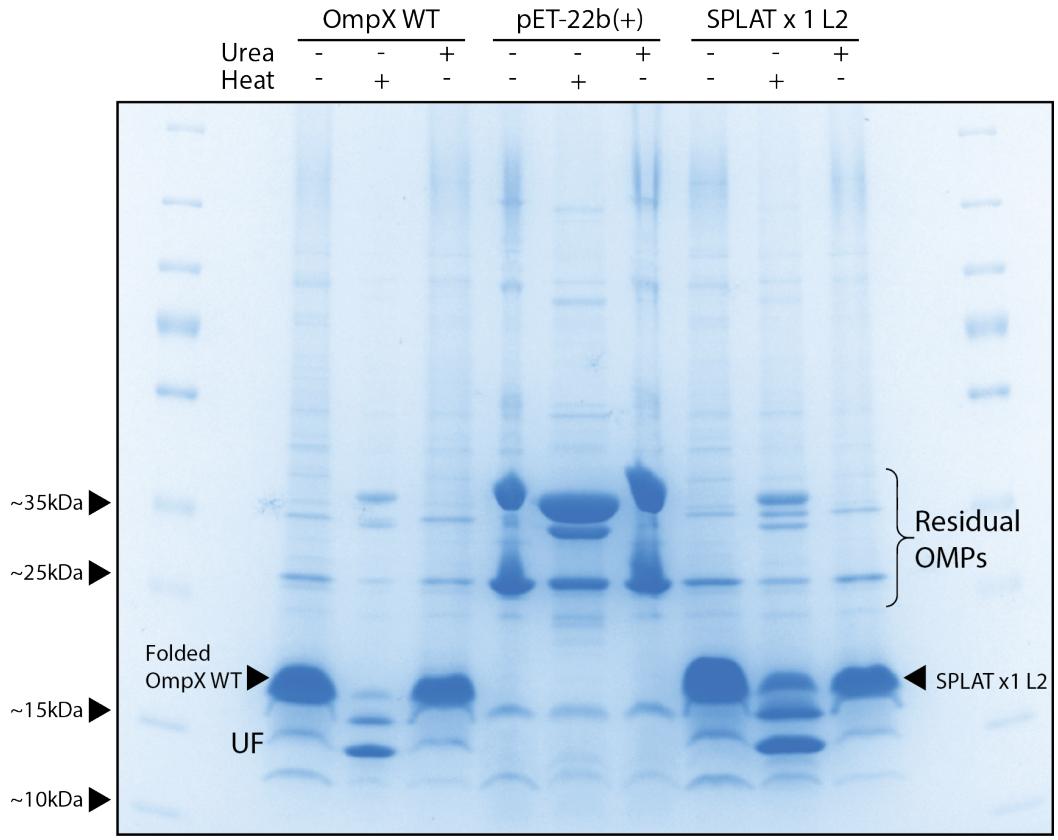

Figure 4.10: Outer membrane prepartions of *E. coli* expressing OmpX, SPLATx1 L2 and an empty vector (pET-22b(+)). The OM was isolated by selective solubilization of the IM with detergent. OM preparations were either heated at 95°C for 10 minutes or washed with urea. OmpX and SPLATx1 L2 folded *in vivo* and resisted the urea wash.

Figures 4.11 to 4.15 shows OM preparations of *E. coli* expressing OmpX constructs with insert in loop 2 and loop 3. All constructs exhibited heat-modifiability except for AGPGA x4 L2+L3. All of the constructs resisted extraction by urea. This indicates that the constructs could fold *in vivo*. However, it was clear a large amount of unfolded protein was present in several of the unheated OM preparations. Most of the unfolded bands disappeared after urea extraction, suggesting that the unfolded protein could associate with OM peripherally.

As observed *in vitro* (Figure 4.8), the apparent molecular weight of the folded protein does not change even after introduction of large loop insertions. The constructs with the largest inserts (x4) had a heat shift that is more difficult to differentiate as these constructs has a molecular weight similar to the apparent molecular weight of the folded protein. The OM preparations of cells expressing the largest x4 constructs all had an additional band appearing above the position of the folded band (~18 kDa). The difference in molecular weight between this extra band and the unfolded protein corresponds to the molecular weight of the signal peptide (2.2 kDa). It is therefore possible that this extra band is caused by contamination of either aggregated protein or a result of incomplete dissolution of the IM. As the x4 loop inserts folded inefficiently *in vitro*, it is possible that the constructs are also folded slower by the BAM complex. Slowing down the BAM complex could then cause an accumulation of unfolded protein at the IM.

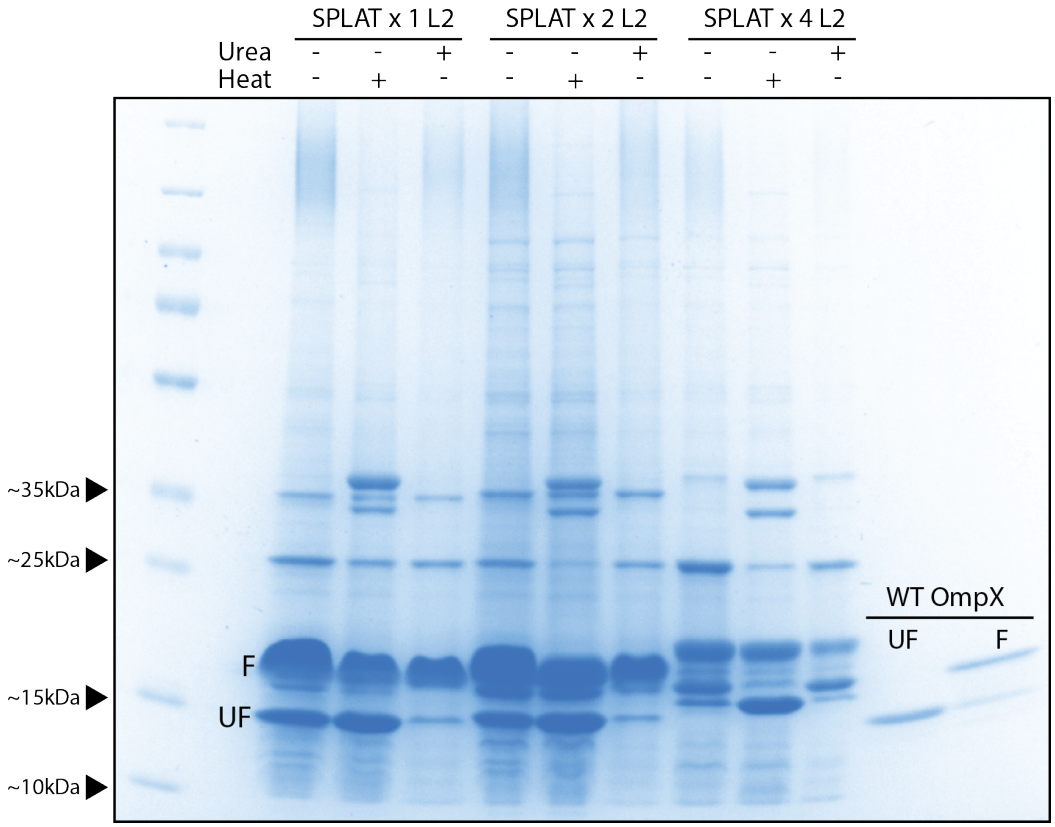

Figure 4.11: Outer membrane prepartions of *E. coli* expressing OmpX with SPLAT inserts in loop 2. The OM was isolated by selective solubilization of the IM with detergent. OM preparations were either heated at 95°C for 10 minutes or washed with urea. All constructs folded *in vivo* and resisted the urea wash.

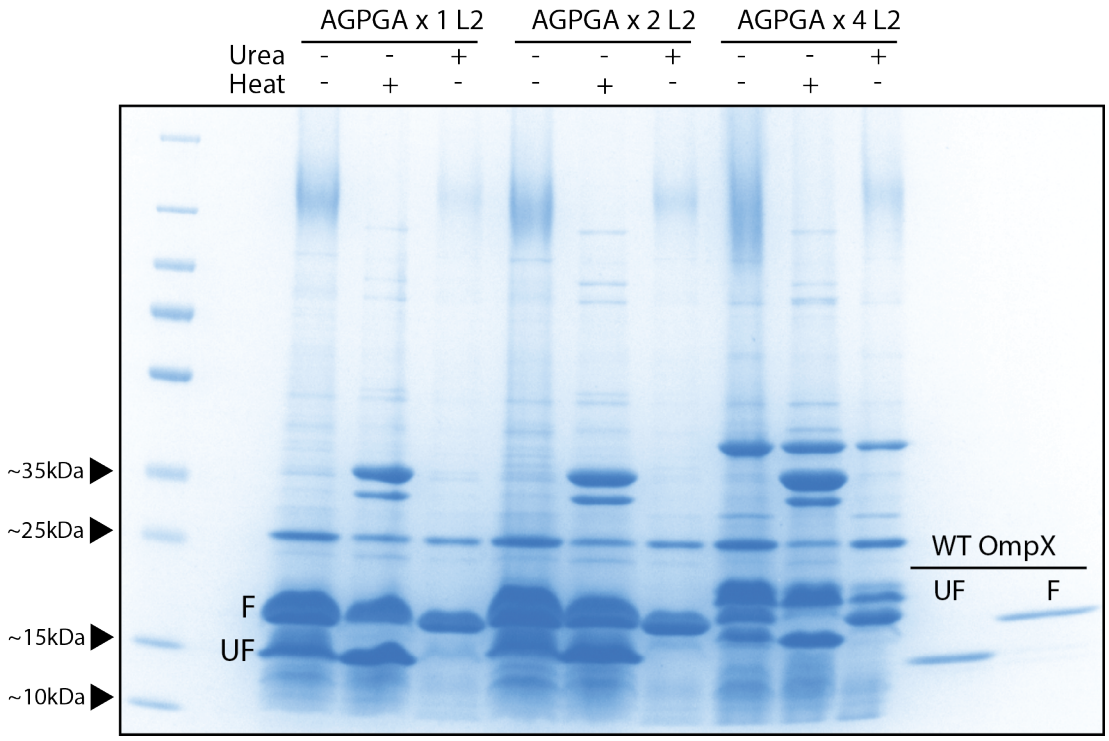

Figure 4.12: Outer membrane prepartions of *E. coli* expressing OmpX with AGPGA inserts in loop 2. The OM was isolated by selective solubilization of the IM with detergent. OM preparations were either heated at 95°C for 10 minutes or washed with urea. All constructs folded *in vivo* and resisted the urea wash.

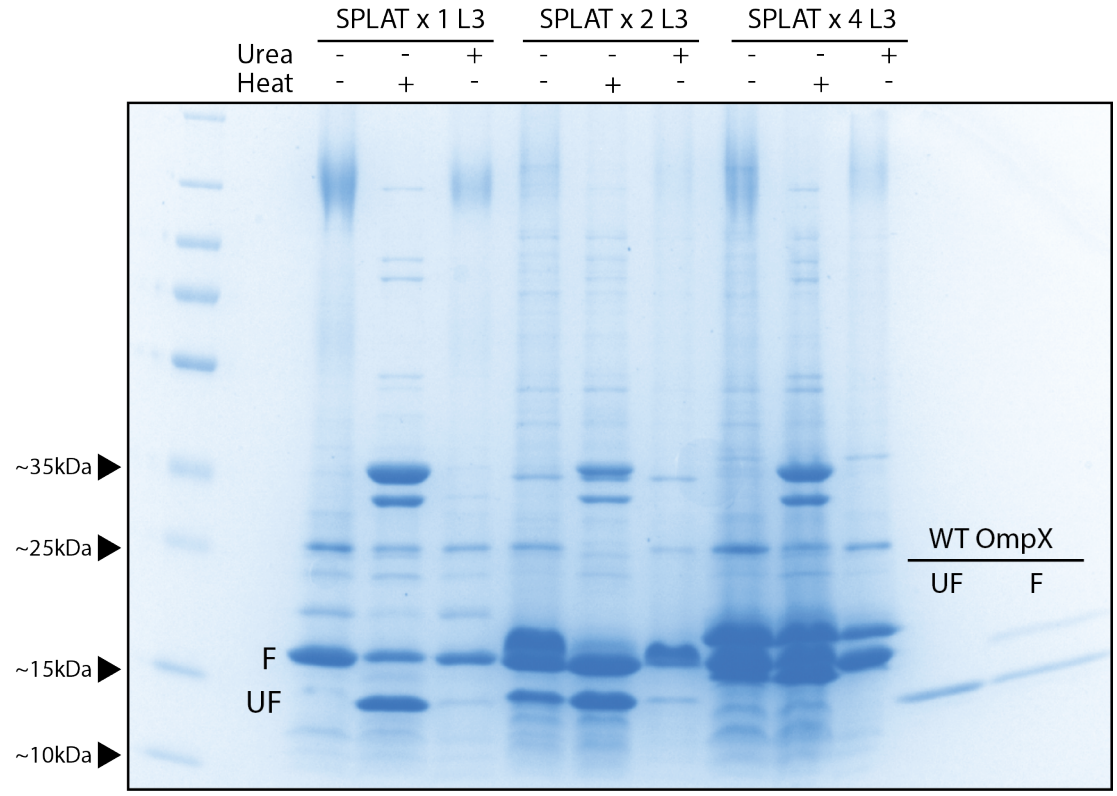

Figure 4.13: Outer membrane prepartions of *E. coli* expressing OmpX with SPLAT inserts in loop 3. The OM was isolated by selective solubilization of the IM with detergent. OM preparations were either heated at 95°C for 10 minutes or washed with urea. All constructs folded *in vivo* and resisted the urea wash.

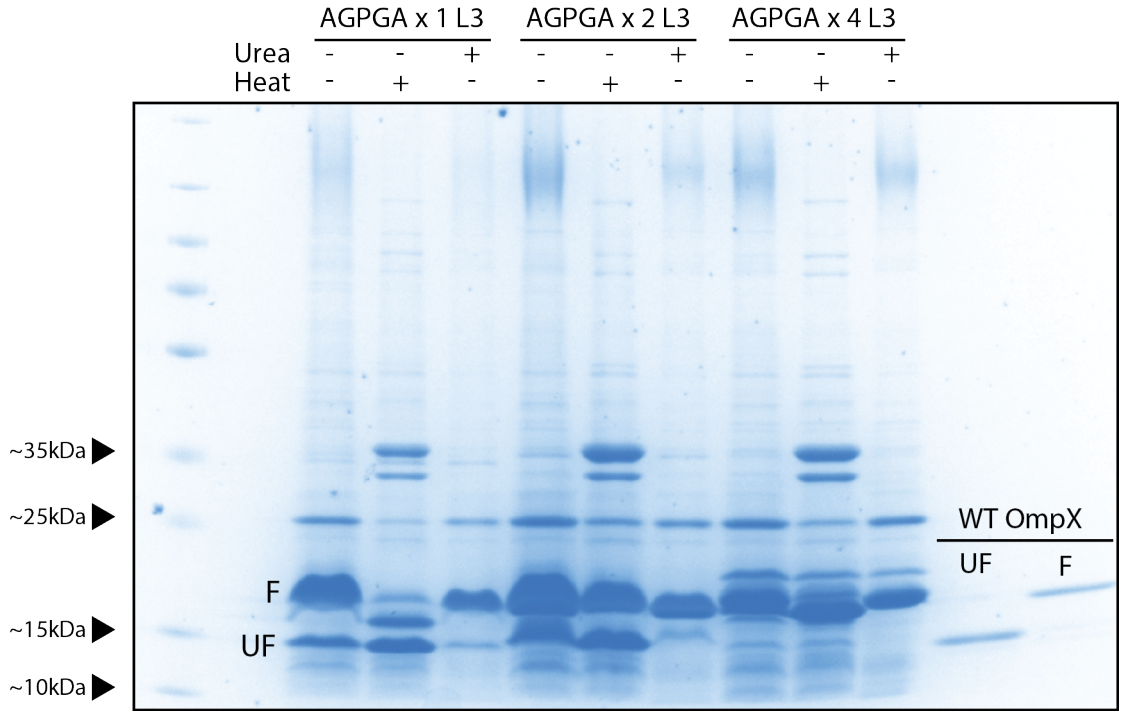

Figure 4.14: Outer membrane prepartions of *E. coli* expressing OmpX with AGPGA inserts in loop 3. The OM was isolated by selective solubilization of the IM with detergent. OM preparations were either heated at 95°C for 10 minutes or washed with urea. All constructs folded *in vivo* and resisted the urea wash.

Figure 4.7 shows the OM preparation of the double inserts. SPLAT x4 L2+L3 folded at the slowest rate of tested constructs *in vitro* and could still fold *in vivo*. AGPGA x4 L2+L3 did not fold *in vitro*, and no discernable heat-modifiability was visible *in vivo* either. As noted previously, this construct should be tested under semi native conditions to see if the loss of head-modifiability is caused by increased sensitivity to SDS. The fact that the *in vitro* folding test are consistent with the OM preparations showcases the utility of testing constructs *in vitro*. Loop modifications that reduce or prevent folding *in vitro* are likely to exhibit negative effects if expressed *in vivo*.

The yield of the OM isolation in cells expressing the double inserts was significantly reduced. The urea washed sample of SPLAT x4 L2+L3 was especially faint, however, bands are noticeable at the position of the folded and unfolded band. The reduced yield might be a side effect of the expressed constructs. The isolation should be repeated of a culture with a higher optical density to compensate for the reduced yield. The fact that AGPGA x4 L2+L3 appears in the OM isolation, but shows no folding shift, suggests that this construct might form a staggered complex with BamA. Such a staggered complex could be useful to understand the mechanism of how the BAM-complex folds OMPs (J. Lee, Xue, et al. 2016).

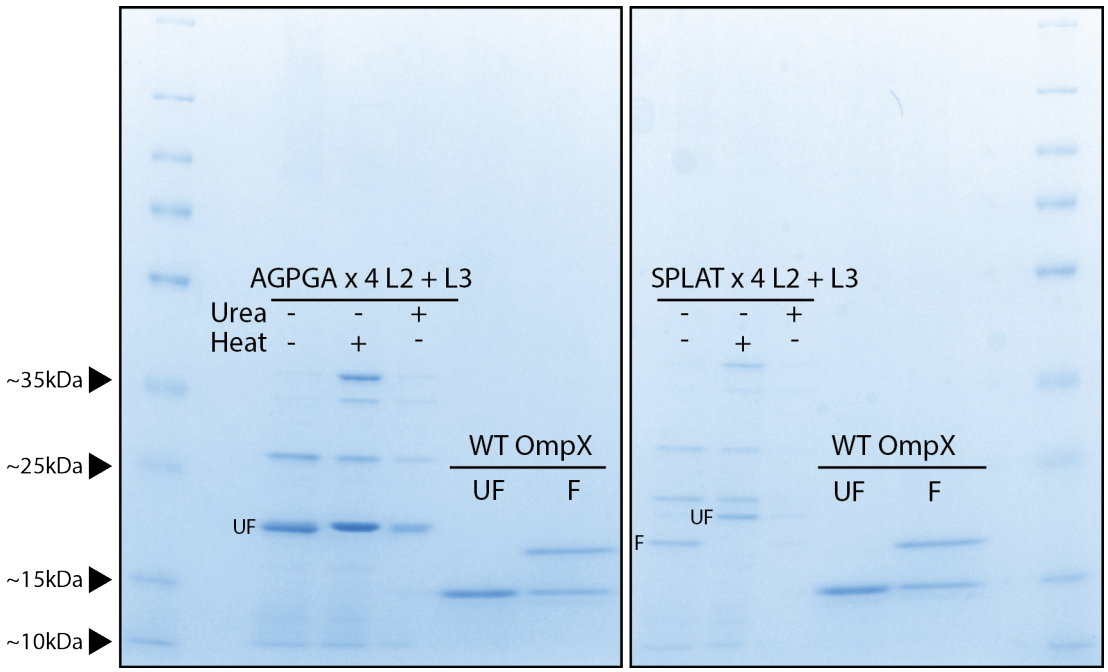

Figure 4.15: Outer membrane prepartions of *E. coli* expressing OmpX with SPLATx4 and AGPGAx4 inserts in loop 2 and loop 3. The OM was isolated by selective solubilization of the IM with detergent. OM preparations were either heated at 95°C for 10 minutes or washed with urea. No heat shift was detectable in AGPGAx4 L2+L3, but could still resist the urea wash. SPLATx4 L2+L3 folded *in vivo* and resisted the urea wash.

4.5 2D crystallization of OmpX88

2D crystallization of the construct "OmpX88" was attempted as a part of a side project. OmpX88 is a construct where the protein OmpX is duplicated and connected by a "DP" linker into a 16-stranded ß-barrel (Arnold et al. 2007). Outer membrane ß-barrel are composed of repeating units of ß-hairpins. Gene duplication is believed to be an important mechanism in the evolution of protein with such repeating units (Remmert et al. 2010). OmpX88 was designed to test of if gene duplication of OMPs could result in functional ß-barrels. OmpX88 exhibits heat-modifiability *in vitro*, indicating the construct can fold. Single channel conductance measurements suggested, however, that the barrel has a smaller diameter than what is expected by its strand number (Arnold et al. 2007). It is possible that the ß-barrel of OmpX88 has collapsed into a more oval shape compared to OmpX. Electron crystallography of 2D OmpX88 crystals would likely result in data that could be used to solve a structure with a sufficient resolution to resolve the overall shape of the ß-barrel within a lipid bilayer.

Electron crystallography is based electron diffraction of 2D crystals (Nannenga et al. 2013). 2D protein crystals can be produced by reconstituting the protein of interest into a lipid bilayer. Reconstitution can be done by mixing detergent solubilized lipids with detergent solubilized protein. The detergent is then removed by dialysis under specific buffer conditions to allow for growth of the 2D crystal (C. Kim et al. 2010). Conditions that results in growth of 2D crystals are limited and depend on a variety of factors. Typically, the lipid to detergent ratio (LPR, mg/mg), lipid type, detergent type, pH and salt concentration are initially varied to identify conditions that allow for crystal growth. Screening is generally slow as the tested conditions must each be examined with a transmission electron microscope to identify promising conditions.

Figures 4.16A and 4.16B shows selected images from the initial crystallization screen where the lipid types DMPC and *E. coli* polar lipid extract were tested. These lipid types are frequently used for screening of 2D crystals (C. Kim et al. 2010). Samples with E. coli polar lipid extract formed stacked planar lipid sheets (figure 4.16A), however, no diffracting crystals were observed in the sample. Samples with DMPC formed large unordered lipidic structures.

Planar lipid sheets are considered to be a good step in the direction of formation of 2D-crystalls (C. Kim et al. 2010). *E. coli* polar lipids were then selected for further screening. In the second screen, more variations of pH and divalent concentration was tested. In one sample (1.5 LPR, 10 mM $MgCl_2$, pH7) a single diffracting crystal could be observed (figure 4.16C). However, the same sample also contained various lipid structures which suggests inhomogeneous crystallization conditions (Figure 4.16).

The sample was used as a baseline for further screening. To create sufficient data, it was necessary to create a sample with more crystals. No crystals could be detected in further screenings however (Figure 4.16E and F). Figure 4.16E shows various vesicular structures, which might indicate successful reconstitution, but that the protein is not optimally packed in the bilayer (C. Kim et al. 2010). Technical issues related to the dialysis block caused excess sample evaporation, which prevented completion of the crystallization screening. The samples were dialyzed in a custom, home-made, plate (Appendix 4). The plate was not completely airtight which allowed for evaporation of water from the sample wells. This resulted in unpredictable changes to the tested

conditions making it difficult to replicate results. However, the results do indicate that *E. coli* polar lipid extract are good choice and that mild concentrations of a divalent could be beneficial for crystal growth.

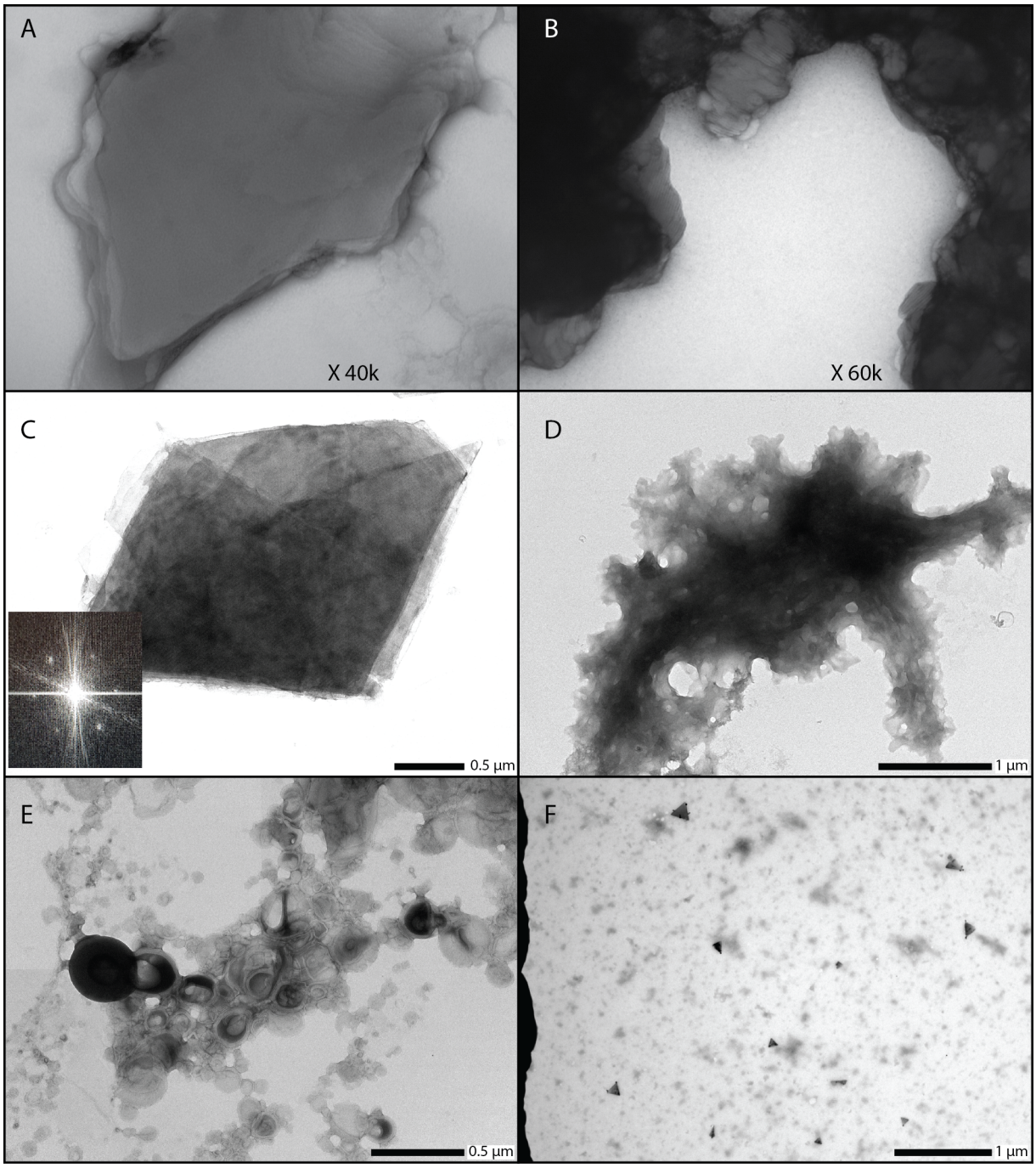

Figure 4.16: Negative stain of selected samples from the 2D-crystallization screening of OmpX88. A) Stacked lipid sheets of *E. coli* polar lipids at 0.66 LPR. B) Lipidic structure of DMPC at 0.5 LPR. C) Diffracting crystal of stacked OmpX88 2D-crystals at 1.5 LPR (*E. coli* polar lipid, 10mM MgCl, pH 7). D) Lipidic structure. Same conditon as C. E) Lipidic structure/ lipid vesicles of E. coli polar lipids at 1.5 LPR (90mM NaCl, 10mM $MgCl_2$, pH 8). F) Triangular shapes of unknown composition at 1.0 LPR (10mM NaCl, 30mM $MgCl_2$, pH7).

5. Conclusion and future goals

The 2D crystallization of OmpX88 was attempted as a side project and was unsuccessful. Some conditions that appeared to be promising for growth of 2D crystals were determined. *E. coli* polar lipids and neutral pH are likely beneficial for crystal growth. Future screenings should involve testing of different types of detergents for reconstituting the protein as only a single detergent was tested in this work.

The main aim of this project was to examine the effects of the extracellular loops on folding of OmpX into SB12 detergent micelles *in vitro*. Insertion of small inserts, regardless of composition, improved the efficiency of the folding kinetics. It is possible that the inserts prevented regular secondary structure formation in the loops that normally reduce the folding rate of WT OmpX. Increasing the size of the insert further reduces the folding rate. Large hydrophilic inserts cause a reduction in folding yield and reduced folding rate. The largest hydrophilic inserts prevented folding of OmpX altogether. The largest amphipathic inserts in contrast reduced the folding rate, but did not prevent folding. Deleting five hydrophilic residues at loop 3 resulted in a construct that folded much faster than WT OmpX, with a significantly improved folding yield. The results indicates clearly that the composition of the loops significantly affects the folding of OMPs.

The OmpX constructs with the different inserts were expressed *in vivo*. All of the constructs that could fold *in vitro* were observed to do so as well *in vivo*. The largest hydrophilic insert that could not fold *in vitro*, was transported and integrated to the OM, but could apparently not be folded. This suggests that the insert caused the construct to stagger on the BAM-complex. Further experiments should examine folding by a method that is less harsh than SDS-PAGE. It is possible that the construct only appears unfolded because of increased sensitivity to SDS. Circular dichroism or native-page should resolve this question. Taken together, these results indicate that modifications to the loops are permissible, but that large hydrophilic inserts might have severe effects on folding of OMPs.

The amount of tested inserts might not be sufficient to explain exactly how the composition of the loops affect folding. Further experiments should involve a more comprehensive set of inserts to determine that the patterns observed in this work is consistent. Specifically, further work should examine the effects of inserts with charged and aromatic inserts.

Based on the results it is recommended that modifications to the loops of OMPs should not be excessively large and hydrophilic. In the case of OmpX specifically, it is recommended to modify loop 2 in favor of loop 3. Loop 3 appeared to be more sensitive to the inserts.

Bibliography

Arnold, Thomas et al. (Mar. 2007). "Gene Duplication of the Eight-stranded β-Barrel OmpX Produces a Functional Pore: A Scenario for the Evolution of Transmembrane β-Barrels." en. In: *Journal of Molecular Biology* 366.4, pp. 1174–1184. ISSN: 0022-2836. DOI: 10.1016/j.jmb.2006.12.029.

Baba, Tomoya et al. (Feb. 2006). "Construction of Escherichia coli K-12 in-frame, single-gene knockout mutants: the Keio collection." In: *Molecular Systems Biology* 2, p. 2006.0008. ISSN: 1744-4292. DOI: 10.1038/msb4100050.

Bakelar, Jeremy, Susan K. Buchanan, and Nicholas Noinaj (Jan. 2016). "The structure of the β-barrel assembly machinery complex." en. In: *Science* 351.6269, pp. 180–186. ISSN: 0036-8075, 1095-9203. DOI: 10.1126/science.aad3460.

Bertani, G. (Sept. 1951). "STUDIES ON LYSOGENESIS I." In: *Journal of Bacteriology* 62.3, pp. 293–300. ISSN: 0021-9193.

Blair, Jessica M. A. et al. (Jan. 2015). "Molecular mechanisms of antibiotic resistance." en. In: *Nature Reviews Microbiology* 13.1, pp. 42–51. ISSN: 1740-1534. DOI: 10.1038/nrmicro3380.

Browning, Douglas F. et al. (Dec. 2013). "Mutational and Topological Analysis of the Escherichia coli BamA Protein." en. In: *PLOS ONE* 8.12, e84512. ISSN: 1932-6203. DOI: 10.1371/journal.pone.0084512.

Burgess, Nancy K. et al. (Sept. 2008). "β-Barrel Proteins That Reside in the Escherichia coli Outer Membrane in Vivo Demonstrate Varied Folding Behavior in Vitro." In: *The Journal of Biological Chemistry* 283.39, pp. 26748–26758. ISSN: 0021-9258. DOI: 10.1074/jbc.M802754200.

Caroff, Martine and Alexey Novikov (2020). "Lipopolysaccharides: structure, function and bacterial identifications." en. In: *OCL* 27, p. 31. ISSN: 2272-6977, 2257-6614. DOI: 10.1051/ocl/2020025.

Chatzi, Katerina E. et al. (Aug. 2014). "SecA-mediated targeting and translocation of secretory proteins." en. In: *Biochimica et Biophysica Acta (BBA) - Molecular Cell Research*. Protein trafficking and secretion in bacteria 1843.8, pp. 1466–1474. ISSN: 0167-4889. DOI: 10.1016/j.bbamcr.2014.02.014.

Chrambach, A. and D. Rodbard (Apr. 1971). "Polyacrylamide Gel Electrophoresis." en. In: *Science* 172.3982, pp. 440–451. ISSN: 0036-8075, 1095-9203. DOI: 10.1126/science.172.3982.440.

Chung, C T, S L Niemela, and R H Miller (Apr. 1989). "One-step preparation of competent Escherichia coli: transformation and storage of bacterial cells in the same solution." In: *Proceedings of the National Academy of Sciences of the United States of America* 86.7, pp. 2172–2175. ISSN: 0027-8424.

Clifton, Luke A et al. (Oct. 2015). "An Accurate In Vitro Model of the E. coli Envelope." In: *Angewandte Chemie (International Ed. in English)* 54.41, pp. 11952–11955. ISSN: 1433-7851. DOI: 10.1002/anie.201504287.

Cox, Katherine et al. (Feb. 2008). "Outer membrane proteins: comparing X-ray and NMR structures by MD simulations in lipid bilayers." en. In: *European Biophysics Journal* 37.2, pp. 131–141. ISSN: 1432-1017. DOI: 10.1007/s00249-007-0185-8.

Dalbey, Ross E. and Andreas Kuhn (Nov. 2012). "Protein Traffic in Gram-negative bacteria – how exported and secreted proteins find their way." In: *FEMS Microbiology Reviews* 36.6, pp. 1023–1045. ISSN: 0168-6445. DOI: 10.1111/j.1574-6976.2012.00327.x.

Denks, Kärt et al. (Mar. 2014). "The Sec translocon mediated protein transport in prokaryotes and eukaryotes." In: *Molecular Membrane Biology* 31.2-3, pp. 58–84. ISSN: 0968-7688. DOI: 10.3109/09687688.2014.907455.

Deol, Sundeep S. et al. (Dec. 2004). "Lipid-protein interactions of integral membrane proteins: a comparative simulation study." eng. In: *Biophysical Journal* 87.6, pp. 3737–3749. ISSN: 0006-3495. DOI: 10.1529/biophysj.104.048397.

Doerner, Pamela Arden and Marcelo C. Sousa (June 2017). "Extreme Dynamics in the BamA β-Barrel Seam." In: *Biochemistry* 56.24, pp. 3142–3149. ISSN: 0006-2960. DOI: 10.1021/acs.biochem.7b00281.

Duguay, Amy R. and Thomas J. Silhavy (Nov. 2004). "Quality control in the bacterial periplasm." eng. In: *Biochimica Et Biophysica Acta* 1694.1-3, pp. 121–134. ISSN: 0006-3002. DOI: 10.1016/j.bbamcr.2004.04.012.

Ferguson, A. D. et al. (June 2000). "A conserved structural motif for lipopolysaccharide recognition by procaryotic and eucaryotic proteins." eng. In: *Structure (London, England: 1993)* 8.6, pp. 585–592. ISSN: 0969-2126. DOI: 10.1016/s0969-2126(00)00143-x.

Fernández, César, Koba Adeishvili, and Kurt Wüthrich (Feb. 2001). "Transverse relaxation-optimized NMR spectroscopy with the outer membrane protein OmpX in dihexanoyl phosphatidylcholine micelles." en. In: *Proceedings of the National Academy of Sciences* 98.5, pp. 2358–2363. ISSN: 0027-8424, 1091-6490. DOI: 10.1073/pnas.051629298.

Fernández, César, Christian Hilty, et al. (Mar. 2004). "NMR Structure of the Integral Membrane Protein OmpX." en. In: *Journal of Molecular Biology* 336.5, pp. 1211–1221. ISSN: 0022-2836. DOI: 10.1016/j.jmb.2003.09.014.

Franklin, Meghan Whitney and Joanna S. G. Slusky (Sept. 2018). "Tight Turns of Outer Membrane Proteins: An Analysis of Sequence, Structure, and Hydrogen Bonding." en. In: *Journal of Molecular Biology* 430.18, Part B, pp. 3251–3265. ISSN: 0022-2836. DOI: 10.1016/j.jmb.2018.06.013.

Freudl, Roland (Oct. 1989). "Insertion of peptides into cell-surface-exposed areas of the Escherichia coli OmpA protein does not interfere with export and membrane assembly." en. In: *Gene* 82.2, pp. 229–236. ISSN: 0378-1119. DOI: 10.1016/0378-1119(89)90048-6.

Gasteiger, Elisabeth et al. (2005). "Protein Identification and Analysis Tools on the ExPASy Server." en. In: *The Proteomics Protocols Handbook*. Ed. by John M. Walker. Springer Protocols Handbooks. Totowa, NJ: Humana Press, pp. 571–607. ISBN: 978-1-59259-890-8. DOI: 10.1385/1-59259-890-0:571.

Ghai, Ishan and Shashank Ghai (2018). "Understanding antibiotic resistance via outer membrane permeability." eng. In: *Infection and Drug Resistance* 11, pp. 523–530. ISSN: 1178-6973. DOI: 10.2147/IDR.S156995.

Gram, C. (1884). "Ueber die isolirte Farbung der Schizomyceten in Schnitt-und Trockenpraparaten." In: *Fortschritte der Medicin* 2, pp. 185–189.

Gupta, Radhey S. (Aug. 2011). "Origin of diderm (Gram-negative) bacteria: antibiotic selection pressure rather than endosymbiosis likely led to the evolution of bacterial cells with two membranes." In: *Antonie Van Leeuwenhoek* 100.2, pp. 171–182. ISSN: 0003-6072. DOI: 10.1007/s10482-011-9616-8.

Hagan, Christine L., Thomas J. Silhavy, and Daniel Kahne (June 2011). "β-Barrel Membrane Protein Assembly by the Bam Complex." In: *Annual Review of Biochemistry* 80.1, pp. 189–210. ISSN: 0066-4154. DOI: 10.1146/annurev-biochem-061408-144611.

Hegde, Ramanujan S. and Harris D. Bernstein (Oct. 2006). "The surprising complexity of signal sequences." en. In: *Trends in Biochemical Sciences* 31.10, pp. 563–571. ISSN: 0968-0004. DOI: 10.1016/j.tibs.2006.08.004.

Heller, K B (June 1978). "Apparent molecular weights of a heat-modifiable protein from the outer membrane of Escherichia coli in gels with different acrylamide concentrations." In: *Journal of Bacteriology* 134.3, pp. 1181–1183. ISSN: 0021-9193.

Hong, Heedeok et al. (July 2007). "Role of Aromatic Side Chains in the Folding and Thermodynamic Stability of Integral Membrane Proteins." In: *Journal of the American Chemical Society* 129.26, pp. 8320–8327. ISSN: 0002-7863. DOI: 10.1021/ja068849o.

Horne, Jim E., David J. Brockwell, and Sheena E. Radford (July 2020). "Role of the lipid bilayer in outer membrane protein folding in Gram-negative bacteria." en. In: *Journal of Biological Chemistry* 295.30, pp. 10340–10367. ISSN: 0021-9258, 1083-351X. DOI: 10.1074/jbc.REV120.011473.

Hussain, Sunyia, Janine H. Peterson, and Harris D. Bernstein (Mar. 2020). "Bam complex-mediated assembly of bacterial outer membrane proteins synthesized in an in vitro translation system." en. In: *Scientific Reports* 10.1, p. 4557. ISSN: 2045-2322. DOI: 10.1038/s41598-020-61431-2.

Kim, Changki et al. (June 2010). "An automated pipeline to screen membrane protein 2D crystallization." In: *Journal of structural and functional genomics* 11.2, pp. 155–166. ISSN: 1345-711X. DOI: 10.1007/s10969-010-9088-5.

Kleinschmidt, J. H., T. den Blaauwen, et al. (Apr. 1999). "Outer membrane protein A of Escherichia coli inserts and folds into lipid bilayers by a concerted mechanism." eng. In: *Biochemistry* 38.16, pp. 5006–5016. ISSN: 0006-2960. DOI: 10.1021/bi982465w.

Kleinschmidt, J. H., M. C. Wiener, and L. K. Tamm (Oct. 1999). "Outer membrane protein A of E. coli folds into detergent micelles, but not in the presence of monomeric detergent." In: *Protein Science : A Publication of the Protein Society* 8.10, pp. 2065–2071. ISSN: 0961-8368.

Kleinschmidt, Jörg H. (June 2006). "Folding kinetics of the outer membrane proteins OmpA and FomA into phospholipid bilayers." en. In: *Chemistry and Physics of Lipids*.

Protein:Lipid Interactions 141.1, pp. 30–47. ISSN: 0009-3084. DOI: 10.1016/j.chemphyslip.2006.02.004.

Kleinschmidt, Jörg H. (Sept. 2015). "Folding of β-barrel membrane proteins in lipid bilayers — Unassisted and assisted folding and insertion." en. In: *Biochimica et Biophysica Acta (BBA) - Biomembranes*. Lipid-protein interactions 1848.9, pp. 1927–1943. ISSN: 0005-2736. DOI: 10.1016/j.bbamem.2015.05.004.

Kleinschmidt, Jörg H. et al. (Mar. 2011). "Association of Neighboring β-Strands of Outer Membrane Protein A in Lipid Bilayers Revealed by Site-Directed Fluorescence Quenching." en. In: *Journal of Molecular Biology* 407.2, pp. 316–332. ISSN: 0022-2836. DOI: 10.1016/j.jmb.2011.01.021.

Klose, M. et al. (Sept. 1988). "The influence of amino substitutions within the mature part of an Escherichia coli outer membrane protein (OmpA) on assembly of the polypeptide into its membrane." eng. In: *The Journal of Biological Chemistry* 263.26, pp. 13297–13302. ISSN: 0021-9258.

Knowles, Timothy J. et al. (Mar. 2009). "Membrane protein architects: the role of the BAM complex in outer membrane protein assembly." en. In: *Nature Reviews Microbiology* 7.3, pp. 206–214. ISSN: 1740-1534. DOI: 10.1038/nrmicro2069.

Koebnik, R. and V. Braun (Feb. 1993). "Insertion derivatives containing segments of up to 16 amino acids identify surface- and periplasm-exposed regions of the FhuA outer membrane receptor of Escherichia coli K-12." en. In: *Journal of Bacteriology* 175.3, pp. 826–839. ISSN: 0021-9193, 1098-5530. DOI: 10.1128/jb.175.3.826-839.1993.

Koebnik, R., K. P. Locher, and P. Van Gelder (July 2000). "Structure and function of bacterial outer membrane proteins: barrels in a nutshell." eng. In: *Molecular Microbiology* 37.2, pp. 239–253. ISSN: 0950-382X. DOI: 10.1046/j.1365-2958.2000.01983.x.

Koebnik, Ralf (June 1999). "Structural and Functional Roles of the Surface-Exposed Loops of the β-Barrel Membrane Protein OmpA from Escherichia coli." In: *Journal of Bacteriology* 181.12, pp. 3688–3694. ISSN: 0021-9193.

Krojer, Tobias et al. (June 2008). "Structural basis for the regulated protease and chaperone function of DegP." en. In: *Nature* 453.7197, pp. 885–890. ISSN: 1476-4687. DOI: 10.1038/nature07004.

Lång, Hannu (Dec. 2000). "Outer membrane proteins as surface display systems." en. In: *International Journal of Medical Microbiology* 290.7, pp. 579–585. ISSN: 1438-4221. DOI: 10.1016/S1438-4221(00)80004-1.

Lee, James, David Tomasek, et al. (Nov. 2019). "Formation of a β-barrel membrane protein is catalyzed by the interior surface of the assembly machine protein BamA." In: *eLife* 8. Ed. by Ramanujan S Hegde and John Kuriyan, e49787. ISSN: 2050-084X. DOI: 10.7554/eLife.49787.

Lee, James, Mingyu Xue, et al. (Aug. 2016). "Characterization of a stalled complex on the β-barrel assembly machine." en. In: *Proceedings of the National Academy of Sciences* 113.31, pp. 8717–8722. ISSN: 0027-8424, 1091-6490. DOI: 10.1073/pnas.1604100113.

Lennox, E. S. (July 1955). "Transduction of linked genetic characters of the host by bacteriophage P1." en. In: *Virology* 1.2, pp. 190–206. ISSN: 0042-6822. DOI: 10.1016/0042-6822(55)90016-7.

Lerouge, Inge and Jos Vanderleyden (2002). "O-antigen structural variation: mechanisms and possible roles in animal/plant–microbe interactions." en. In: *FEMS Microbiology Reviews* 26.1, pp. 17–47. ISSN: 1574-6976. DOI: https://doi.org/10.1111/j.1574-6976.2002.tb00597.x.

Lin, Jun, Shouxiong Huang, and Qijing Zhang (Mar. 2002). "Outer membrane proteins: key players for bacterial adaptation in host niches." en. In: *Microbes and Infection* 4.3, pp. 325–331. ISSN: 1286-4579. DOI: 10.1016/S1286-4579(02)01545-9.

Madeira, Fábio et al. (July 2019). "The EMBL-EBI search and sequence analysis tools APIs in 2019." en. In: *Nucleic Acids Research* 47.W1, W636–W641. ISSN: 0305-1048, 1362-4962. DOI: 10.1093/nar/gkz268.

Manns, Joanne M. (2011). "SDS-Polyacrylamide Gel Electrophoresis (SDS-PAGE) of Proteins." en. In: *Current Protocols in Microbiology* 22.1, A.3M.1–A.3M.13. ISSN: 1934-8533. DOI: https://doi.org/10.1002/9780471729259.mca03ms22.

Maruvada, Ravi and Kwang Sik Kim (Jan. 2011). "Extracellular Loops of the Eschericia coli Outer Membrane Protein A Contribute to the Pathogenesis of Meningitis." In: *The Journal of Infectious Diseases* 203.1, pp. 131–140. ISSN: 0022-1899. DOI: 10.1093/infdis/jiq009.

Maurya, Svetlana Rajkumar, Deepti Chaturvedi, and Radhakrishnan Mahalakshmi (June 2013). "Modulating lipid dynamics and membrane fluidity to drive rapid folding of a transmembrane barrel." en. In: *Scientific Reports* 3.1, p. 1989. ISSN: 2045-2322. DOI: 10.1038/srep01989.

Mecsas, J. et al. (Feb. 1995). "Identification and characterization of an outer membrane protein, OmpX, in Escherichia coli that is homologous to a family of outer membrane proteins including Ail of Yersinia enterocolitica." en. In: *Journal of Bacteriology* 177.3, pp. 799–804. ISSN: 0021-9193, 1098-5530. DOI: 10.1128/jb.177.3.799-804.1995.

Megrian, Daniela et al. (2020). "One or two membranes? Diderm Firmicutes challenge the Gram-positive/Gram-negative divide." en. In: *Molecular Microbiology* 113.3, pp. 659–671. ISSN: 1365-2958. DOI: https://doi.org/10.1111/mmi.14469.

Meuskens, Ina et al. (Nov. 2017). "A New Strain Collection for Improved Expression of Outer Membrane Proteins." In: *Frontiers in Cellular and Infection Microbiology* 7. ISSN: 2235-2988. DOI: 10.3389/fcimb.2017.00464.

Miller, Samuel I. and Nina R. Salama (2018). "The gram-negative bacterial periplasm: Size matters." eng. In: *PLoS biology* 16.1, e2004935. ISSN: 1545-7885. DOI: 10.1371/journal.pbio.2004935.

Mogensen, Jesper E. and Daniel E. Otzen (July 2005). "Interactions between folding factors and bacterial outer membrane proteins." eng. In: *Molecular Microbiology* 57.2, pp. 326–346. ISSN: 0950-382X. DOI: 10.1111/j.1365-2958.2005.04674.x.

Molloy, M. P. et al. (May 2000). "Proteomic analysis of the Escherichia coli outer membrane." eng. In: *European Journal of Biochemistry* 267.10, pp. 2871–2881. ISSN: 0014-2956. DOI: 10.1046/j.1432-1327.2000.01296.x.

Moyes, Rita B., Jackie Reynolds, and Donald P. Breakwell (2009). "Differential Staining of Bacteria: Gram Stain." en. In: *Current Protocols in Microbiology* 15.1, A.3C.1–A.3C.8. ISSN: 1934-8533. DOI: https://doi.org/10.1002/9780471729259.mca03cs15.

Murzin, Alexey G., Arthur M. Lesk, and Cyrus Chothia (Mar. 1994). "Principles determining the structure of β-sheet barrels in proteins I. A theoretical analysis." en. In: *Journal of Molecular Biology* 236.5, pp. 1369–1381. ISSN: 0022-2836. DOI: 10.1016/0022-2836(94)90064-7.

Nakamura, Kenzo and Shoji Mizushima (Dec. 1976). "Effects of Heating in Dodecyl Sulfate Solution on the Conformation and Electrophoretic Mobility of Isolated Major Outer Membrane Proteins from Escherichia coli K-12." en. In: *The Journal of Biochemistry* 80.6, pp. 1411–1422. ISSN: 0021-924X. DOI: 10.1093/oxfordjournals.jbchem.a131414.

Nannenga, Brent L. et al. (2013). "Overview of Electron Crystallography of Membrane Proteins: Crystallization and Screening Strategies Using Negative Stain Electron Microscopy." In: *Current protocols in protein science / editorial board, John E. Coligan ... [et al.]* 0 17. ISSN: 1934-3655. DOI: 10.1002/0471140864.ps1715s72.

Noinaj, Nicholas, Adam J. Kuszak, and Susan K. Buchanan (2015). "Heat Modifiability of Outer Membrane Proteins from Gram-Negative Bacteria." In: *Methods in molecular biology (Clifton, N.J.)* 1329, pp. 51–56. ISSN: 1064-3745. DOI: 10.1007/978-1-4939-2871-2_4.

Noinaj, Nicholas, Adam J. Kuszak, James C. Gumbart, et al. (Sept. 2013). "Structural insight into the biogenesis of β-barrel membrane proteins." en. In: *Nature* 501.7467, pp. 385–390. ISSN: 1476-4687. DOI: 10.1038/nature12521.

Otto, Karen and Malte Hermansson (Jan. 2004). "Inactivation of ompX Causes Increased Interactions of Type 1 Fimbriated Escherichia coli with Abiotic Surfaces." en. In: *Journal of Bacteriology* 186.1, pp. 226–234. ISSN: 0021-9193, 1098-5530. DOI: 10.1128/JB.186.1.226-234.2004.

Paetzel, Mark, Ross E Dalbey, and Natalie C. J Strynadka (July 2000). "The structure and mechanism of bacterial type I signal peptidases: A novel antibiotic target." en. In: *Pharmacology & Therapeutics* 87.1, pp. 27–49. ISSN: 0163-7258. DOI: 10.1016/S0163-7258(00)00064-4.

Park, Min et al. (Mar. 2015). "Isolation and characterization of the outer membrane of Escherichia coli with autodisplayed Z-domains." en. In: *Biochimica et Biophysica Acta (BBA) - Biomembranes* 1848.3, pp. 842–847. ISSN: 0005-2736. DOI: 10.1016/j.bbamem.2014.12.011.

Parwin, Shabnam, Sashi Kalan, and Preeti Srivastava (Jan. 2019). "Bacterial Cell Surface Display." In: *Next Generation Biomanufacturing Technologies*. Vol. 1329. ACS Symposium Series 1329. American Chemical Society, pp. 81–108. ISBN: 978-0-8412-3500-7. DOI: 10.1021/bk-2019-1329.ch005.

Patel, Geetika J. et al. (Nov. 2009). "The Periplasmic Chaperone Skp Facilitates Targeting, Insertion, and Folding of OmpA into Lipid Membranes with a Negative Membrane Surface Potential." In: *Biochemistry* 48.43, pp. 10235–10245. ISSN: 0006-2960. DOI: 10.1021/bi901403c.

Pautsch, Alex et al. (1999). "Strategy for membrane protein crystallization exemplified with OmpA and OmpX." en. In: *Proteins: Structure, Function, and Bioinformatics* 34.2, pp. 167–172. ISSN: 1097-0134. DOI: https://doi.org/10.1002/(SICI)1097-0134(19990201)34:2<167::AID-PROT2>3.0.CO;2-H.

Phale, Prashant S. et al. (Nov. 1998). "Stability of Trimeric OmpF Porin: The Contributions of the Latching Loop L2." In: *Biochemistry* 37.45, pp. 15663–15670. ISSN: 0006-2960. DOI: 10.1021/bi981215c.

Plummer, Ashlee M. and Karen G. Fleming (Oct. 2016). "From Chaperones to the Membrane with a BAM!" In: *Trends in biochemical sciences* 41.10, pp. 872–882. ISSN: 0968-0004. DOI: 10.1016/j.tibs.2016.06.005.

Popot, Jean-Luc (Dec. 2014). "Folding membrane proteins in vitro: A table and some comments." en. In: *Archives of Biochemistry and Biophysics* 564, pp. 314–326. ISSN: 0003-9861. DOI: 10.1016/j.abb.2014.06.029.

Powers, T and P Walter (Aug. 1997). "Co-translational protein targeting catalyzed by the Escherichia coli signal recognition particle and its receptor." In: *The EMBO Journal* 16.16, pp. 4880–4886. ISSN: 0261-4189. DOI: 10.1093/emboj/16.16.4880.

Rath, Arianna, Fiona Cunningham, and Charles M. Deber (Sept. 2013). "Acrylamide concentration determines the direction and magnitude of helical membrane protein gel shifts." en. In: *Proceedings of the National Academy of Sciences* 110.39, pp. 15668–15673. ISSN: 0027-8424, 1091-6490. DOI: 10.1073/pnas.1311305110.

Rath, Arianna, Mira Glibowicka, et al. (Feb. 2009). "Detergent binding explains anomalous SDS-PAGE migration of membrane proteins." eng. In: *Proceedings of the National Academy of Sciences of the United States of America* 106.6, pp. 1760–1765. ISSN: 1091-6490. DOI: 10.1073/pnas.0813167106.

Rath, Parthasarathi, Timothy Sharpe, and Sebastian Hiller (Jan. 2020). "The electrostatic core of the outer membrane protein X from E. coli." en. In: *Biochimica et Biophysica Acta (BBA) - Biomembranes*. Molecular biophysics of membranes and membrane proteins 1862.1, p. 183031. ISSN: 0005-2736. DOI: 10.1016/j.bbamem.2019.183031.

Rath, Parthasarathi, Timothy Sharpe, Bastian Kohl, et al. (2019). "Two-State Folding of the Outer Membrane Protein X into a Lipid Bilayer Membrane." en. In: *Angewandte Chemie International Edition* 58.9, pp. 2665–2669. ISSN: 1521-3773. DOI: 10.1002/anie.201812321.

Remmert, M. et al. (June 2010). "Evolution of Outer Membrane β-Barrels from an Ancestral ββ Hairpin." In: *Molecular Biology and Evolution* 27.6, pp. 1348–1358. ISSN: 0737-4038. DOI: 10.1093/molbev/msq017.

Rice, Jeffrey J. et al. (Apr. 2006). "Bacterial display using circularly permuted outer membrane protein OmpX yields high affinity peptide ligands." eng. In: *Protein*

Science: A Publication of the Protein Society 15.4, pp. 825–836. ISSN: 0961-8368. DOI: 10.1110/ps.051897806.

Ried, Georg et al. (Mar. 1994). "Membrane topology and assembly of the outer membrane protein OmpA of Escherichia coli K12." en. In: *Molecular and General Genetics MGG* 243.2, pp. 127–135. ISSN: 1432-1874. DOI: 10.1007/BF00280309.

Rojas, Enrique R. et al. (July 2018). "The outer membrane is an essential load-bearing element in Gram-negative bacteria." In: *Nature* 559.7715, pp. 617–621. ISSN: 0028-0836. DOI: 10.1038/s41586-018-0344-3.

Rosano, Germán L. and Eduardo A. Ceccarelli (2014). "Recombinant protein expression in Escherichia coli: advances and challenges." English. In: *Frontiers in Microbiology* 5. ISSN: 1664-302X. DOI: 10.3389/fmicb.2014.00172.

Sanger, F. and A. R. Coulson (May 1975). "A rapid method for determining sequences in DNA by primed synthesis with DNA polymerase." en. In: *Journal of Molecular Biology* 94.3, pp. 441–448. ISSN: 0022-2836. DOI: 10.1016/0022-2836(75)90213-2.

Schiffrin, Bob, David J. Brockwell, and Sheena E. Radford (Dec. 2017). "Outer membrane protein folding from an energy landscape perspective." In: *BMC Biology* 15.1, p. 123. ISSN: 1741-7007. DOI: 10.1186/s12915-017-0464-5.

Schindelin, Johannes et al. (July 2012). "Fiji: an open-source platform for biological-image analysis." en. In: *Nature Methods* 9.7, pp. 676–682. ISSN: 1548-7105. DOI: 10.1038/nmeth.2019.

Schleifer, Karl Heinz and Otto Kandler (1972). "Peptidoglycan .Types of Bacterial Cell Walls and their Taxonomic Implications." en. In: *BACTERIOL. REV.* P. 71.

Schulz, Georg E (Jan. 2003). "Transmembrane β-barrel proteins." en. In: *Advances in Protein Chemistry*. Vol. 63. Membrane Proteins. Academic Press, pp. 47–70. DOI: 10.1016/S0065-3233(03)63003-2.

Silhavy, Thomas J., Daniel Kahne, and Suzanne Walker (May 2010). "The Bacterial Cell Envelope." In: *Cold Spring Harbor Perspectives in Biology* 2.5. ISSN: 1943-0264. DOI: 10.1101/cshperspect.a000414.

Sperandeo, Paola, Alessandra M. Martorana, and Alessandra Polissi (Nov. 2017). "Lipopolysaccharide biogenesis and transport at the outer membrane of Gram-negative bacteria." en. In: *Biochimica et Biophysica Acta (BBA) - Molecular and Cell Biology of Lipids* 1862.11, pp. 1451–1460. ISSN: 1388-1981. DOI: 10.1016/j.bbalip.2016.10.006.

Stoorvogel, J., M. J. van Bussel, and J. A. van de Klundert (Jan. 1991). "Biological characterization of an Enterobacter cloacae outer membrane protein (OmpX)." en. In: *Journal of Bacteriology* 173.1, pp. 161–167. ISSN: 0021-9193, 1098-5530. DOI: 10.1128/jb.173.1.161-167.1991.

Studier, F. William and Barbara A. Moffatt (May 1986). "Use of bacteriophage T7 RNA polymerase to direct selective high-level expression of cloned genes." en. In: *Journal of Molecular Biology* 189.1, pp. 113–130. ISSN: 0022-2836. DOI: 10.1016/0022-2836(86)90385-2.

Surrey, Thomas and Fritz Jähnig (Nov. 1995). "Kinetics of Folding and Membrane Insertion of a β-Barrel Membrane Protein." en. In: *Journal of Biological Chemistry* 270.47, pp. 28199–28203. ISSN: 0021-9258, 1083-351X. DOI: 10.1074/jbc.270.47.28199.

Sutcliffe, Iain C. (Oct. 2010). "A phylum level perspective on bacterial cell envelope architecture." English. In: *Trends in Microbiology* 18.10, pp. 464–470. ISSN: 0966-842X, 1878-4380. DOI: 10.1016/j.tim.2010.06.005.

Tomasek, David et al. (2020). "Structure of a nascent membrane protein as it folds on the BAM complex." eng. In: *Nature* 583.7816, pp. 473–478. ISSN: 1476-4687. DOI: 10.1038/s41586-020-2370-1.

Tsirigotaki, Alexandra et al. (Jan. 2017). "Protein export through the bacterial Sec pathway." en. In: *Nature Reviews Microbiology* 15.1, pp. 21–36. ISSN: 1740-1534. DOI: 10.1038/nrmicro.2016.161.

Typas, Athanasios et al. (Dec. 2011). "From the regulation of peptidoglycan synthesis to bacterial growth and morphology." In: *Nature reviews. Microbiology* 10.2, pp. 123–136. ISSN: 1740-1526. DOI: 10.1038/nrmicro2677.

Ventola, C. Lee (Apr. 2015). "The Antibiotic Resistance Crisis." In: *Pharmacy and Therapeutics* 40.4, pp. 277–283. ISSN: 1052-1372.

Vogt, Joachim and Georg E Schulz (Oct. 1999). "The structure of the outer membrane protein OmpX from Escherichia coli reveals possible mechanisms of virulence." en. In: *Structure* 7.10, pp. 1301–1309. ISSN: 0969-2126. DOI: 10.1016/S0969-2126(00)80063-5.

Vollmer, Waldemar (Jan. 2012). "Bacterial outer membrane evolution via sporulation?" en. In: *Nature Chemical Biology* 8.1, pp. 14–18. ISSN: 1552-4469. DOI: 10.1038/nchembio.748.

Vollmer, Waldemar, Didier Blanot, and Miguel A. De Pedro (2008). "Peptidoglycan structure and architecture." en. In: *FEMS Microbiology Reviews* 32.2, pp. 149–167. ISSN: 1574-6976. DOI: https://doi.org/10.1111/j.1574-6976.2007.00094.x.

Wimley, William C (Aug. 2003). "The versatile β-barrel membrane protein." en. In: *Current Opinion in Structural Biology* 13.4, pp. 404–411. ISSN: 0959-440X. DOI: 10.1016/S0959-440X(03)00099-X.

Wimley, William C. and Stephen H. White (Oct. 1996). "Experimentally determined hydrophobicity scale for proteins at membrane interfaces." en. In: *Nature Structural Biology* 3.10, pp. 842–848. ISSN: 1545-9985. DOI: 10.1038/nsb1096-842.

Winther, Anja Ruud (Dec. 2015). "Fluorescent biomarkers for membrane seperation." English. MA thesis. The University of Oslo.

Wu, Runrun et al. (Jan. 2020). "The big BAM theory: An open and closed case?" en. In: *Biochimica et Biophysica Acta (BBA) - Biomembranes*. Molecular biophysics of membranes and membrane proteins 1862.1, p. 183062. ISSN: 0005-2736. DOI: 10.1016/j.bbamem.2019.183062.

Wülfing, Christoph and Andreas Plückthun (1994). "Protein folding in the periplasm of Escherichia coli." en. In: *Molecular Microbiology* 12.5, pp. 685–692. ISSN: 1365-2958.

Xu, Zhaohui and Sang Yup Lee (Nov. 1999). "Display of Polyhistidine Peptides on the Escherichia coli Cell Surface by Using Outer Membrane Protein C as an Anchoring Motif." In: *Applied and Environmental Microbiology* 65.11, pp. 5142–5147. ISSN: 0099-2240.

Yamashita, Satoshi et al. (Nov. 2011). "Structural insights into Ail-mediated adhesion in Yersinia pestis." In: *Structure (London, England : 1993)* 19.11, pp. 1672–1682. ISSN: 0969-2126. DOI: 10.1016/j.str.2011.08.010.

Yan, Zhaofeng et al. (Feb. 2017). "Structural insights into the secretin translocation channel in the type II secretion system." en. In: *Nature Structural & Molecular Biology* 24.2, pp. 177–183. ISSN: 1545-9985. DOI: 10.1038/nsmb.3350.

Appendix 1 - Abbreviations

Table 6.1: Buffers and chemicals

Abbreviation	Full form
Amp	Ampicillin
ATP	Adenosine triphosphate
BAM	ß-barrel assembly machinery
BSA	Bovine serum albumin
CMC	critical micelle concentration
CV	Column volume
DNA	Deoxyribonucleic acid
dNTP	Deoxynucleotide
DMPC	1,2-dimyristoyl-sn-glycero-3-phosphocholine
E. coli	*Escherichia coli*
EV	Empty vector
EDTA	Ethylenediaminetetraacetic acid
GTP	Guanoside 5′-triphosphate
HEPES	4-(2-hydroxyethyl)-1-piperazineethanesulfonic acid
HRP	Horseradish peroxidase
IM	Inner membrane
IPTG	Isopropyl ß-D-1-thiogalactopyranoside
Kan	Kanamycin
LB	Lysogeny broth
LPP	major outer membrane lipoprotein
LPR	Lipid to protein ratio
LPS	Lipopolysaccharides
MWCO	Molecular weight cut-off
OD_{600}	Optical density
OM	Outer membrane
OMP	Outer membrane protein
OmpX	Outer membrane protein X
OG	N-Octyl-β-D-glucoside

Abbreviation	Full form
PBS	Phosphate-buffered saline
PBST	Phosphate-buffered saline with Tween 20
PCR	Polymerase chain reaction
pI	Isoelectric point
POTRA	Polypeptide transport-associated
RT	Room temperature
SB12	N-Dodecyl-N,N-dimethylammonio-3-propane sulfonate
SDS-PAGE	Sodium dodecyl sulfate - polyacrylamide gel electrophoresis
Sec	General secretion
SRP	Signal recognition particle
TAT	Twin arginine translocase
TAE	Tris-acetate-EDTA
Tet	Tetracyclin
TF	Trigger factor
TSS	Transformation and storage solution
WT	Wild type

Appendix 2 - Media, buffers and solutions

Table 7.1: Buffers and chemicals

Media\Buffer	Components	Company
Lysogeny Broth (LB)	10 g NaCl	Merck KGaA
	10 g Tryptone enzymatic digest	Merck KGaA
LB agar	25 g LB broth	BD
	10 g Bactopor agar	BD
	ddH_2O to 1 L	
TSS buffer	075 mL $MgCl_2$ (1M)	Merc
	2.5 g PEG 8000	Sigma-Aldrich
	1.23 mL DMSO	Sigma-Aldrich
	25 mL LB	
50x TAE	242 g Tris base	VWR chemicals
	57.1 mL glacial acetic acid	Sigma-Aldrich
	20.81 EDTA	VWR chemicals
	ddH_2O to 1 L	
TAE agarose 0.8% (w/v)	Agarose	Lonza
	50x TAE	VWR Chemical
	GelRed® Nucleic Acid Stain	SigmaAldrich
	ddH_2O to	
6x DNA loading buffer	3.5 mL 100% Glycerol	VWR
	35 μL 3M Tris-HCl, pH8	Angus
	20 μL EDTA (0.5 M, pH 8)	AppliChem
	25 mg bromophenol blue	Sigma-Aldrich
	ddH_2O to 10 mL	
T4 PNK buffer	3 μ Primer (100 μM)	
	5 μL 10X PNK buffer	NEB
	0.5 μL ATP (100 μL)	NEB

Media\Buffer	Components	Company
	1 μL T4 PNK	NEB
	ddH_2O to 50 μL	
4x SDS sample buffer	40 mL 20% SDS	AppliChem
	0.04 g bromophenol blue sodium salt	Sigma-Aldrich
	6.6 mL 3 M Tris pH 7.5	Angus
	40% glycerol bidistilled	VMW chemicals
	0.4 mL 0.5 M EDTA	AppliChem
	ddH_2O to 100 mL	
10x SDS Running buffer	30 g Tris	Angus
	144 g glycine	VWR chemichals
	10 g SDS	AppliChem
	ddH_2O to 1000 mL	
Staining solution	1.25 g Coomassie R	Sigma-Aldrich
	100 mL Acetic acid	Sigma-Aldrich
	500 mL Ethanol	Angus
	400 mL ddH_2O	
Destaining solution	400 mL Ethanol	Arcus
	100 mL Acetic acid	Sigma-Aldrich
Western Transfer buffer	25 mM Tris	Angus
	150 mM glycine	Sigma-Aldrich
	10% isopropanol	VWR chemicals
10x PBS	1.3 M NaCl	Merck
	70 mM Na_2HPO_4	Sigma-Aldrich
	30 mM NaH_2PO_4	Sigma-Aldrich
TBS	20 mM Tris HCL	Angus
	150 mM NaCl	Merck
TBS-T	20 mM Tris HCL	Angus
	150 mM NaCl	Merck
	0.05% tween 20	Sigma

Media\Buffer	Components	Company
Blocking buffer	2% BSA	VWR chemicals
	TBS-T	
Urea extraction buffer	15 mM HEPES pH 7.4	Sigma
	100 mM glycine	Sigma
	6 M urea	Merc

Appendix 3 - Primers

Table 8.1: Primer sequences and PCR conditions

Primer 1	SPLATfwdL2
PCR	Phusion polymerase with GC enhancer. 61°C annealing
Sequence	AGCCCACTAGCAACAGGTGACTACAACAAAAACCAGTACTACG
Primer 2	AGPGAfwdL2
PCR	Phusion polymerase with GC enhancer. 61°C annealing
Sequence	GCAGGACCAGGAGCAGGTGACTACAACAAAAACCAGTACTACG
Primer 3	revL2
PCR	Phusion polymerase with GC enhancer. 61°C annealing
Sequence	AGAGCTTGCAGTACGGCTT
Primer 4	SPLATfwdL3
PCR	Phusion polymerase with GC enhancer. 61°C annealing
Sequence	AGCCCACTAGCAACAACCTACAAACACGACACCAGC
Primer 5	AGPGAfwdL3
PCR	Phusion polymerase with GC enhancer. 61°C annealing
Sequence	GCAGGACCAGGAGCAACCTACAAACACGACACCAGC
Primer 6	revL3
PCR	Phusion polymerase with GC enhancer. 61°C annealing
Sequence	CGGGTATTCAGTGGTCTGGAATTT
Primer 7	AGPGAx2revL2
PCR	Phusion polymerase. 62°C annealing
Sequence	TGCTCCTGGTCCTGCGCTTGCAGTACGGCTTTTCTCG
Primer 8	SPLATx2revL2
PCR	Phusion polymerase. 62°C annealing
Sequence	TGTTGCTAGTGGGctAGAGCTTGCAGTACGGCTT
Primer 9	SPLATx2revL3
PCR	Phusion polymerase. 62°C annealing
Sequence	TGTTGCTAGTGGAGACGGGTATTCAGTGGTCTGGAATTT
Primer 10	AGPGAx2fwdL2
PCR	Phusion polymerase. 62°C annealing
Sequence	GCGGGTCCGGGTGCGTCTGGTGACTACAACAAAAACCAGTACTAC
Primer 11	SPLATx2fwdL2
PCR	Phusion polymerase. 62°C annealing
Sequence	AGTCCGCTTGCGACAGGTGACTACAACAAAAACCAGTACTACG
Primer 12	AGPGAx2fwdL3
PCR	Phusion polymerase. 62°C annealing
Sequence	GCGGGTCCGGGTGCGTACAAACACGACACCAGCGACTACG

Primer 13	AGPGAx2revL3
PCR	Phusion polymerase. 62°C annealing
Sequence	TGCTCCTGGTCCTGCGGTCGGGTATTCAGTGGTCTGGAATT
Primer 14	SPLATx4fwdL2
PCR	Phusion polymerase. 69°C annealing
Sequence	AGTCCGCTTGCGACAAGTCCGCTTGCGACAGGTGACTACAACAAAAACCAGTACTACGGC
Primer 15	SPLATx4revL2
PCR	Phusion polymerase. 69°C annealing
Sequence	TGTTGCTAGTGGGCTTGTTGCTAGTGGGCTAGAGCTTGCAGTACGGCTTTTCTCG
Primer 16	SPLATx4fwdL3
PCR	Phusion polymerase. 62°C annealing
Sequence	AGCCCACTTGCAACAAGCCCACTAGCAACTCCGACCTACAAACACGACACCAGC
Primer 17	SPLATx4revL3
PCR	Phusion polymerase. 62°C annealing
Sequence	TGTAGCTAGAGGAGAAGTAGCAAGAGGTGAGTATTCAGTGGTCTGGAATTTACCATAACCCACA
Primer 18	AGPGAx4fwdL2
PCR	Phusion polymerase. 68°C annealing
Sequence	GCGGGTCCGGGTGCGGCGGGTCCGGGTGCGTCTGGTGACTACAACAAAAACCAGTACTAC
Primer 19	AGPGAx4revL2
PCR	Phusion polymerase. 68°C annealing
Sequence	TGCTCCTGGTCCTGCTGCTCCTGGTCCTGCGCTTGCAGTACGGCTTTTCTCG
Primer 20	AGPGAx4fwdL3
PCR	Phusion polymerase with GC enhancer. 67°C annealing
Sequence	GCGGGTCCGGGTGCGGCGGGTCCGGGTGCGTACAAACACGACACCAGCGACTACG
Primer 21	AGPGAx4revL3
PCR	Phusion polymerase with GC enhancer. 67°C annealing
Sequence	TGCTCCTGGTCCTGCTGCTCCTGGTCCTGCGGTCGGGTATTCAGTGGTCTGGAATT
Primer 22	delEYPTYfwdL3
PCR	Q5 polymerase with GC enhancer. 61°C annealing
Sequence	AAACACGACACCAGCGACTACG
Primer 23	delEYPTYrevL3
PCR	Q5 polymerase with GC enhancer. 61°C annealing
Sequence	AGTGGTCTGGAATTTACCATAACCCACAC
Primer 24	delFwdL3
PCR	Phusion polymerase. 61°C annealing
Sequence	GAATACCCGACCTACTTCTCCTACGGTGCGGGTCTG
Primer 25	delRevL3
PCR	Phusion polymerase. 61°C annealing
Sequence	ACCCACACCCACTACACCGTAGA
Primer 26	T7 forward Binds the T7 promotor. Used for sequencing of constructs

Sequence	CCCTATAGTGAGTCGTATTA
Primer 27	T7 reverse Binds the T7 terminator. Used for sequencing of constructs.
Sequence	GCTAGTTATTGCTCAGCGG

Appendix 4 - Supplementary figures

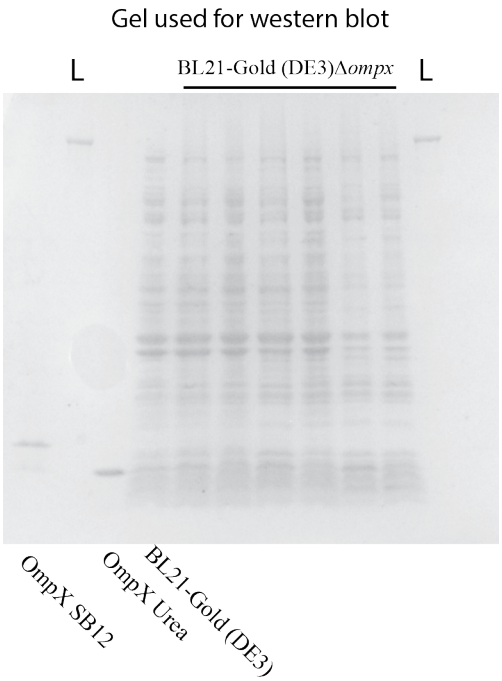

Figure 9.1: After transfer of protein to the PVDF membrane the gel was stained in Coomassie R. The gels shows that protein was not completely transferred to the membrane. Folded and unfolded OmpX is visible in the wells labeled "OmpX SB12" and "OmpX Urea" respectievly. The western blot of this gel is in section 4.2.

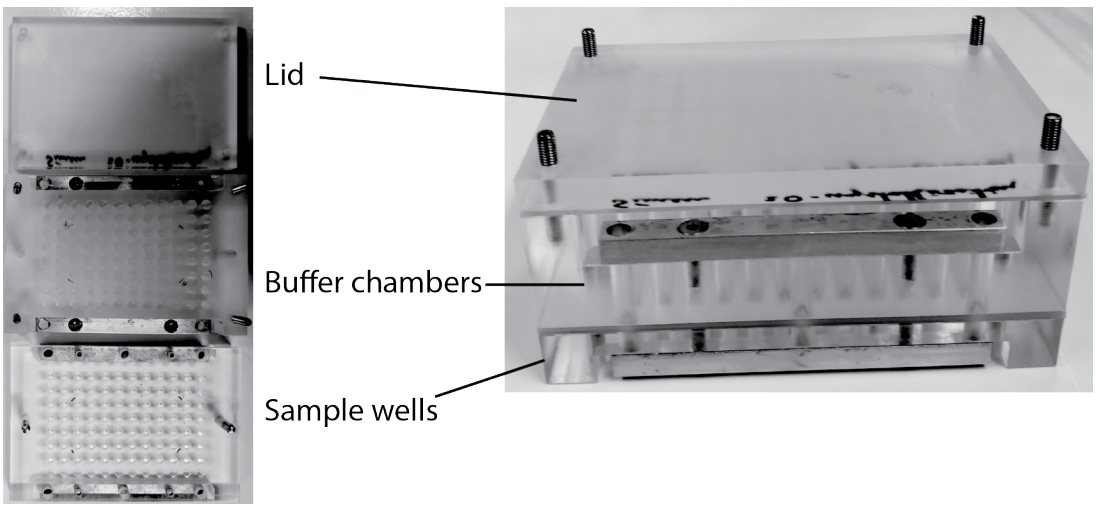

Figure 9.2: Dialasis block used for crystallization of OmpX88. The design is based on. The design was fitted with a lid so that the block could be placed sideways without the buffer falling out. The individual parts of the block were machined by the Instrument Laboratory (I-Lab) at UiO. The sample wells hold 50 µL and the buffer chambers hold 950 µL.

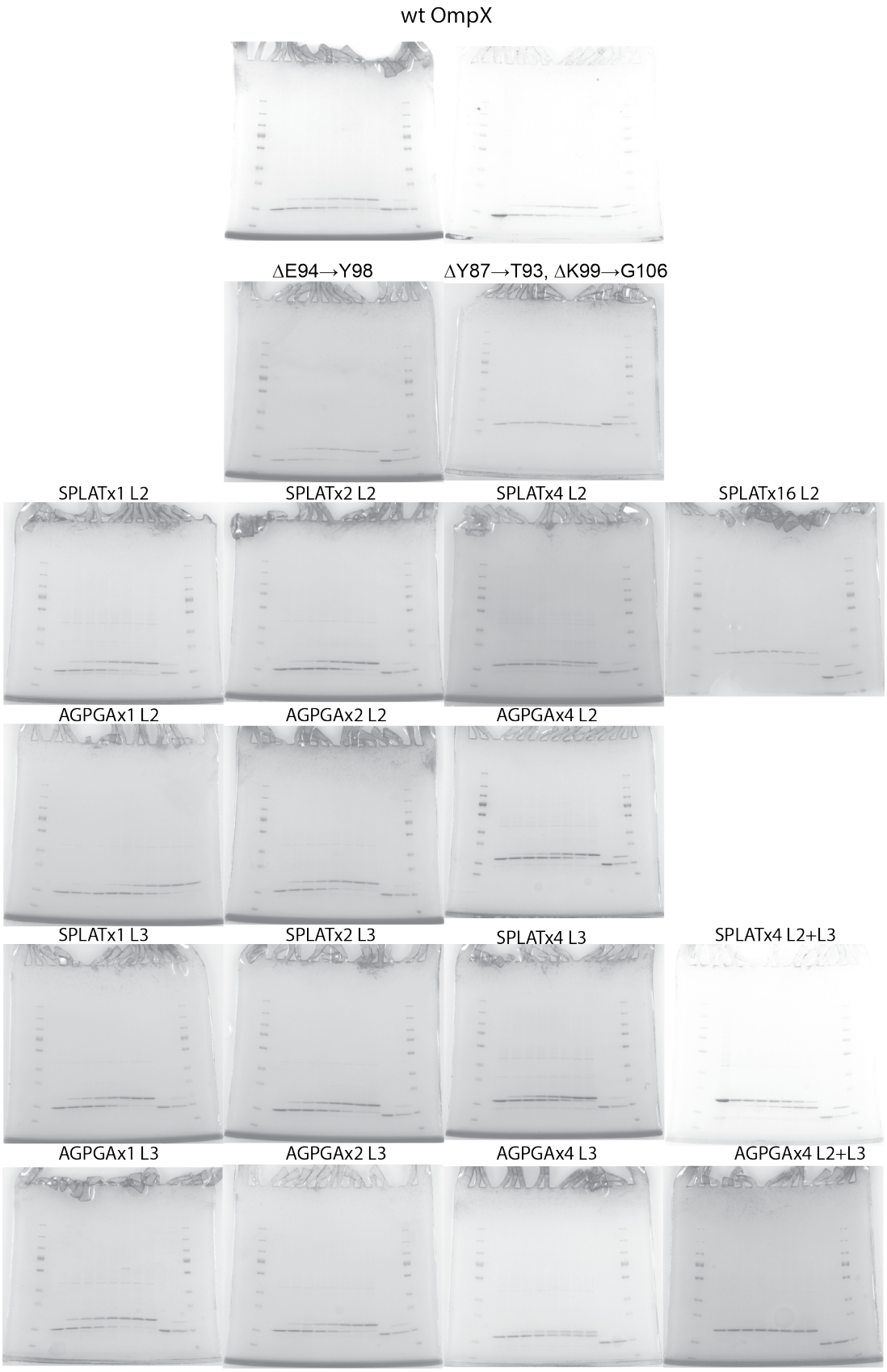

Figure 9.3: Uncropped folding assays of the various OmpX constructs used to dermine folding kinetics. Seven timepoints were sampled in the different folding kinetics. The ladder used was PageRuler™Plus Prestained protein ladder. See section 4.5 for the folding kinetics.